Rewetting Phenomena and Measurements

of True Quench Temperature

by

Peter W.K. Lau

A thesis
presented to the School of Graduate Studies and Research
at the University of Ottawa
in partial fulfillment of the
requirements for the degree of
Master of Applied Science
in
Department of Mechanical Engineering

Rewetting Phenomena and Measurements of True Quench Temperature

by

Peter W.K. LAU

ABSTRACT

Accurate prediction of the consequences of a loss-of-coolant-accident (LOCA) requires precise calculation of fuel-coolant heat transfer during the subsequent emergency-core-cooling phase. The rewetting phenomenon and the minimum film boiling temperature play an important role in the study of the LOCA analysis.

In the present experiments, the true quench temperature and location of initial rewet with respect to system parameters were studied. The experiments were performed in a single tube geometry with bottom flooding.

The data cover a pressure range of 101 to 687 kPa, mass flux from 50 to 682 kg/m^{2}s, inlet subcooling from 2 to 30^{o}C and local quality from -0.0315 to 0.1990.

It is found that the true quench temperature depends on pressure, mass flux, inlet subcooling and local quality. A true quench temperature correlation of the form:

$$T_Q = 145.98 + 0.1347\ P + 0.1605\ G + 3.5069\ \Delta T_{sub}$$

was derived, with the root mean square error of 7.75%. An attempt to correlate T_Q based on local quality, mass flux and pressure was not very successful. This is due to the strong entrance effect.

Special artificial cold spot tests were also conducted to check the length effect on the true quench temperature.

ACKNOWLEDGEMENT

I would like to express my deepest appreciation and gratitude to Professor S.C. Cheng for his constant encouragement, guidance and stimulation throughout the course of this study.

I wish to extend special thanks to Dr. D.C. Groeneveld of AECL, who provided excellent ideas and suggestions throughout the work.

I also wish to thank the technical staffs and members of Mechanical Engineering department for their cooperation and assistance.

Special thanks to Mr. J.H. Woodall of AECL for his excellent technique in perfecting the fabrication of the test section. Also Mr. K.T. Poon and Mr. W.W.L. Ng are gratefully acknowledged for their assistance in the experimental work.

Finally, an expression of thanks is extended to Argonne National Laboratory, Illinois, U.S.A., for their financial support.

TABLE OF CONTENTS

ABSTRACT ii

ACKNOWLEDGEMENT iv

LIST OF FIGURES viii

LIST OF TABLES xii

NOMENCLATURE xiii

Chapter | page

I. INTRODUCTION 1

II. LITERATURE REVIEW 3

2.1 Boiling Curve 3
2.2 Flow Regimes 6
2.2.1 Single phase liquid flow 6
2.2.2 Bubbly flow 6
2.2.3 Inverted annular flow 8
2.2.4 Slug flow 9
2.2.5 Dispersed flow 10
2.2.6 Single phase vapour 10
2.3 Flow pattern map for vertical flow 11
2.4 Rewetting mechanisms 13
2.4.1 Hydrodynamic mechanism 13
2.4.2 Thermodynamic mechanism 14
2.5 Types of Rewetting 15
2.5.1 Forced convection rewet 15
2.5.1.1 Impulse cooling collapse 15
2.5.1.2 Axial conduction controlled rewet . . 17
2.5.1.3 Dispersed flow rewet 18
2.5.2 Free convection rewet 20
2.5.2.1 Leidenfrost cooling 20
2.5.2.2 Collapse of vapour film during pool boiling 22
2.6 Parametric effects 23
2.6.1 Mass flux 23
2.6.2 Subcooling 26
2.6.3 Pressure 26
2.6.4 Quality 26
2.6.5 Thermal properties of heated surface . . . 29

III. EXPERIMENTAL DESIGN 31

3.1 Open loop facilities 31
3.1.1 General 31
3.1.2 Storage tank 33
3.1.3 Preheater 33
3.1.4 Test section assembly 34
3.1.5 Test section power supply 38
3.1.6 Open loop procedure 41
3.2 Closed loop facilities 43
3.2.1 General 43
3.2.2 Storage tank 45
3.2.3 Surge tank 45
3.2.4 Piping 46
3.2.5 Others 46
3.2.6 Closed loop procedure 46

IV. EXPERIMENTAL RUNS AND DATA REDUCTION 49

4.1 General 49
4.1.1 10,000 and 10,100 run series 49
4.1.2 10,200 run series 51
4.1.3 10,200A run series 51
4.1.4 10,300 run series 53
4.2 Data reduction 59

V. RESULTS AND DISCUSSION 61

5.1 10,000 and 10,100 run series 62
5.2 10,200 run series 64
5.3 10,200A run series 64
5.4 10,300 run series 71
5.5 Parametric trends study 88
5.5.1 Mass flux effect 88
5.5.2 Inlet subcooling effect 89
5.5.3 Quality effect 89
5.5.4 Pressure effect 90
5.6 General discussion 91
5.7 Correlation and comparison 95

VI. CONCLUSIONS 107

BIBLIOGRAPHY 110

<u>Appendix</u> <u>page</u>

A. HEAT LOSSES TEST 113

B. COOLDOWN TEST OF THE BOTTOM HOT PATCH 115

C. MATHEMATICAL METHOD FOR DETERMINATING FILM BOILING HEAT FLUX 116

D. SAMPLE CALCULATION OF LOCAL QUALITY 121

E. CONTINUOUS SYSTEM MODELING PROGRAM 125

F. SPSS PROGRAM FOR CORRELATION OF TRUE QUENCH TEMPERATURE 134

LIST OF FIGURES

Figure		Page
2.1	Boiling Curve	4
2.2	Flow Regimes in a Directly Heated Tube	7
2.3	Flow Pattern Map for Vertical Flow	12
2.4	Types of Rewetting	16
2.5	Axial Conduction Controlled Rewet	19
2.6	Dispersed Flow Rewet	21
2.7	Film Boiling Minimum ΔT_w vs Equilibrium Quality - Effect of Mass Flux	24
2.8	Effect of Mass Flux on Boiling Curve of Distilled Water for $\Delta T_{sub} = 0°C$	25
2.9	Effect of Subcooling on Boiling Curve	25
2.10	Effect of Subcooling on ΔT_{min}	27
2.11	Effect of Quality on ΔT_{min}	28
2.12	Comparison of Boiling Curves obtained from Different Heated Surface Test Sections - Effect of Heated Surface Properties	30
3.1	Schematic Diagram of the Experimental Loop for Atmospheric Pressure	32
3.2	Schematic Diagram of the Test Section	35
3.3	Schematic Diagram of the Bottom Hot Patch	36
3.4	Typical Temperature-Time Trace of Test Section Thermocouples during Test	39
3.5	Schematic Diagram of the Pressurized Experimental Loop	44
3.6	An Insulated Test Section Assembly	47

Figure		Page

3.7	Experimental Equipment	47
3.8	Surge Tank and Water Storage Tank	48
3.9	Overall View of the Experimental Apparatus	48
5.1	Measured Quench Temperature vs Mass Flux and Local Quality for 10,000 and 10,100 Run Series	63
5.2	Measured Quench Temperature vs Mass Flux and Local Quality for 10,200 Run Series	65
5.3	Measured Quench Temperature vs Local Quality for Fixed Mass Flux for 10,200 Run Series	66
5.4	Measured Quench Temperature vs Inlet Subcooling for Fixed Mass Flux for 10,200 Run Series	67
5.5	Measured Quench Temperature vs Mass Flux for Fixed Local Quality for 10,200 Run Series	68
5.6	Measured Quench Temperature vs Inlet Subcooling for Fixed Local Quality for 10,200 Run Series	69
5.7	Measured Quench Temperature vs Mass Flux and Local Quality for 10,300 Run Series at P=206 kPa	72
5.8	Measured Quench Temperature vs Mass Flux and Local Quality for 10,300 Run Series at P=344 kPa	73
5.9	Measured Quench Temperature vs Mass Flux and Local Quality for 10,300 Run Series at P=550 kPa	74
5.10	Measured Quench Temperature vs Mass Flux and Local Quality for 10,300 Run Series at P=687 kPa	75
5.11	Measured Quench Temperature vs Inlet Subcooling for Fixed Mass Flux for 10,300 Run Series at P=206 kPa	76
5.12	Measured Quench Temperature vs Inlet Subcooling for Fixed Mass Flux for 10,300 Run Series at P=344 kPa	77

Figure		Page

5.13 Measured Quench Temperature vs Inlet Subcooling for Fixed Mass Flux for 10,300 Run Series at P=550 kPa 78

5.14 Measured Quench Temperature vs Inlet Subcooling for Fixed Mass Flux for 10,300 Run Series at P=687 kPa 79

5.15 Measured Quench Temperature vs Local Quality for Fixed Mass Flux for 10,300 Run Series at P=206 kPa 80

5.16 Measured Quench Temperature vs Local Quality for Fixed Mass Flux for 10,300 Run Series at P=344 kPa 81

5.17 Measured Quench Temperature vs Local Quality for Fixed Mass Flux for 10,300 Run Series at P=550 kPa 82

5.18 Measured Quench Temperature vs Local Quality for Fixed Mass Flux for 10,300 Run Series at P=687 kPa 83

5.19 Measured Quench Temperature vs Mass Flux for Fixed Local Quality for 10,300 Run Series 84

5.20 Measured Quench Temperature vs Inlet Subcooling for Fixed Local Quality for 10,300 Run Series 85

5.21 Measured Quench Temperature vs Pressure for Fixed Mass Flux and Inlet Subcooling for 10,300 Run Series 86

5.22 Measured Quench Temperature vs Pressure for Fixed Local Quality and Mass Flux for 10,300 Run Series 87

5.23 True Quench Temperature and Apparent Quench Temperature at Various Locations for Run 10,214 93

5.24 True Quench Temperature and Apparent Quench Temperature at Various Locations for Run 10,233 94

Figure | Page

5.25 Comparison of Correlation with Experimental Data from 10,300 Run Series at P=206 kPa 96

5.26 Comparison of Correlation with Experimental Data from 10,300 Run Series at P=550 kPa 97

5.27 Comparison of Correlation with Experimental Data from 10,300 Run Series at G=200 kg/m^2s 98

5.28 Comparison of Correlation with Experimental Data from 10,300 Run Series at G=400 kg/m^2s 99

5.29 Comparison of Correlation with Experimental Data from 10,300 Run Series at ΔT_{sub} =20°C 100

5.30 Comparison of Correlation with Experimental Data from 10,300 Run Series at ΔT_{sub} =30°C 101

A.1 Heat Losses vs Average Wall Temperature for 10,300 Run Series 114

C.1 Nodal Points Distribution 117

LIST OF TABLES

Table		Page
4.1	10,000 and 10,100 Run Series Data	50
4.2	10,200 Run Series Data	52
4.3	Cold Spot Test, 10,200A Run Series Data	54
4.4A	10,300 Run Series Data at P=206 kPa	55
4.4B	10,300 Run Series Data at P=344 kPa	56
4.4C	10,300 Run Series Data at P=550 kPa	57
4.4D	10,300 Run Series Data at P=687 kPa	58
5.1	Minimum Film Boiling Temperature [Fung]	103
5.2	Minimum Film Boiling Temperature [Stewart]	104

NOMENCLATURE

A	area
BHP	bottom hot patch
C	specific heat
D	diameter
G	mass flux
h	enthalpy
h	heat transfer coefficient
hp	horsepower
HF	heat flux
j	superficial phase velocity
k	thermal conductivity
L	length
m	mass flow rate
P	pressure
q	heat flux
Q	heat content
r	radius
t	time
T	temperature
THP	top hot patch

x, X	quality
α	thermal diffusivity
δ	thickness
ρ	density

Subscripts

amb	ambient
c, crit	critical
c	copper
f	liquid
g	vapour
in	inner
l, liq	liquid
min	minimum
n	nodal point
out	outer
Q	quench
sat	saturate
sub	subcooling
t	test section
w, wall	wall

Chapter I

INTRODUCTION

The safety aspect of heat transfer problems associated with water-cooled nuclear reactors under hypothetical loss-of-coolant-accident (LOCA) conditions continues to attract great attention from present heat transfer researchers.

Following a postulated loss-of-coolant-accident in a water-cooled reactor, the lack of adequate cooling can result in dryout occuring over a considerable part of the core. The fuel elements in dryout will experience a significant rise in surface temperature. The establishment of adequate emergency core cooling will slowly lower these temperatures by precursory cooling, radiation and axial conduction. The injected water will only wet the fuel sheath when the surface temperature has been reduced to below the minimum film boiling temperature.

Determination of the minimum film boiling temperature is of great importance in reactor safety analysis. This minimum film boiling temperature separates the high temperature region, where inefficient film boiling or vapour cooling takes place, from the lower temperature region, where more efficient transition boiling occurs. It thus provides a limit to the application of transition boiling and film boiling correlations.

A large number of terms have been used to describe the phenomenon at the boundary between transition boiling and film boiling, eg., rewetting, quenching, sputtering, DFFB (departure from film boiling), film boiling collapse, Leidenfrost phenomenon and minimum film boiling. A variety of correlations have been proposed to predict the corresponding temperature and heat flux. Unfortunately, none of these studied the true quench phenomenon and the associated true quench temperature in the flow boiling situation in the absence of the axial conduction.

The purpose of this study is to measure the true quench temperature and to investigate its parametric trends. The termination of the film boiling phenomenon encountered in this study is a result of the spontaneous collapse of a vapour film following a gradual reduction in the surface temperature. The experiments were performed on a single tube geometry with bottom flooding.

To anchor the quench front originated from both ends of the test section, a relatively new hot patch technique is used to establish steady-state film boiling for water during forced convection inside a directly-heated channel.

Chapter II
LITERATURE REVIEW

2.1 BOILING CURVE

In pool boiling, when a surface is exposed to a liquid and is maintained at a temperature above the saturation temperature of the liquid, a change in phase from liquid to vapour may occur. A boiling curve can be obtained by plotting the heat flux versus the corresponding surface temperature such as the one shown in Fig. 2.1.

It has now been well-established that there are three basic modes of boiling; namely, nucleate boiling, transition boiling and film boiling. Each occurs over a range of superheats measured at the surface [1].

In the case of a temperature controlled surface, the boiling curve is continuous as shown in Fig. 2.1. The region A to B represents nucleate boiling, so called because bubbles are formed repeatedly at fixed nucleation sites on the surface. This mode of boiling is characterized by the continuous contact between the liquid and the heated surface. With further increase in superheat, the heat flux

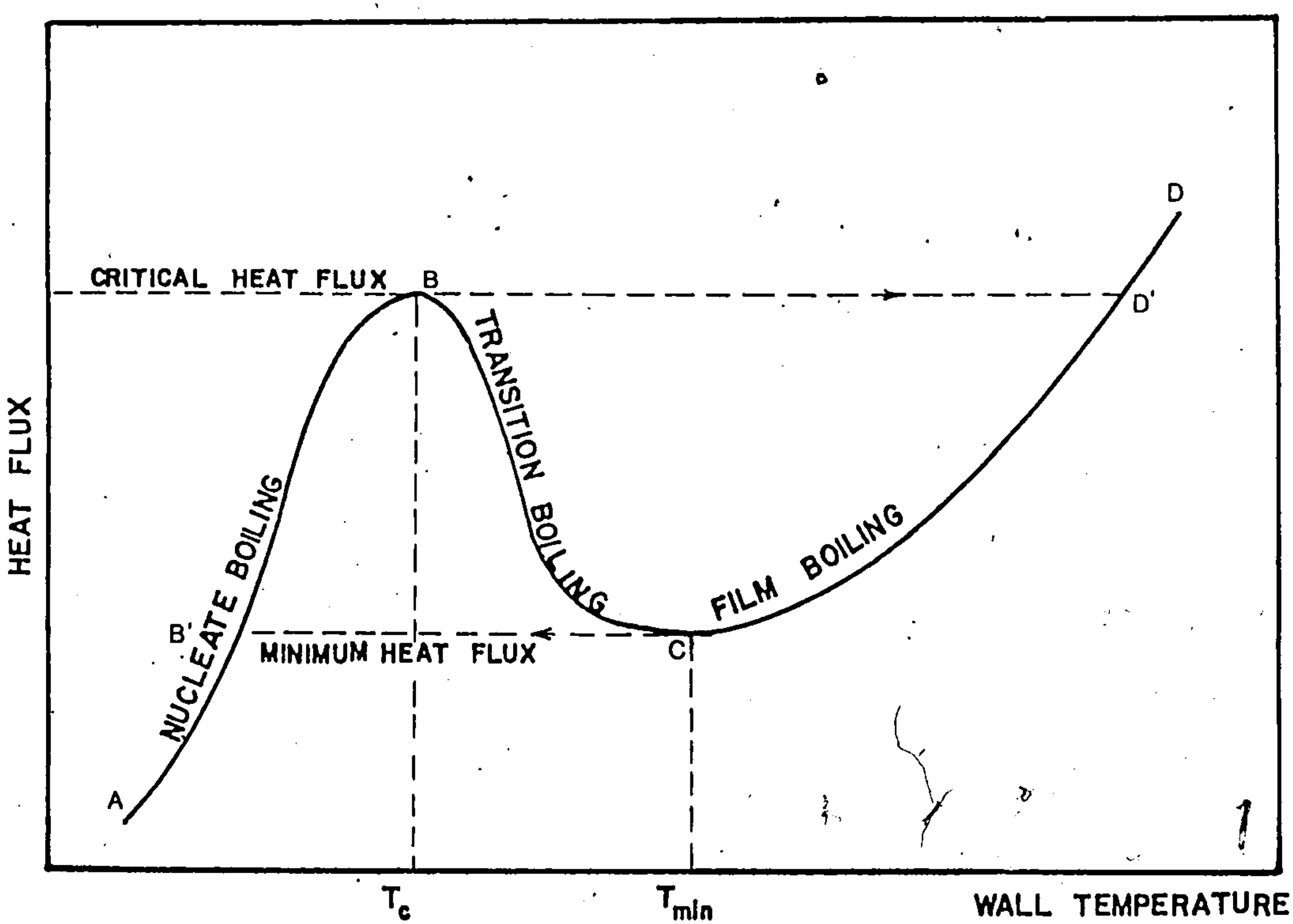

FIG. 2.1 BOILING CURVE

decreases at region BC in Fig. 2.1. This mode is called transition boiling, in which the liquid-surface contact is intermittent. The region C to D is film boiling. It exists over a higher superheat heating surface, and it is characterized by the formation of a continuous blanket of vapour film which separates the liquid coolant from the hot surface. This mode of heat transfer is very inefficient when compared to nucleate boiling.

If the heating surface is heat-flux controlled, raising the heat flux would bring nucleate boiling directly into film boiling with a large increase of superheat, such as the path ABD'D. At point B, the maximum limit of nucleate boiling is reached. The heat flux at this point is called critical heat flux (CHF), and is also known as dryout, burnout, first boiling crisis and departure from nucleate boiling (DNB).

On the contrary, reducing the heat flux would bring the boiling from the film boiling mode to the nucleation mode through path DCB'A. Point C is the limit for stable film boiling. The heat flux at this point is called the minimum film boiling heat flux, and the temperature of this point is known as the minimum film boiling temperature.

2.2 FLOW REGIMES

For a forced convective flow of a subcooled liquid at the inlet of a uniformly heated vertical tube, several flow regimes are likely to occur as the mass quality increases downstream. These are, namely: single phase liquid, bubbly flow, inverted annular flow, slug flow, dispersed flow and single phase vapour. Figure 2.2 shows the possible configurations of the flow structures inside a heated channel.

2.2.1 Single phase liquid flow

Single phase forced convective heat transfer.

2.2.2 Bubbly flow

Bubbles are generated at the heated wall and remain in the wall region, since the bulk of the liquid is still subcooled. The liquid becomes saturated further downstream, bubbly flow bubbles exist in the core region and coalesce to form larger bubbles. The heat is transferred through forced convection to the liquid or through nucleate boiling to the bubbles, which in turn transfer some of their latent heat to the liquid by condensation [2].

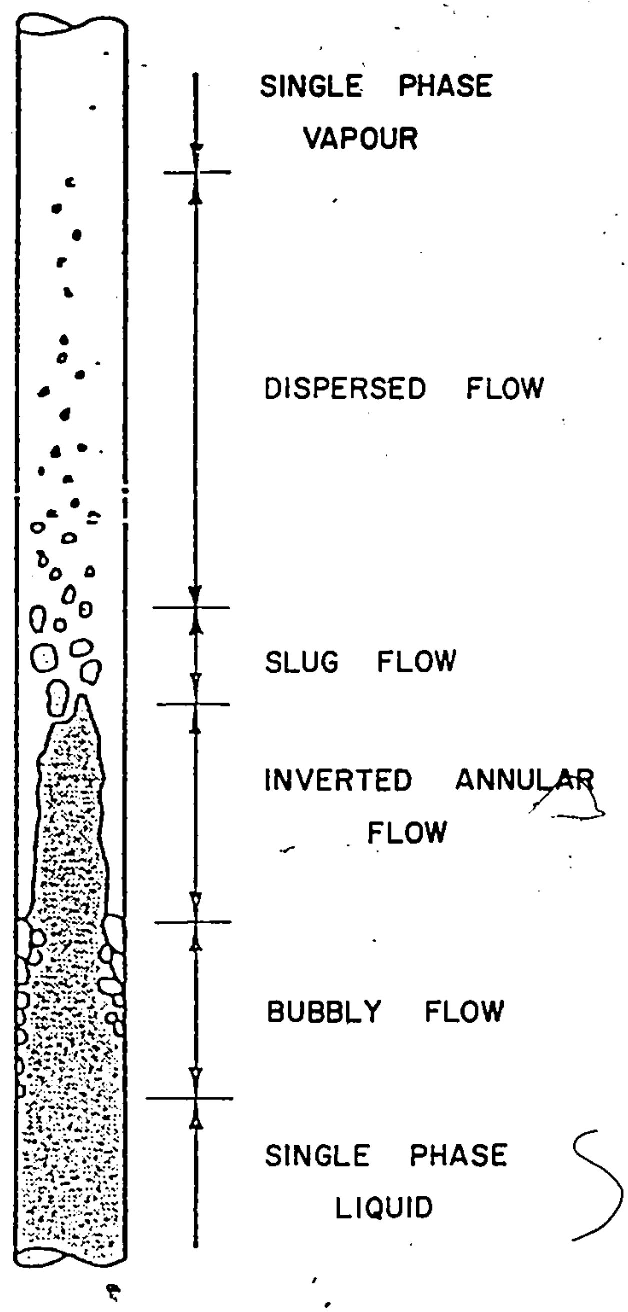

FIG. 2.2 FLOW REGIMES IN A DIRECTLY HEATED TUBE

2.2.3 Inverted annular flow

This flow regime occurs at the upstream of the test section. The vapour is generated and forms a vapour blanket over the entire heated wall surface; hence, the vapour film separates a continuous liquid core in the center of the tube from the heated surface.

The vapour-liquid interface is irregular. These irregularites occur at random locations, but appear to retain their identity to some degree as they pass up the tube with velocities of the same order as that of the liquid core. The vapour in the film adjacent to the heating surface would appear to travel at a higher velocity. Vapour bubbles may be present in the liquid core, but will have little influence except to modify the core velocity and density.

Inverted annular film boiling typically involves heat transfer from the hot wall to the vapour blanket and subsequently from the vapour to the liquid core. Some heat will also be transferred directly from the wall to the liquid core by radiation. Heat transfer across the vapour-liquid interface takes place by conduction followed by forced convection evaporation once the initially subcooled liquid core reaches the saturation temperature [3].

Theoretical models of the inverted annular film boiling regime always neglect the boiling process and vapour generation at the quench front. Recent photographic study of inverted annular film boiling in a quartz tube [4] has indicated the existence of two distinct regions of inverted annular film boiling. The first region occurs immediately above the quench front and is characterized by a smooth vapour film of constant thickness separating the bulk liquid phase from the hot wall. The vapour layer thickness in that region depends on the flow velocity and subcooling. The second region taking place further downstream, a wavy and unstable vapour-liquid interface is observed.

2.2.4 Slug flow

The slug flow is usually encountered at lower mass flows. It is formed just downstream of the inverted annular flow region when the liquid core breaks up into slugs of liquid.

Some theories for the onset of slug flow have been proposed. Chi [5] suggested that the liquid core breaks up into slugs which are equal in length to the most unstable wavelength of interfacial waves. Subcooling tends to stabilize the liquid-vapour interface, and thus inhibits the formation of slug flow. Kalinin et al. [6] observed that immediately after the introduction of liquid to their test section, the sudden increase in vapour volume, due to vapour generation at the leading edge of the liquid, caused a back pressure which decelerated the flow. The higher pressure and the lower flow rate caused a decrease in vapourization, after which, the higher pressure would cause the flow to surge forward. This cycle was repetitive, with a liquid slug separating from the liquid core with each cycle [7].

2.2.5 Dispersed flow

Dispersed flow sometimes happens at the downstream of the test section, especially at the low flow rate and small degree of subcooling. In this flow regime, the liquid is present as droplets entrained in the vapour. The wall may be cooled both by convection to vapour and by the droplets entering the vapour boundary layer and possible contacting the wall. It is assumed that when the dispersed phase is finely dispersed, the two phase flow can be assumed to be a homogeneous mixture [1].

2.2.6 Single phase vapour

Here all droplets have evaporated and the single phase forced convective heat transfer applies again.

2.3 FLOW PATTERN MAP FOR VERTICAL FLOW

Figure 2.3 shows a flow pattern map [8] obtained from observations on low-pressure air-water and high-pressure steam-water flow in small diameter vertical tubes. The axes represent the superficial momentum fluxes of the liquid ($\rho_f j_f^2$) and vapour ($\rho_g j_g^2$) phase, respectively. These superficial momentum fluxes can also be expressed in terms of the mass velocity (G) and the vapour quality (X):

$$\rho_f j_f^2 = \frac{[G(1-X)]^2}{\rho_f} \tag{2.1}$$

$$\rho_g j_g^2 = \frac{(GX)^2}{\rho_g} \tag{2.2}$$

This map must be regarded as no more than a rough guide. It is clear that the momentum fluxes alone are not adequate to represent the influence of fluid physical properties or the channel diameter [9].

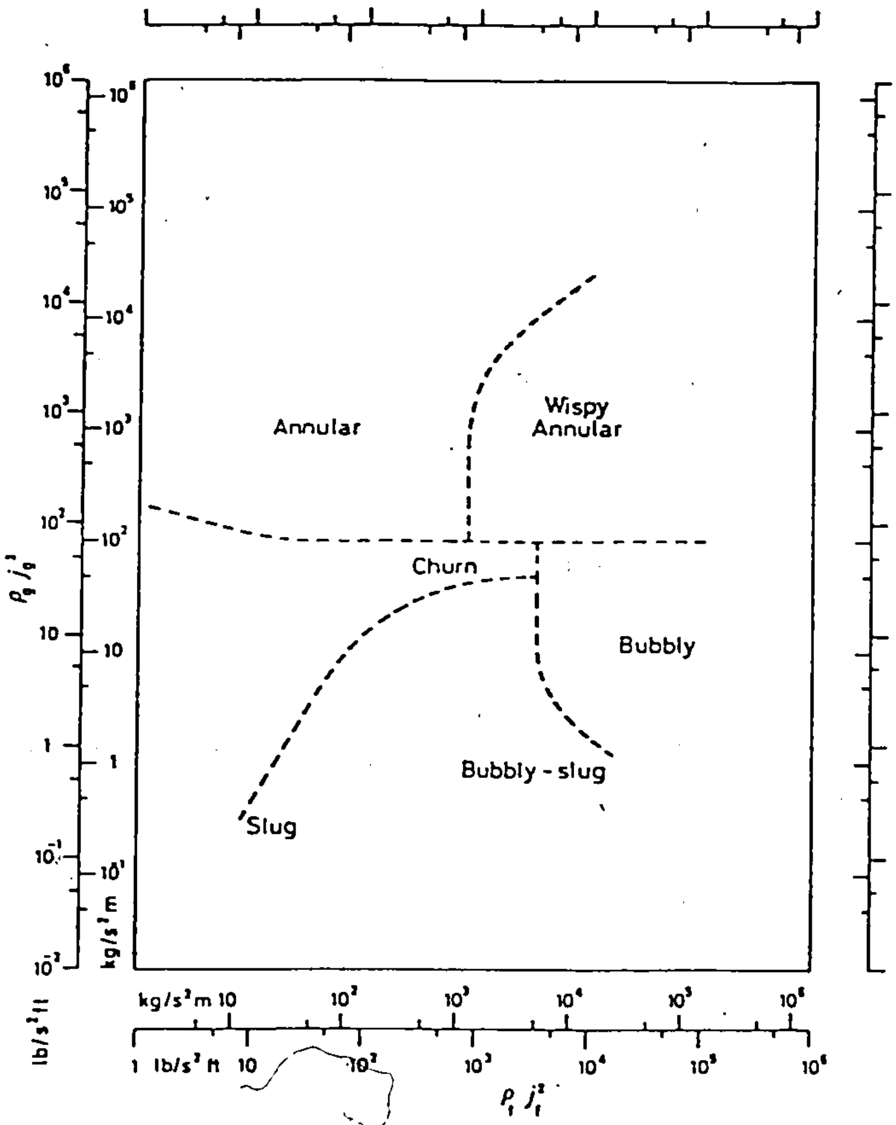

FIG. 2.3 FLOW PATTERN MAP FOR VERTICAL FLOW (HEWITT AND ROBERTS [8])

2.4 REWETTING MECHANISMS

In pool boiling, two principal mechanisms have been proposed for the rewetting, the hydrodynamic mechanism and the thermodynamic mechanism.

2.4.1 Hydrodynamic mechanism

The separation of the liquid-vapour interface from the wall can be maintained only as long as the vapour generation rate exceeds the vapour removal rate, i.e., vapour forces balance out liquid forces. If the fluid properties or the heated surface is changed to affect this vapour generation stability, then the vapour layer may collapse; hence rewet.

Using the concept of Taylor Instability, Berenson [10] assumed that the Leidenfrost temperature would occur where vapour-liquid interface oscillations become unstable due to force imbalance. Such imbalance occurs when bubble spacing at the interface has reached the critical wavelength for which the amplitude of the disturbances (bubbles) grows most rapidly. Physically, the vapour-liquid interface is wavy, bubbles are released to the liquid at regular intervals, and liquid spikes form between the released bubbles sometimes wetting the heated surface.

2.4.2 Thermodynamic mechanism

It is assumed that the liquid can never exist beyond a "maximun liquid temperature", which depends only on the liquid properties and hence is a unique function of pressure. Thus, a heated surface whose temperature is beyond the "maximum liquid temperature" cannot support liquid contact [11].

2.5 TYPES OF REWETTING

2.5.1 Forced convection rewet

Iloeje et al. [12] isolated three different controlling mechanisms for forced convective rewet. These are: impulse cooling collapse, axial conduction controlled rewet and dispersed flow rewet. Groeneveld [11] presents various types of rewetting as shown in Fig. 2.4. This figure includes the three controlling mechanisms mentioned above.

2.5.1.1 Impulse cooling collapse

At the wall temperature higher than the rewetting temperature in the inverted-annular vapour film boiling regime, the liquid-vapour interface is wavy and it fluctuates about a mean position. If the wall temperature or heat flux is lowered, the vapour thickness decreases and eventually the liquid may contact the wall. Depending on the temperature level and the rate of heat supply to the cooled region of material beneath the liquid, permanent liquid-wall contact is either maintained or the liquid is pushed away from the surface with the formation of vapour. In the latter case, each contact is equivalent to an impulsive cooling of the surface. In a quenching process, repeated contacts will lower the surface temperature enough to permit rewet. Type 1 of Fig. 2.4 shows the configuration of collapse of vapour film.

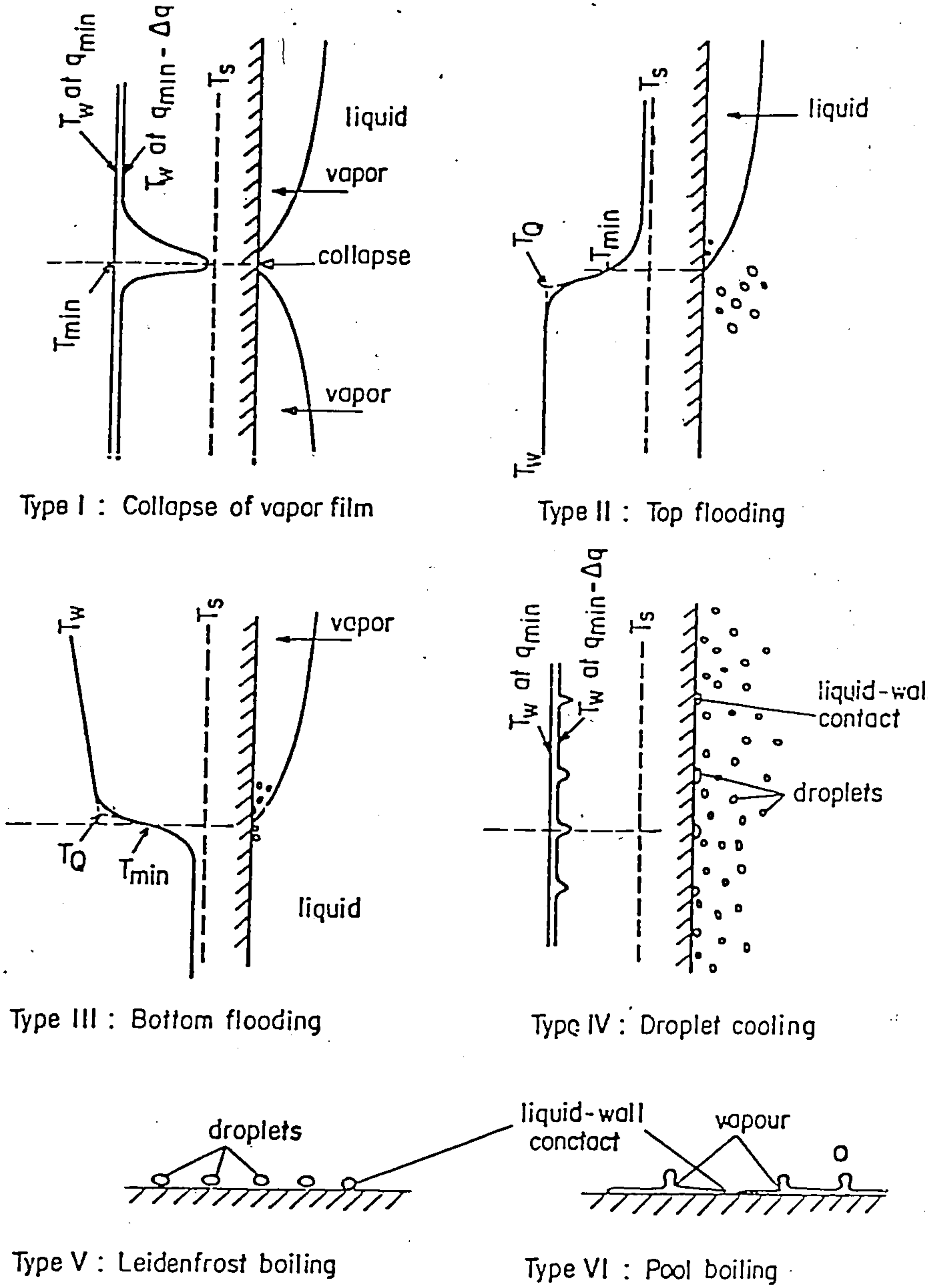

FIG. 2.4 TYPES OF REWETTING (GROENEVELD [11])

There is one model proposed by Kalinin et al. [13], in which a conduction analysis is performed to obtain the temperature of beginning and ending of the film boiling crisis (i.e., the collapse of vapour film). The wall temperature corresponding to the minimum heat flux in forced convective flow can be obtained from their empirical correlation:

$$\frac{T_{min}-T_{sat}}{T_{crit}-T_{liq}} = 1.65\left\{0.1+0.6\,\frac{(\rho ck)_l}{(\rho ck)_w}+1.5\left[\frac{(\rho ck)_l}{(\rho ck)_w}\right]^{\frac{1}{2}}\right\} \tag{2.3}$$

However this model seems to be incomplete because the hydrodynamic parameter of the flow rate is completely absent.

Recently, the impulse cooling collapse type of rewetting has been studied by Groeneveld [11], Cheng et al. [14] [15] and Stewart [16]. Correlations for the true quench temperature of this type of rewetting have also been proposed by Cheng and Stewart.

2.5.1.2 Axial conduction controlled rewet

In a system with an already wetted upstream surface, i.e., the type 2 and 3 configurations of Fig. 2.4, Simon and Simoneau [17] suggested that the transition from film boiling to nucleate boiling in an electrically heated system appears to be governed by axial conduction as shown in Fig. 2.5. Wall conduction transfers the heat from the film boiling side to the nucleate boiling side and causes the surface temperature to drop as a function of time. Transition from film boiling to nucleate boiling occurs when the wall temperature at each position along the heating surface reaches the wetting temperature. Furthermore, Simon and Simoneau also mentioned that the value of the wetting temperature corresponds to the maximum superheat of a fluid and this condition is determined by using the Van der Waals equation of state.

The theoretical equation of Spieglar et al. [18] to be used for the determination of the wetting temperature difference as a function of pressure is as follows:

$$\frac{T_{wet}}{T_c} = 0.13 \frac{P}{P_c} + 0.84 \tag{2.4}$$

The above equation implies that the rewetting temperature is determined by the thermodynamic properties of the boiling fluid.

2.5.1.3 Dispersed flow rewet

In the dispersed flow regime, Iloeje et al. [12] postulated that transition is controlled by the limiting effects of two processes; namely, heat transfer to the vapour assuming no effect of the existence of droplets, and

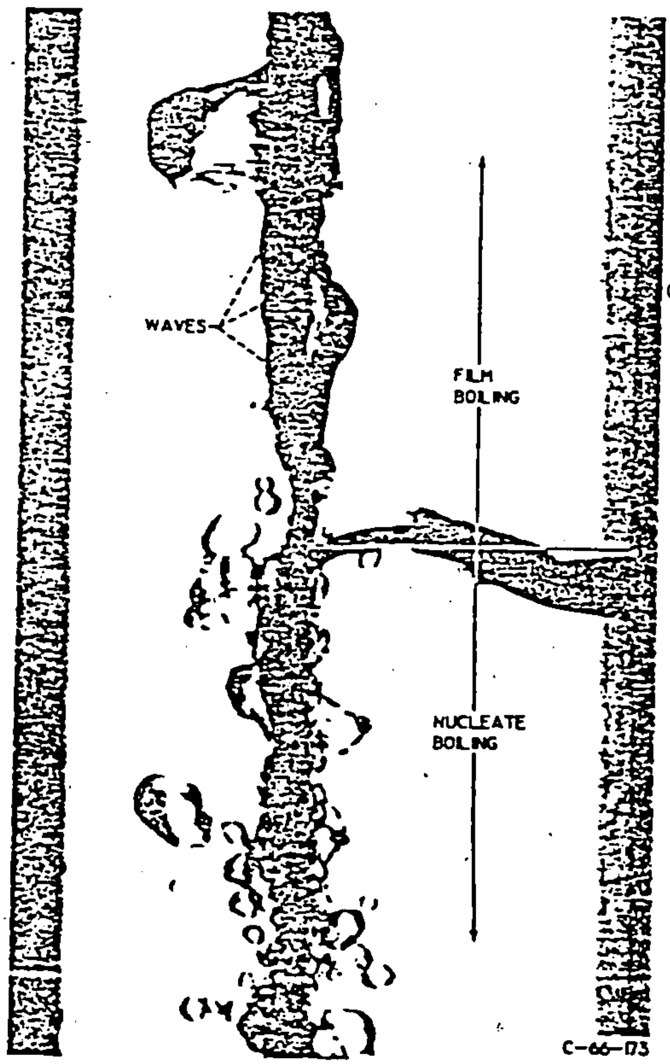

Nucleate transition region in vicinity of transition heat flux (upward flow). Velocity, 0.27 m/sec; heat flux, 6.9×10^4 w/m^2.

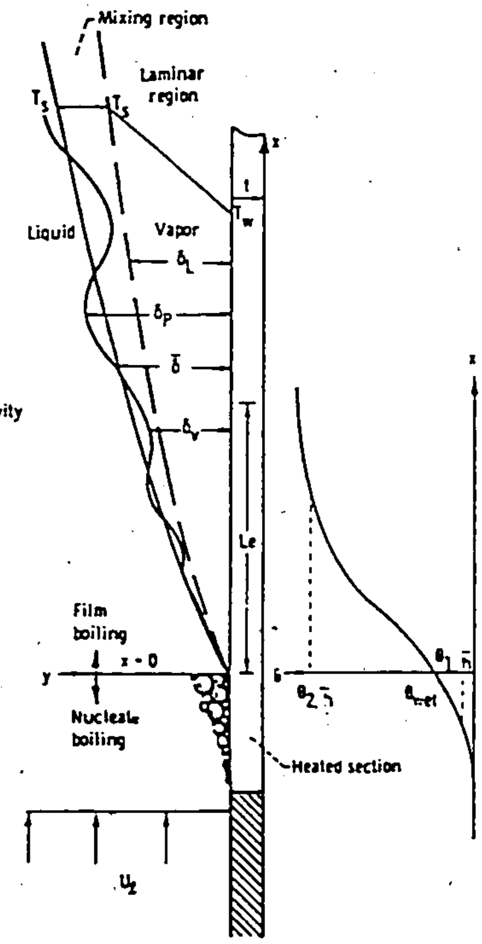

Film boiling model.

FIG. 2.5 AXIAL CONDUCTION CONTROLLED REWET (SIMON AND SIMONEAU [17]) heat transfer due to the presence of the droplets, which may or may not be touching the surface.

The sum of the two heat transfer components gives the total heat flux and indicates the location of the minimum heat flux and ΔT_{min}. Fig. 2.6 shows the change of each component with wall temperature.

Note that this type of minimum film boiling is characterized by the absence of a propagating rewetting front. It is thus similar to the type 1 (Fig. 2.4) film boiling configuration, except that the liquid phase is dispersed in the vapour instead of being continuous [11].

2.5.2 Free convection rewet

2.5.2.1 Leidenfrost cooling

The type 5 in Fig. 2.4 illustrates the heat transfer configuration of Leidenfrost cooling [11]. The heated surface is cooled by stationary discrete droplets separated from the heated surface by a vapour film. A reduction in the heated surface temperature will lead to an insufficient vapour generation rate to maintain droplet-wall separation and eventually wet the heated surface. The temperature corresponding to the first contact of the droplets with the wall is usually referred to as the Leidenfrost temperature.

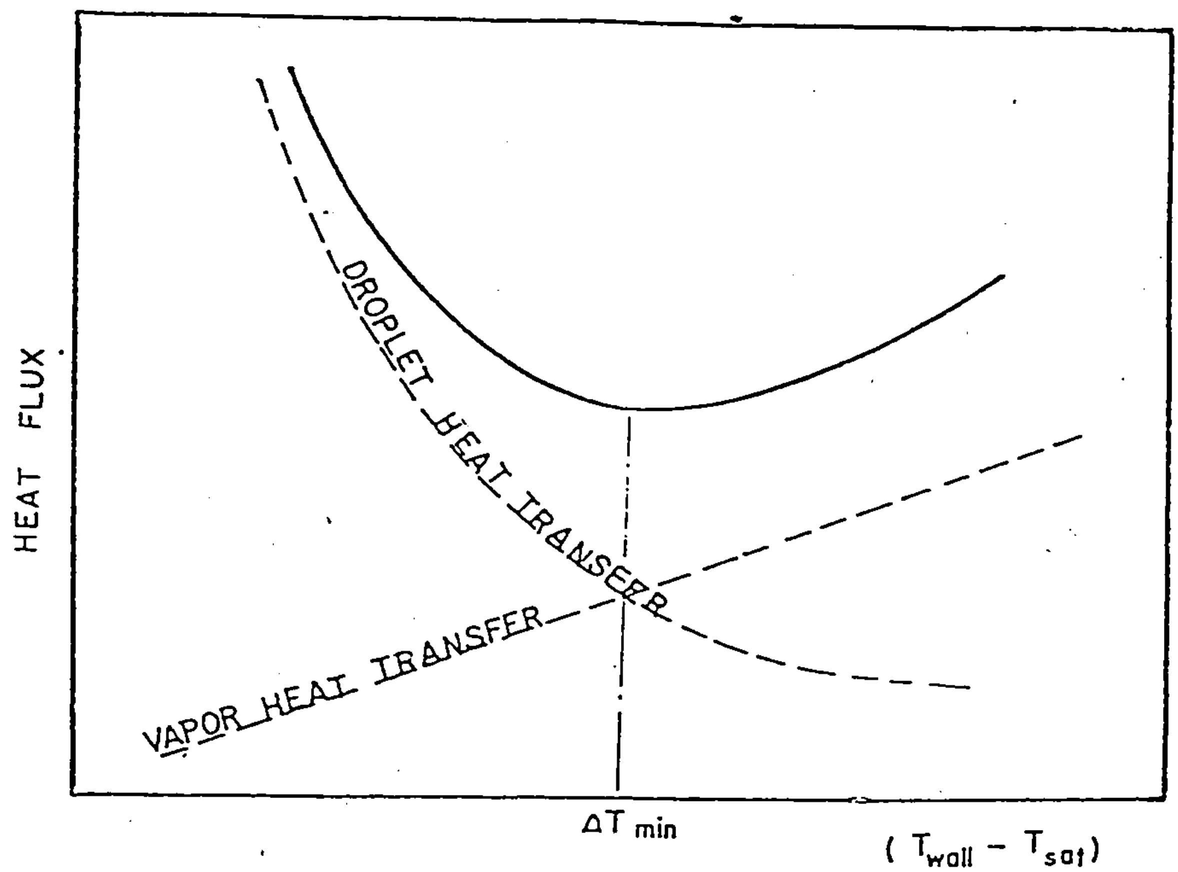

FIG. 2.6 DISPERSED FLOW REWET (ILOEJE, ET AL [12])

2.5.2.2 Collapse of vapour film during pool boiling

Pool film boiling is a stable vapour film covering the entire heating surface. The vapour is released from the film periodically in the form of regularly spaced bubbles. Heat transfer is accomplished principally by conduction and convection through the vapour film. The collapse of vapour film is due to the vapour generation rate becoming smaller than the vapour removal rate. The corresponding temperature and heat flux may be predicted theoretically from the Taylor's instability theory [19].

2.6 PARAMETRIC EFFECTS

In the literature, most of the earlier work on forced convection quench temperature experiments measured the apparent quench temperature. Here, the apparent quench temperature refers to the quench temperature with the influence of axial conduction. The following paragraphs will discuss the effects of various system parameters on the apparent quench temperature.

2.6.1 Mass flux

In Plummer et al. [20] forced convection experiments, they clearly indicated that the quench temperature increases with mass flux as shown in Fig. 2.7. In Fig. 2.8, Cheng et al. [21] while studying the transition boiling phenomenon under forced convective conditions, also found that q_{min} and T_{min} increase for increasing mass flux.

The above observations appear reasonable, since at high mass flux there would be more violent mixing, reduced superheating of the vapour and increasing momentum of the droplets. Consequently, the chances of impingement would be greater for higher flow; thus, quench would occur at a higher wall temperature [22].

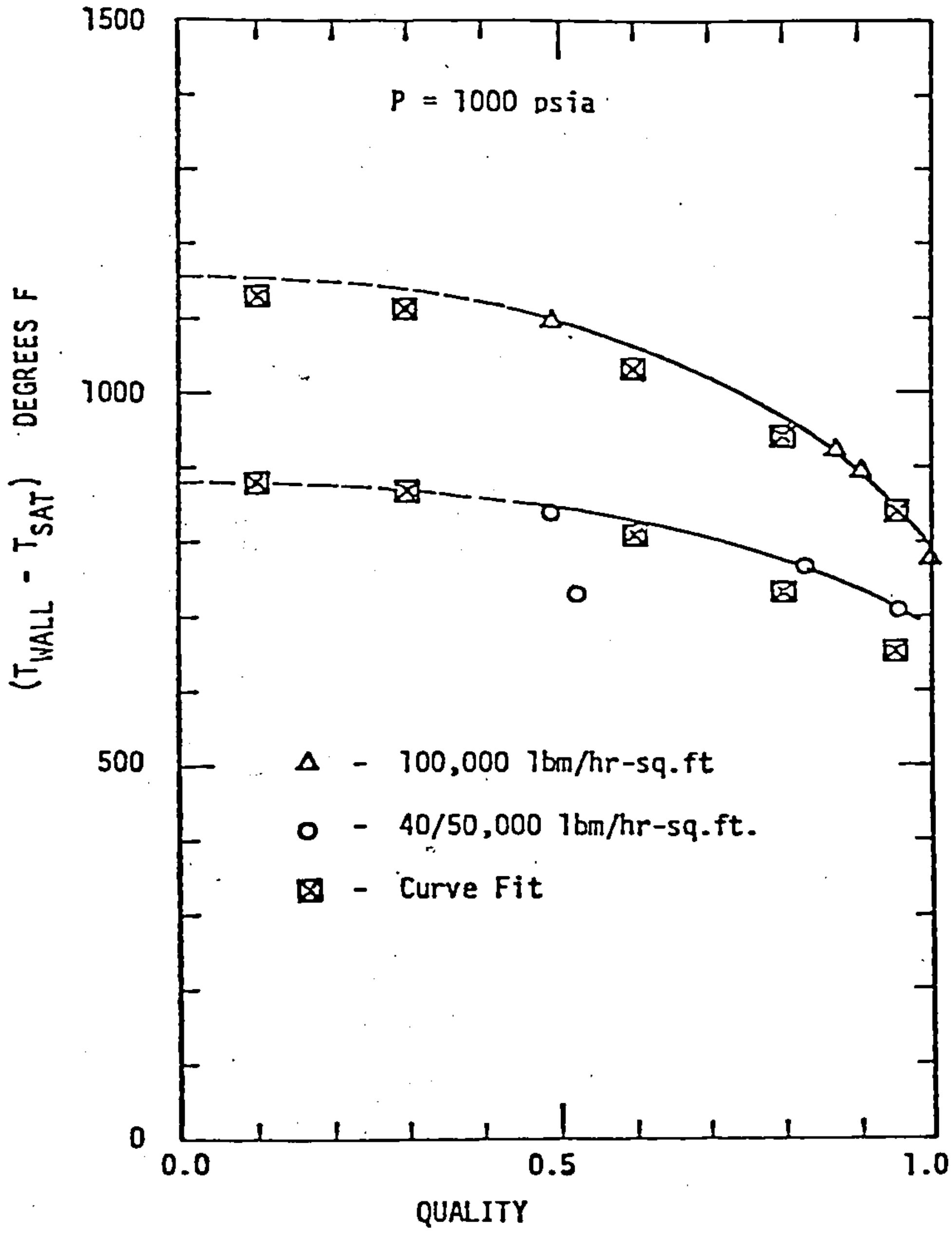

FIG. 2.7 FILM BOILING MINIMUM ΔT_w VS EQUILIBRIUM QUALITY - EFFECT OF MASS FLUX (PLUMMER, ET AL [20])

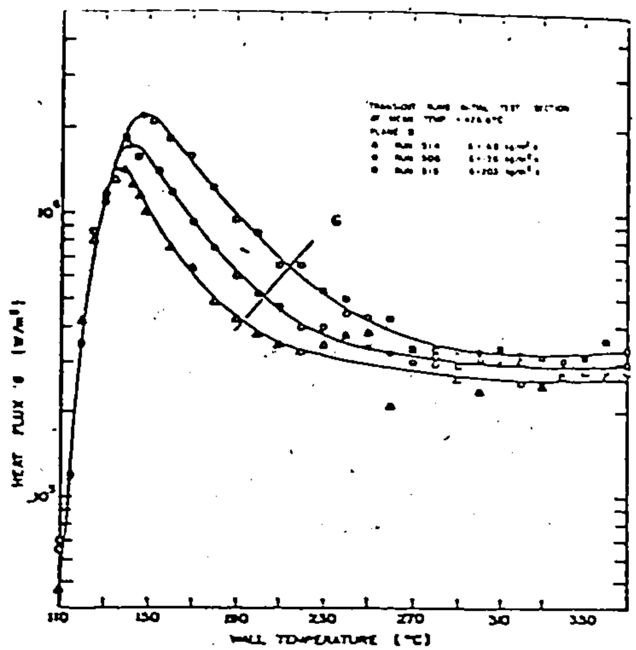

FIG. 2.8 EFFECT OF MASS FLUX ON BOILING CURVE OF DISTILLED WATER FOR ΔT_{SUB} = 0°C (CHENG, ET AL [21])

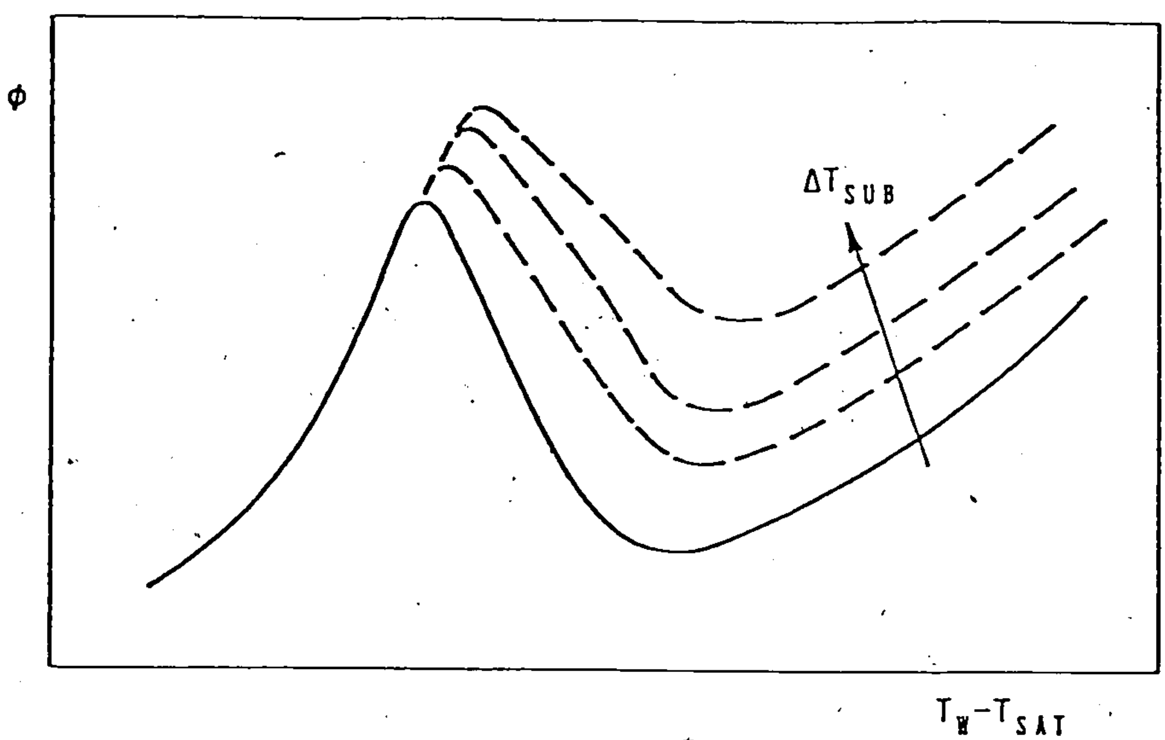

FIG. 2.9 EFFECT OF SUBCOOLING ON BOILING CURVE (GROENEVELD, ET AL [23])

2.6.2 Subcooling

All experimental studies indicate that T_{min} or T_Q increases with an increase in subcooling as shown in Fig. 2.9 [23] and Fig. 2.10 [11]. The effect of higher subcooling is similar to that of higher mass flux. Therefore, it is expected that quench would occur at a higher wall temperature.

2.6.3 Pressure

In the literature, it has been found that the T_Q increases with increasing pressure. One possible explanation may be stated as follows: the vapour forces necessary to overcome the liquid forces at higher pressure would be greater than at normal pressure. Since the pressure generation is due to heat energy, the higher temperature would be required to maintain the vapour-liquid interface [22]. However, Groeneveld observed a reverse trend when pressure is above 4MPa [11].

2.6.4 Quality

The effect of this parameter is still not well understood. In Fig. 2.11, Plummer et al. [20] found that the quench temperature increases with a decrease in quality, while in Steward and Groeneveld's [24] minimum film boiling

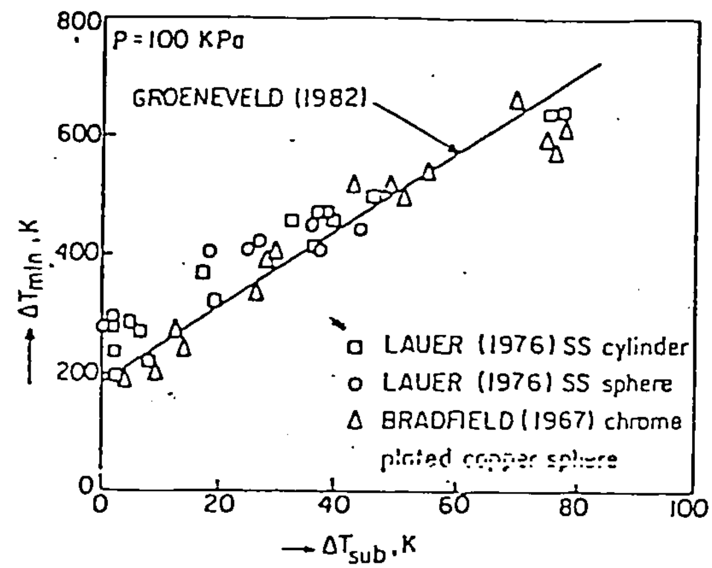

FIG. 2.10 EFFECT OF SUBCOOLING ON ΔT_{MIN} (GROENEVELD [11])

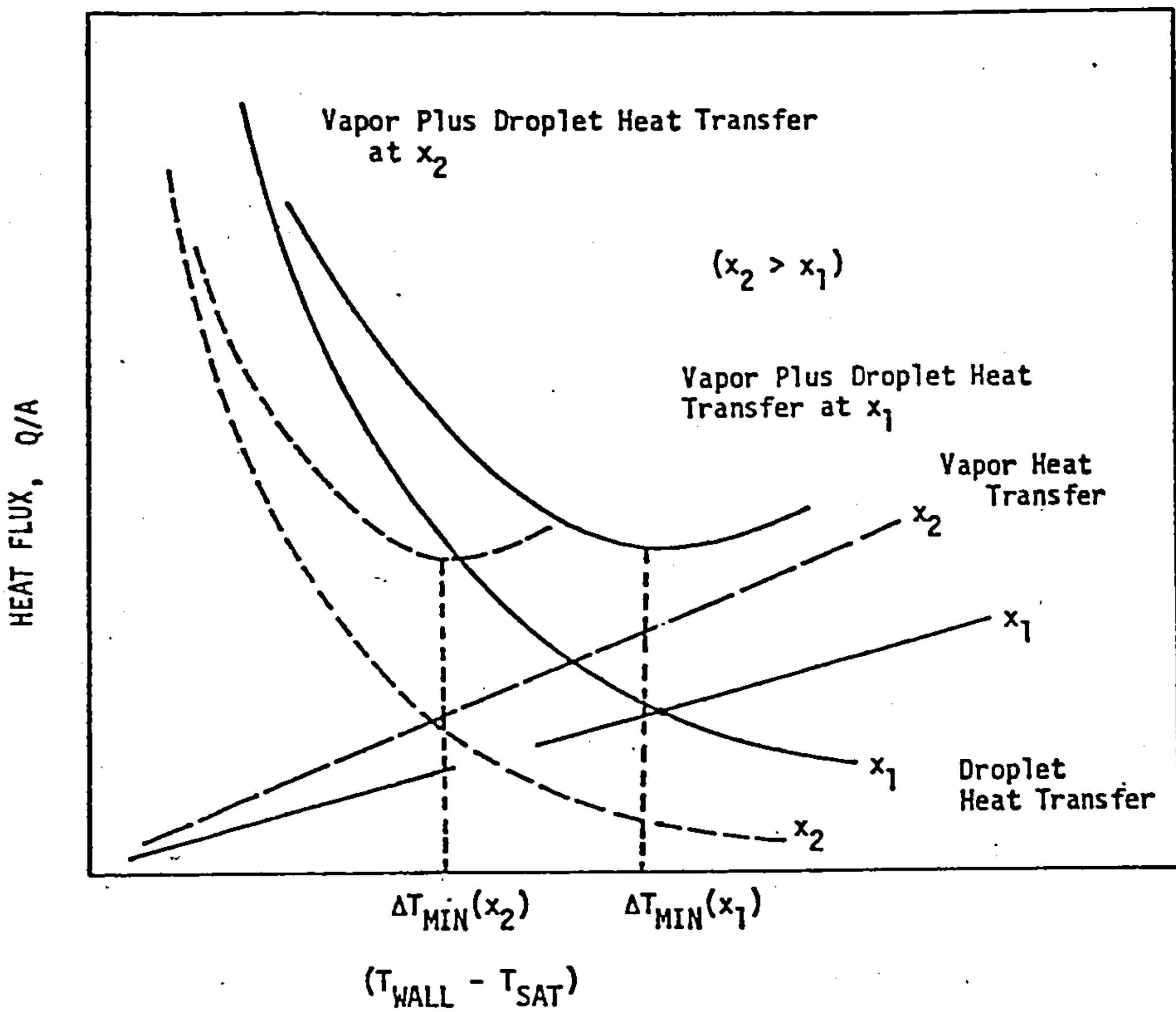

FIG. 2.11 EFFECT OF QUALITY ON ΔT_{MIN} (PLUMMER, ET AL [20])

temperature study, a quality range up to 13% is covered and shows no significant effect of quality on T_{min}.

2.6.5 Thermal properties of heated surface

Ragheb et al. [25] presented the effects of $k\rho c_p$ on boiling curves during their transition boiling experiments. Figure 2.12 shows rewetting occurs at lower wall superheat for heated surfaces having a higher value of $k\rho c_p$. Notice that the copper surface has the highest value of $k\rho c_p$; thus, it quenchs at the lowest wall temperature.

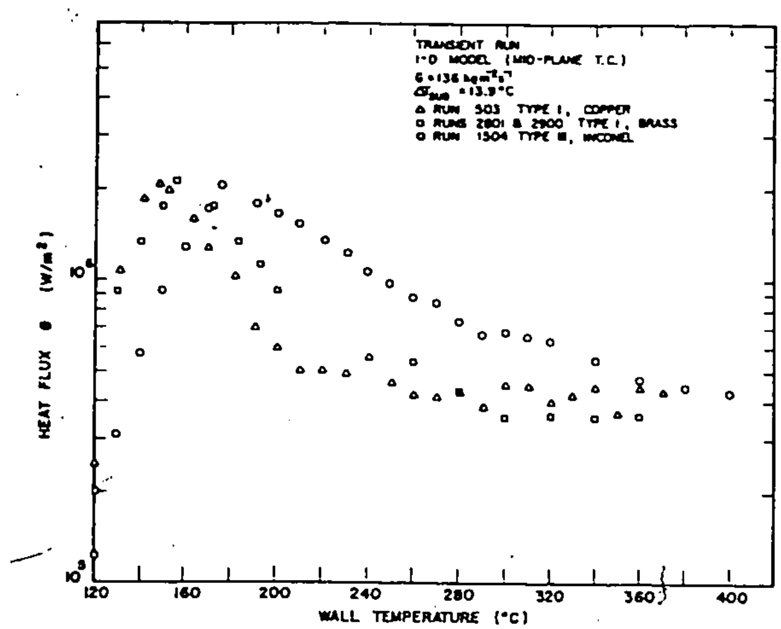

FIG. 2.12 COMPARSION OF BOILING CURVES OBTAINED FROM DIFFERENT HEATED SURFACE TEST SECTIONS - EFFECT OF HEATED SURFACE PROPERTIES (RAGHEB, ET AL [25])

Chapter III
EXPERIMENTAL DESIGN

There are two different experimental flow loops for the experiment. One is an open loop for the atmospheric pressure true quench temperature measurements, and the other is a closed pressurized loop capable of producing 101 kPa (14.7 psia) to 687 kPa (100 psia) pressure range. Both experimental loops and procedures will be described in the following sections.

3.1 OPEN LOOP FACILITIES

3.1.1 General

A schematic flow diagram of the open loop is shown in Fig. 3.1. It consists mainly of a hot water storage tank, pump, flow meter, preheater, test section and the associated valves and piping.

Provisions of two by-pass loops were incorporated, namely, the pump by-pass and the test section assembly by-pass. These provisions were added to the system to stabilize the flow and promote ease of flow adjustment.

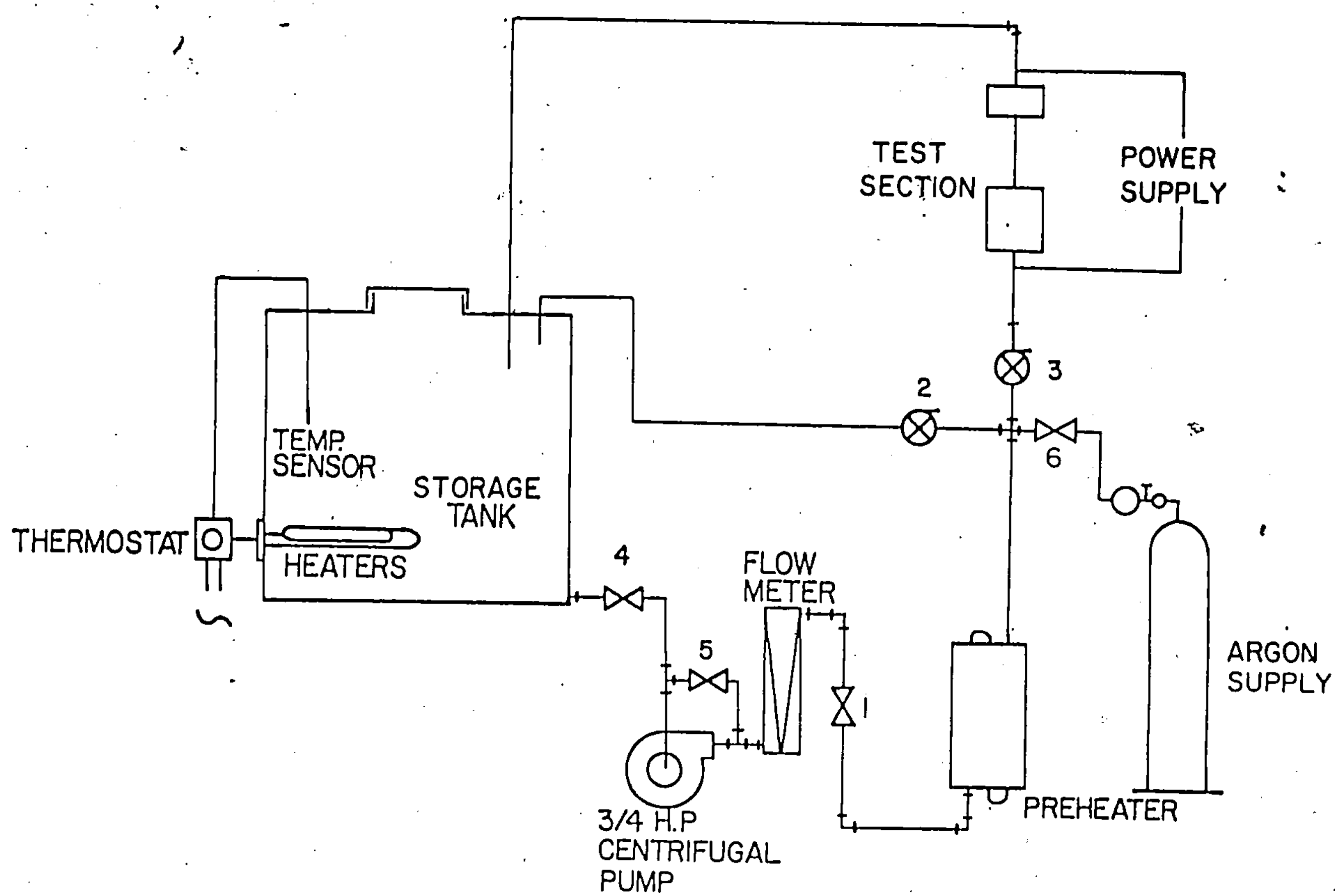

FIG. 3.1 SCHEMATIC DIAGRAM OF THE EXPERIMENTAL LOOP FOR ATMOSPHERIC PRESSURE

Water was circulated by a 3/4 hp centrifugal pump. The flow rate was measured by a rotameter (series 20-4000, S&K instruments) and the flow adjustment was done via the regulatory needle valve 1. Valves 2 and 3 are an ON-OFF type which operate out of phase, i.e., one open and the other closed or vice-versa.

3.1.2 Storage tank

The hot water storage tank was made of 12 gauge aluminum plate with dimensions of 0.46m X 1.00m X 0.80m. It had a capacity of about 50 gallons of distilled water. Styrofoam of 3.8cm thickness was utilized to insulate the entire tank. The tank was powered by three immersion heaters of 3 kW rating each. The heaters draw current via a thermostat which could be adjusted to the desired operating temperature.

3.1.3 Preheater

A 10 cm O.D. and 30 cm long copper block was used as the preheater. Twelve 10.16 cm (4 in.) cartridge heaters of 250 W each were inserted in the copper block, with six heaters at each end. Water ran through a triple bend passage within the preheater. A proportional temperature controller (model R 7355, Honeywell) was employed to control the preheater temperature which was adjusted according to the desired inlet temperature of the test conditions.

3.1.4 Test section assembly

A typical test section is shown schematically in Fig. 3.2. The test section itself was made of Inconel. For the atmospheric test runs, the tube sizes of 1.27 cm - 1.31 cm O.D. and 0.04 cm - 0.084 cm wall thickness were used, whereas for the pressurized test runs, only one tube size of 1.31 cm O.D. and 0.104 cm wall thickness was used.

To anchor quench fronts originating from both ends of the test section, two different sizes of copper hot patches were in use, i.e., the bottom hot patch (BHP) and top hot patch (THP).

The bottom hot patch, as shown in Fig. 3.3, is a cylindrical copper block of 10.16 cm long and 9.53 cm O.D. Eight cartridge heaters of 0.95 cm (3/8 in.) diameter and 10.16 cm (4 in.) in length with 500 W each were tight-fitted in equal space within the hot patch. Two thermocouples (T.C.1 and T.C.2) were mounted in holes drilled through the hot patch. T.C.1 was located at the interface of hot patch and Inconel tube, and T.C.2 was located at the halfway point between the T.C.1 and the outermost hot patch surface. Both were located at the mid-plane. The T.C.2 was connected to

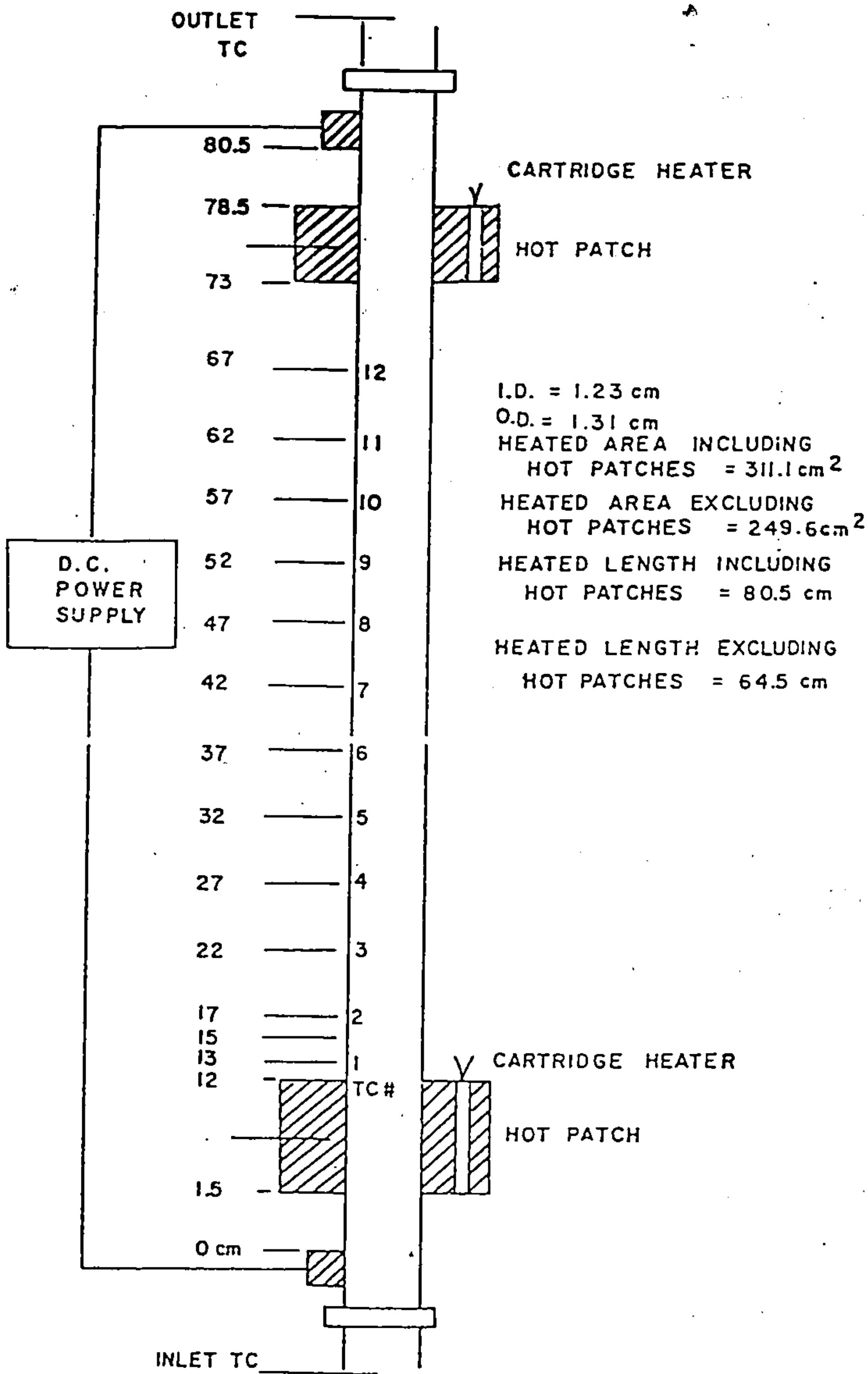

FIG. 3.2 SCHEMATIC DIAGRAM OF THE TEST SECTION

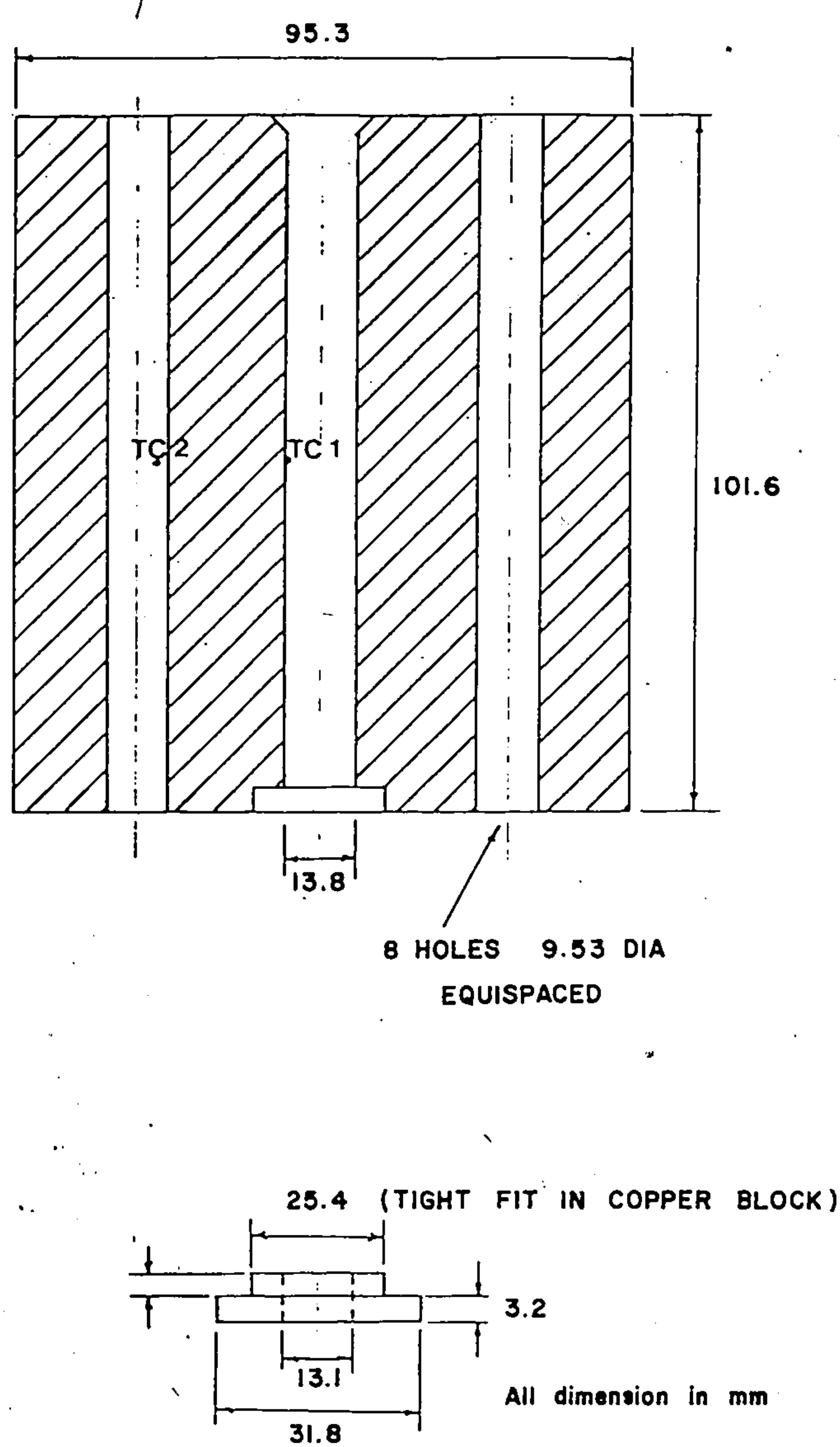

FIG. 3.3 SCHEMATIC DIAGRAM OF THE BOTTOM HOT PATCH

the ON-OFF type temperature controller (model R 7353, 0-1100°C range, Honeywell) for controlling the temperature of the hot patch. The T.C.1 was used to determine the film boiling curve of the hot patch during a separate cooldown test of the hot patch.

A stainless steel ring was brazed onto the test tube to support the copper patch, before the copper patch was soldered to the Inconel tube. The copper patch was soldered in an argon-filled container in order to minimize the oxidation during the process. The normal operating temperature for the BHP was 700°C, thus, high temperature silver solder (melting point at 780°C) was used. An improper soldering process may cause the failure of the performance of the BHP. For instance, if the gap between the central core of the hot patch and the outside surface of the tube is not completely filled with solder, then BHP may not function properly because some spots inside the patch will be rewetted first and the quench front would propagate downstream to the test section. Therefore, extra caution is required in the soldering process.

The top hot patch is relatively short and has the dimensions of 5.72 cm height and 9.53 cm O.D. Eight cartridge heaters of 0.64 cm (1/4 in.) diameter and 5.08 cm (2 in.) in length with 250 W rating each were also fitted into the patch. One thermocouple was mounted in a hole drilled halfway through at the mid-plane of the hot patch. It was also connected to a ON-OFF type temperature controller (model R7353, 0-650°C range, Honeywell) to control the temperature of the hot patch. The operating temperature for the THP was 500°C, 45%-silver silver solder (melting point at 660°C) was used in the soldering process.

About a dozen chromel-alumel thermocouples were spot welded onto the exterior of the tubing at various axial locations as shown in Fig. 3.2. The entire test section assembly was insulated by high temperature ceramic fibre glass to reduce heat losses.

Selected test section thermocouple signals were displayed in a Hewlett Packard 2-channel chart recorder (model 7100B), and a Gould 4-channel chart recorder (model 2400). A sample temperature-time trace is shown in Fig. 3.4.

Due to the small tube wall thickness, the temperature difference between the outside surface wall temperature and the inside surface wall temperature of the test section is negligibly small. Therefore, in the present study, the inside surface wall temperature can be readily replaced by the outside surface wall temperature.

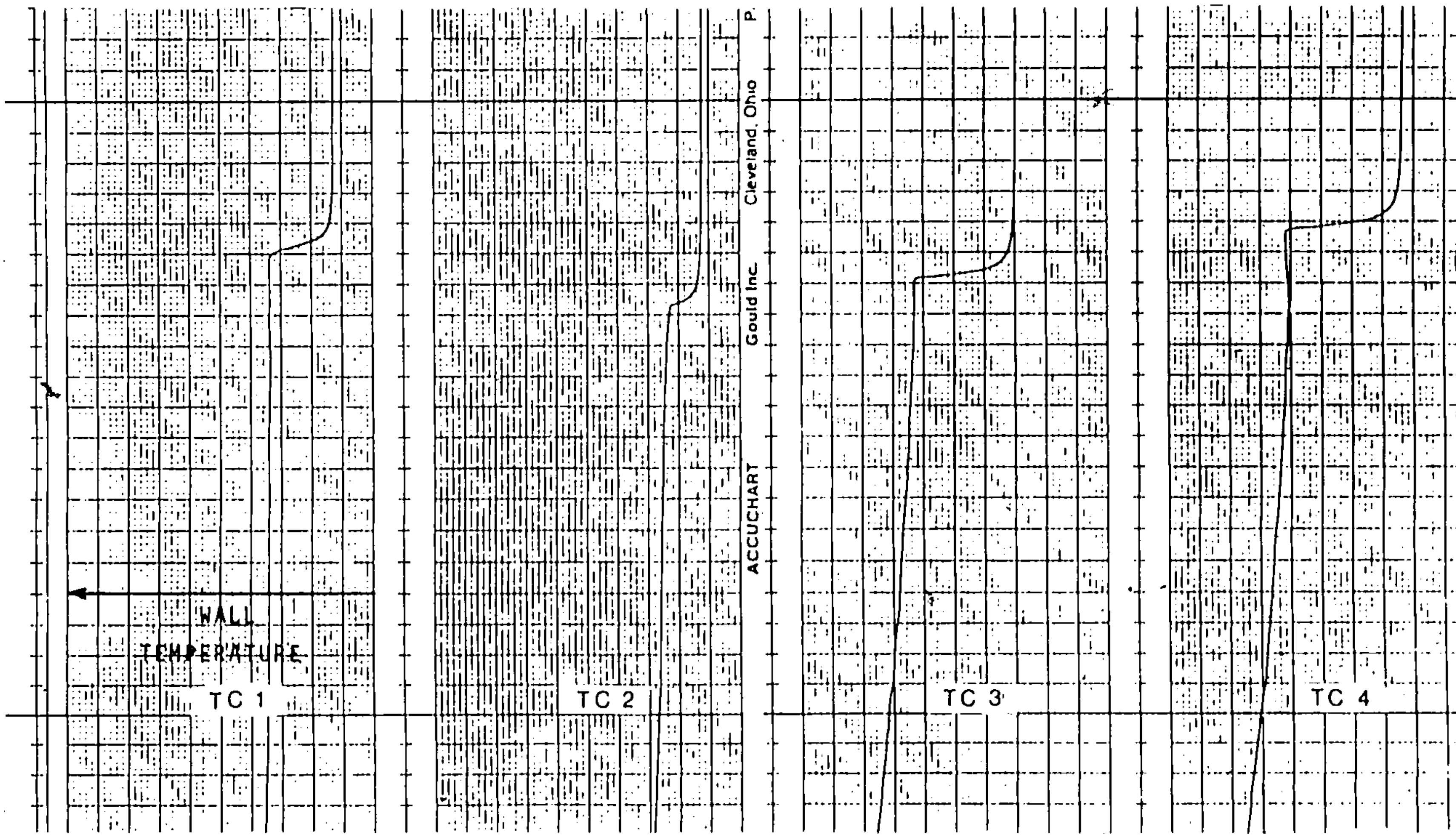

(the sudden drop of the temperature indicate the occurence of rewet)

FIG. 3.4 TYPICAL TEMPERATURE-TIME TRACE OF TEST SECTION THERMOCOUPLES DURING TEST

3.1.5 Test section power supply

A Miller direct current arc welder (model SR-600, serial no. 70-552310) was employed as the test section direct power supply. This machine has a maximum voltage of 40 volts and a maximum current of 600 amperes. The D.C. power machine is chosen because of its steadiness and low voltage operation.

Finally, Pirelli welding cable of 500-ampere capability was used to transmit power between the power supply and the test section.

3.1.6 Open loop procedure

1. Water in the storage tank was first heated to slightly below the desired test inlet temperature by the immersion heaters which were thermostatically controlled.
2. The top and bottom hot patches were then heated to the desired temperatures.
3. The pump was turned on and the flow was first passed through the regulating valve 1, then through the ON-OFF valve 2 (valve 3 closed) and drained back to the storage tank via the test section by-pass loop.
4. The preheater was used to raise the water temperature to the desired test inlet value.
5. The Inconel tube was heated to about 700°C by the Miller Welders power supply with direct heating.
6. The ON-OFF valve 2 was closed and the ON-OFF valve 3 opened to divert the flow into the test section.
7. Starting from the tube temperature of 700°C, the power was reduced stepwise by approximately 5% each time. Sufficient time was allowed for the flow to stabilize between steps. The process was repeated until the first detection of true quench by thermocouples through chart recorders. The test was terminated when the tube started to rewet.

8. For tests at high mass fluxes, sometimes it was necessary to start with a lower mass flux in order to prevent the test section from being quenched when the flow first reached it. The mass flux and the heat flux were then gradually increased to reach the desired flow rate.
9. After each test run, argon gas was circulated through the Inconel tube to purge the residue liquid and to prevent oxidation at high heated surface temperature during the subsequent run.

3.2 CLOSED LOOP FACILITIES

3.2.1 General

The pressurized loop, as shown in Fig. 3.5, consists primarily of a 5-gallon surge tank, 50-gallon hot water storage tank, pump, flow meter, preheater, test section and the associated valves and piping.

Provisions of by-passing the pump and the test section were incorporated to stabilize the flow. The flow was circulated by a 1/4 hp pump (serial no. 167146, Franklin Electric), the flow rate was measured by a rotameter (model 3604 B08C2K1A from Brooks Instrument, with 400 K and 1500 psig limit), and the flow adjustment was done via the regulatory needle valve 1. Valves 2 and 3 are ON-OFF type which operate out-of-phase.

The system was pressurized by argon gas through the regulating valve 4, and the surge tank was used to moderate pressure variation. A solenoid vent valve was used to release the excess pressure during experiments. The system pressure value can be obtained from a pressure transducer (model BKF-1, Bofors Instrument) and a voltmeter.

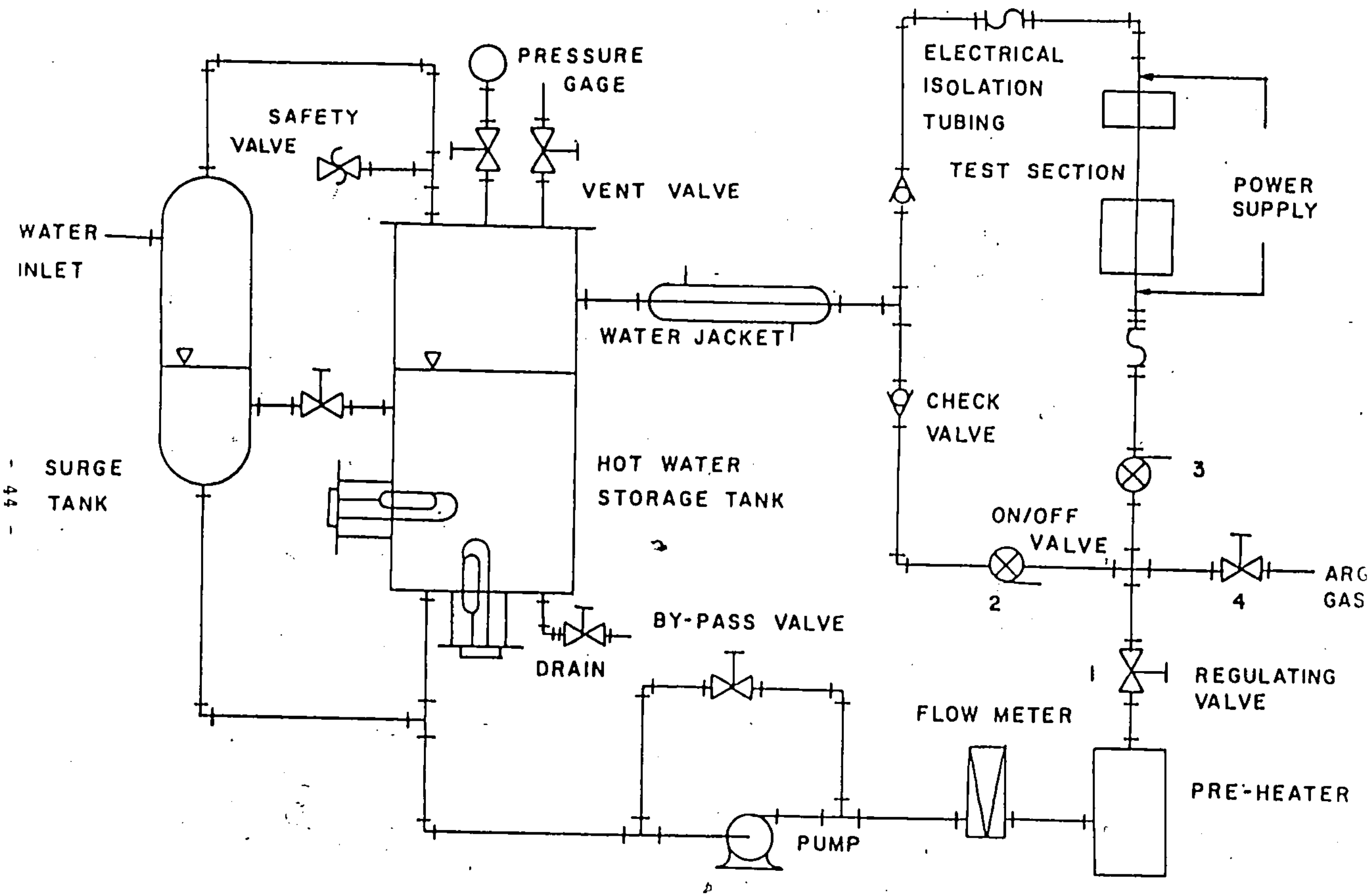

FIG. 3.5 SCHEMATIC DIAGRAM OF THE PRESSURIZED EXPERIMENTAL LOOP

3.2.2 Storage tank

The water storage tank was made of a heavy gauge stainless steel cylinder with two round steel plates welded at both ends. Its dimensions are 0.46m O.D. and 1.68m high with a capacity of about 50 gallons of distilled water. The tank was powered by two immersion heaters of 3 kW rating each. An ON-OFF type Honeywell temperature controller (model R7353, 0-650^{o}C range) was employed to control the water temperature.

To measure the water level inside the tank, a two-meter long translucent rubber hose was vertically hung adjacent to the tank and connected to the drain valve at the bottom of the tank. Before heating up water, the vent valve and the drain valve were open, the water level would then be clearly indicated on the translucent rubber hose.

The tank was designed to operate at the pressure varying from 101 kPa (14.7 psia) to 687 kPa (100 psia). Commercial fibre glass of 5.1 cm thickness was used for insulation.

3.2.3 Surge tank

The surge tank was also made of a heavy gauge stainless steel cylinder with two steel hemispheres welded at each end. The dimensions are 0.21 m O.D. and 0.86 m high. Its main function is to give extra space in the system to moderate pressure variation.

3.2.4 Piping

Most of the path was connected with 1.27 cm (1/2 in.) O.D. 304 stainless steel tube. Swagelok tube fittings were used between tubes. They provided a leak-proof, torque free seal at the tubing connection. Copper piping of 2.54 cm (1 in.) was employed for connecting the pump, because the pump has 2.54 cm (1 in.) O.D. outlet and inlet junction. The high pressure flexible rubber hose (steel reinforced) was utilized to isolate the electric current of the test section from the rest of the loop.

3.2.5 Others

The preheater and the test section assembly were the same as used in the open loop facilities.

3.2.6 Closed loop procedure

After the water in the storage tank was heated up to slightly below the desired test inlet temperature, the system was pressurized to the desired test pressure by injecting argon gas. Thereafter, the procedure would be same as the open loop.

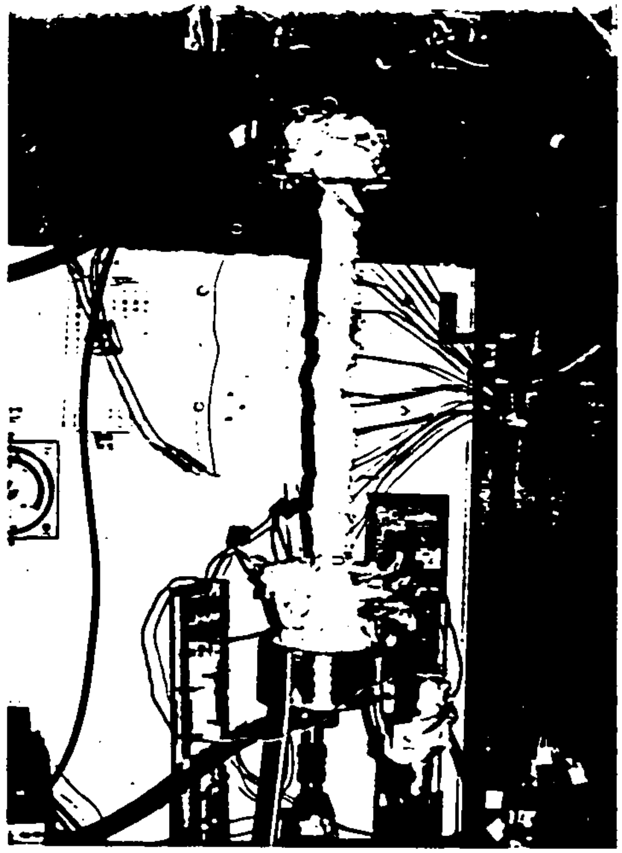

FIG. 3.6 AN INSULATED TEST SECTION ASSEMBLY

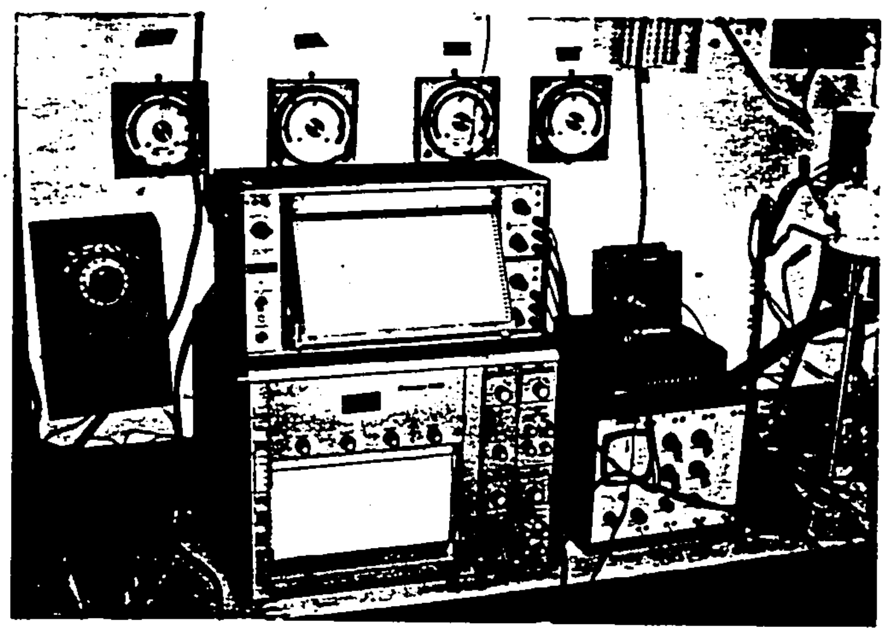

FIG. 3.7 EXPERIMENTAL EQUIPMENT

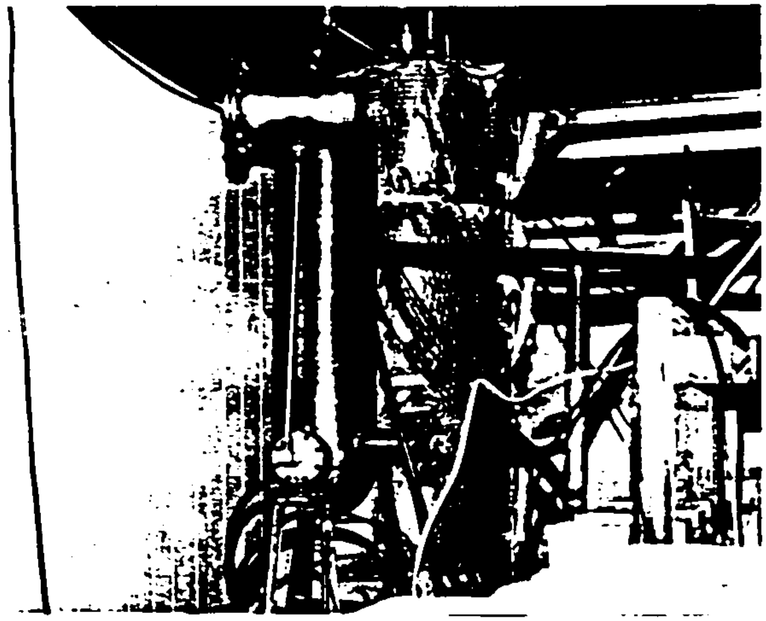

FIG. 3.8 SURGE TANK AND WATER STORAGE TANK

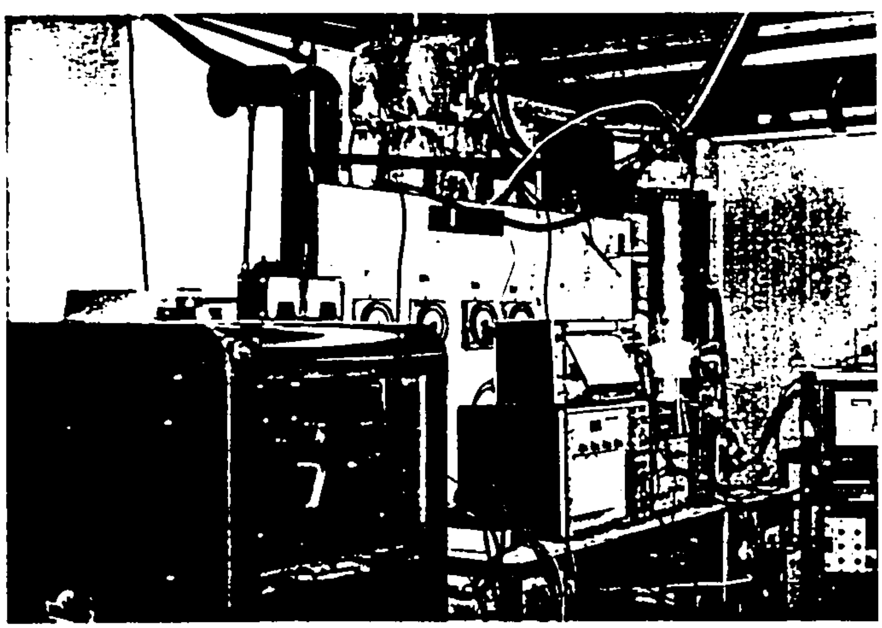

FIG. 3.9 OVERALL VIEW OF THE EXPERIMENTAL APPARATUS

Chapter IV

EXPERIMENTAL RUNS AND DATA REDUCTION

4.1 GENERAL

Four regular run series were conducted for measurements of the true quench temperature, i.e., 10,000, 10,100, 10,200, and 10,300 run series, plus a special run series of 10,200A. All the run series except 10,300 were operated at atmospheric pressure and were done on the open experimental loop. The details of each test run series are discussed below.

4.1.1 10,000 and 10,100 run series

These two run series were performed on the same test section. The features of the test section are described in Table 4.1. In 10,000 run series, two successful data were obtained. They are mass flux of 43 kg/m^2s with inlet subcooling of 16^oC and mass flux of 84 kg/m^2s with inlet subcooling of 10^oC. The temperature of the BHP was set at 600^oC and THP at 400^oC.

TABLE 4.1 10,000 AND 10,100 RUN SERIES DATA

General: Inconel 600 with 36" (91.4 cm) long, 0.514" (1.31 cm) O.D. and 0.0157" (0.04 cm) wall thickness. Gap size of 0.005" ~ 0.007" between the tube and hot patches before soldering. BHP 4" long with temp. set at 600°C (10,000 run series) and 700°C (10,100 run series) and THP 2" long with temp. set at 400°C (10,000 run series) and 500°C (10,100 run series).

Run No.	G (kg/m^2s)	ΔT_{sub} (°C)	Quench temp. (°C)	Quench location (cm)	H.F. due to direct heating at quench ($10^4 W/m^2$)	H.F. from BHP at quench ($10^5 W/m^2$)	x at quench location
10004	43	16	200	15	1.101	3.6	0.0918
10007	84	10	210	5	1.247	3.6	0.0426
10102	84	7	197	10	1.200	4.04	0.0576
10103	105	6	192	10	1.328	4.16	0.0474
10104	147	8	200	10	1.388	4.40	0.0293
10105	219	7	207	5	1.674	4.56	0.0172

For 10,100 run series, the temperature of the BHP and THP were raised from 600°C to 700°C and 400°C to 500°C, respectively. Four runs were conducted with mass flux ranging from 84 to 219 kg/m^{2}s and inlet subcooling from 6°C to 8°C.

4.1.2 10,200 run series

After careful studies of the previous two run series, an improved test section was constructed. The detailed features of the test section are listed in Table 4.2. With better soldering technique and thicker size tubing, the mass flux range was expanded from 53 to 682 kg/m^{2}s, inlet subcooling from 4 to 20°C, and local quality from -0.0227 to 0.0736. The temperature of the BHP and THP were still kept at 700°C and 500°C, respectively.

4.1.3 10,200A run series

The objective of this run series is to study the length effect on quench temperature. This is an extra run series conducted on the same apparatus as that for the 10,200 run series. An artifical cold spot was created at 30cm from the BHP first, and later at 15cm. A bundle of fine copper wires was used to wrap tightly around the cold spot. Six experimental data were obtained. They covered the mass

TABLE 4.2 10,200 RUN SERIES DATA

General: Inconel 718 with 36" (91.4 cm) long, 0.5" (1.27 cm) O.D. and 0.033" (0.084 cm) wall thickness. Gap size of 0.015" (0.038 cm) between the tube and hot patches before soldering. BHP 4" long with temp. set at 700°C and THP 2" long with temp. set at 500°C.

Run No.	G (kg/m^2s)	ΔT_{sub} (°C)	Quench temp. (°C)	Quench location (cm)	H.F. due to direct heating at quench $(10^4 W/m^2)$	H.F. from BHP at quench $(10^5 W/m^2)$	x at quench location
10217	53	5	180	40	1.333	2.25	0.0736
10215	102	4	180	40	1.682	2.4	0.0404
10214	178	4	190	40	1.960	2.6	0.0226
10213	265	4	222	30	2.472	2.75	0.0131
10212	336	4	255	30	3.120	2.9	0.0102
10208	509	4	244	10	6.402	3.2	0.0045
10210	682	4	317	5	9.130	3.6	0.0018
10224	53	10	190	10	2.057	2.6	0.0654
10223	102	10	240	5	2.720	2.7	0.0243
10222	178	8	240	5	4.004	2.8	0.0115
10220	336	10	267	5	6.998	3.0	- 0.0031
10225	509	10	265	3	10.260	3.2	- 0.0077

TABLE 4.2 10,200 RUN SERIES DATA (CONT'D)

Run No.	G (kg/m^2s)	ΔT_{sub} (^oC)	Quench temp. (^oC)	Quench location (cm)	H.F. due to direct heating at quench $(10^4 W/m^2)$	H.F. from BHP at quench $(10^5 W/m^2)$	x at quench location
10230	53	20	220	10	2.194	2.85	0.0535
10231	102	20	267	3	4.088	3.10	0.0116
10233	178	20	320	5	7.872	3.40	- 0.0039
10234	265	20	340	1	1.219	3.65	- 0.0151
10235	336	20	336	1 & 3	1.423	3.90	- 0.0168 & - 0.0181
10236	509	20	346	1 & 3	1.574	4.50	- 0.0217 & - 0.0227

fluxes of 53 and 102 kg/m^2s, inlet subcooling from 2 to 16.5°C. Table 4.3 shows all the experimental run data.

4.1.4 10,300 run series

In this run series, a thicker tube of 0.104 cm wall thickness with slightly larger diameter was used. The features of the test section are presented in Table 4.4.

The experiments were performed on the closed experimental loop. It covered the pressure ranging from 206 kPa (30 psia) to 687 kPa (100 psia), mass flux from 50 to 400 kg/m^2s, inlet subcooling from 10 to 30°C and quality from -0.0315 to 0.1990.

TABLE 4.3 COLD SPOT TESTS, 10,200 A RUN SERIES DATA

Run No.	G (kg/m^2s)	ΔT_{sub} (^oC)	Quench temp. (^oC)	Quench location (cm)	H.F. due to direct heating at quench ($10^4 W/m^2$)	H.F. from BHP at quench ($10^5 W/m^2$)	x at quench location
10201 A	53	12	195	30*	2.031	2.70	0.0769
10202 A	53	6	200	30*	1.832	2.30	0.0731
10203 A	53	3	180	30*	1.082	2.20	0.0694
10211 A	53	16.5	210	15*	1.943	2.80	0.0610
10204 A	102	8	225	15*	1.947	2.60	0.0290
10205 A	102	2	190	15*	1.757	2.25	0.0351
10250	102	8	230	20	2.102	2.55	0.0301
10251	102	5.8	200	25	1.772	2.45	0.0339
10252	102	4	195	30	1.426	2.35	0.0352

*The location of cold spot from the BHP.

TABLE 4.4A 10,300 RUN SERIES DATA AT P=206 kPa

General: Inconel 718 with 36" (91.4 cm) long, 0.514" (1.31 cm) O.D. and 0.0408" (0.104 cm) wall thickness. Gap size of 0.015" (0.038 cm) between the tube and hot patches before soldering. BHP 4" long with temp. set at 700°C and THP 2" long with temp. set at 500°C.

Run. No.	G (kg/m^2s)	ΔT_{sub} (°C)	Quench temp. (°C)	Quench location(cm)	H.F. due to direct heating at quench ($10^4 W/m^2$)	H.F. from BHP at quench ($10^5 W/m^2$)	x at quench location
10301	50	30	245	20	1.763	4.88	0.1243
10302	100	30	268	5	3.646	5.08	0.0345
10303	200	30	343	5	13.63	5.484	-0.0028
10304	300	30	367	5	17.90	5.718	-0.0182
10305	400	30	392	1	19.30	5.953	-0.0300
10306	50	20	225	30	1.416	4.30	0.1258
10307	100	20	245	15	2.103	4.52	0.0457
10308	200	20	285	5	7.55	4.95	0.0085
10309	300	20	320	5	11.60	5.35	-0.0034
10310	400	20	340	5	13.00	5.75	-0.0100
10311	50	10	216	50	1.136	4.36	0.1514
10312	100	10	230	45	1.377	4.045	0.0614
10313	200	10	235	40	2.267	3.417	0.0182
10314	300	10	245	15	3.281	3.539	0.0042
10315	400	10	245	15	5.48	3.662	0.00024

TABLE 4.4B 10,300 RUN SERIES DATA AT P=344 kPa

Run No.	G (kg/m^2s)	ΔT_{sub} (^oC)	Quench temp. (^oC)	Quench location(cm)	H.F. due to direct heating at quench ($10^4 W/m^2$)	H.F. from BHP at quench ($10^5 W/m^2$)	x at quench location
10321	50	30	270	20	2.456	5.02	0.1366
10322	200	30	330	5	13.70	5.503	-0.0033
10323	300	30	341	5	15.60	5.36	-0.0219
10324	400	30	400	5	17.60	5.22	-0.0315
10325	50	20	250	30	1.218	4.87	0.1458
10326	100	20	285	20	2.80	4.85	0.0566
10327	200	20	307	5	7.90	4.84	0.0076
10328	300	20	343	5	11.60	4.697	-0.0076
10329	400	20	343	5	11.80	4.55	-0.0162
10330	50	10	220	50	0.766	4.70	0.1600
10331	100	10	236	30	1.539	4.52	0.0686
10332	200	10	248	25	2.145	4.18	0.0219
10333	300	10	245	30	3.663	4.035	0.0105
10334	400	10	260	30	5.578	3.89	0.0048

TABLE 4.4c 10,300 RUN SERIES DATA AT P=550 kPa

Run No.	G (kg/m^2s)	ΔT_{sub} (^oC)	Quench temp. (^oC)	Quench location(cm)	H.F. due to direct heating at quench ($10^4 W/m^2$)	H.F. from BHP at quench ($10^5 W/m^2$)	x at quench location
10341	50	30	330	20	3.592	5.27	0.1570
10343	200	30	341	5	13.10	5.534	-0.0038
10344	300	30	363	5	15.88	5.718	-0.0208
10345	400	30	374	5	18.37	5.902	-0.0295
10346	50	20	307	20	2.243	5.23	0.1663
10348	200	20	331	5	8.72	5.13	0.0105
10349	300	20	331	5	11.85	5.106	-0.0056
10350	400	20	350	5	14.70	5.08	-0.0140
10351	50	10	295	20	1.81	5.15	0.1721
10352	100	10	319	20	2.93	5.01	0.0815
10353	200	10	288	15	3.49	4.73	0.0274
10355	400	10	280	15	5.744	4.26	0.0028

TABLE 4.4D 10,300 RUN SERIES DATA AT P=687 kPa

Run No.	G (kg/m^2s)	ΔT_{sub} (^oC)	Quench temp. (^oC)	Quench location(cm)	H.F. due to direct heating at quench ($10^4 W/m^2$)	H.F. from BHP at quench ($10^5 W/m^2$)	x at quench location
10362	100	30	343	5	10.25	5.80	0.0557
10363	200	30	370	5	14.61	6.10	0.0017
10364	300	30	378	5	16.08	6.00	-0.0199
10365	400	30	385	5	18.56	5.91	-0.0304
10367	100	20	343	10	3.351	5.36	0.0635
10368	200	20	354	10	9.65	5.67	0.0199
10369	300	20	355	10	13.80	5.424	0.0006
10370	400	20	362	5	14.67	5.184	-0.0140
10371	50	10	318	25	2.411	5.36	0.1991
10372	100	10	330	20	3.266	5.316	0.0896
10374	300	10	341	10	5.28	4.848	0.0126
10375	400	10	300	15	6.94	4.456	0.0048

4.2 DATA REDUCTION

For every run in the experiments, the test section current, voltage and thermocouple signals were recorded. In order to calculate the local quality at the true quench location, it is necessary to determine the test section power, the heat flux of the test section, the heat flux of the bottom hot patch and the heat losses of the test section. Appendix A describes the heat losses test.

To measure the direct power input, a shunt resistor of a known value was placed along the power cable in series with the test section. The current was measured, via the shunt, in terms of millivolt (i.e. 500 A $\equiv$ 50 mV), and the voltage was measured across the two cable clamps on the test section. The test section power was recorded by the datalogger (model 2240B, Fluke) at the time of rewet.

The heat flux of the test section was obtained by dividing the direct power input by the heated surface area inside the tube between two cable clamps excluding the area in contact with both hot patches.

The determination of the heat flux of the bottom hot patch is more complicated. After each run series, a series of quench tests of the bottom hot patch were conducted (Appendix B). The cooldown history of the data thermocouple T.C.1 was used to determine the film boiling heat flux of the BHP via the mathematical model (Appendix C) developed by Cheng et al. [26]. This model involves the calculation of heat flux by solving the Fourier transient equation and using the concept of rate of changing heat content with the bottom hot patch. The Continuous System Modeling Program (CSMP) [27] has been used in obtaining the numerical solution.

Finally, the local quality (x) of the true quench location can be calculated by the heat balance equation:

$$h_l + \frac{\Delta Q}{\dot{m}} = h_f + xh_{fg} \qquad (4.1)$$

where Q represents the heat gained from the BHP plus the heat gained from the test section due to direct heating, and minus heat losses. A sample calculation of local quality is presented in Appendix D.

Chapter V

RESULTS AND DISCUSSION

The recently developed hot patch technique is of great aid in the present experiments. The technique is used to anchor the unwanted quench fronts originated from both ends of the test section during a cooling process by generating a steady-state film boiling condition inside the hot patch. This would permit the measurement of the true quench temperature over a wide range of flow conditions.

A properly functioning hot patch is strongly dependent on the method of soldering. An improper soldering process may cause the failure of the performance of the hot patch, as a result, the quench front initiates from the hot patch.

The temperature of the hot patch should be set at well above the minimum film boiling temperature, but below the melting temperature of the soldering material. After several trials, it was decided that the bottom hot patch temperature should be set at 700°C, and the top hot patch at 500°C. The temperature of the top hot patch was set at lower value because the chance of rewet from the top end is rare.

5.1 10,000 AND 10,100 RUN SERIES

These two run series were considered as trial ones to obtain some experience in performing the experiments. The true quench location was always close to the bottom hot patch. Thus, it was limited to the lower mass flux and small inlet subcooled runs.

In general, as mass flux increases, the quench location moves downward towards the bottom hot patch. For increasing mass flux, heat transfer between the wall and the coolant becomes more efficient. The portion of tube adjacent to the bottom hot patch under the strong influence of hot patch temperature gradient diminishes, resulting in a downward movement of quench location. The observation of the effect of increasing inlet degree subcooling to the quench location exhibits a similar trend to the increase of mass flux. In order to push the quench location further downstream, one must raise the temperature of the hot patch. Therefore, in the 10,100 run series, a slightly higher mass flux can be obtained.

The measured quench temperatures are about 200°C for these two series. Due to the small range of mass flux and inlet subcooling, the study of parametric trends in these run series is not possible. Figure 5.1 shows the plot of measured quench temperature vs flow parameters.

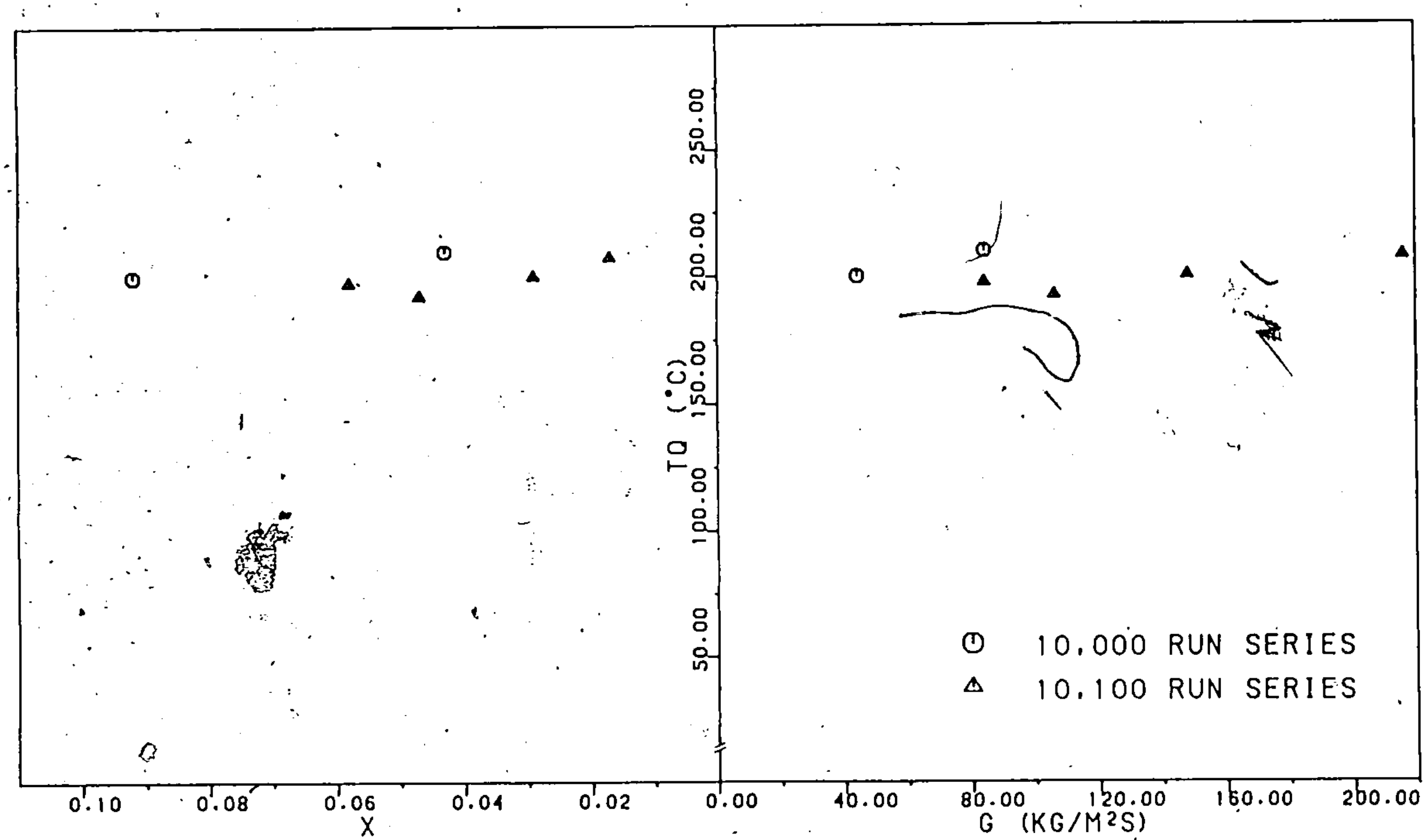

FIG. 5.1 MEASURED QUENCH TEMPERATURE VS MASS FLUX AND LOCAL QUALITY (X) FOR 10,000 AND 10,100 RUN SERIES

5.2 10,200 RUN SERIES

After raising the hot patch temperatures in the last run series, a further modification of the test section is still necessary. In this series, a thicker tube was constructed. It is obvious that a thicker tube requires more power for heating; thus, the quench location would be pushed further downstream under the same flow conditions.

In this series, the measured quench temperature is no longer a constant value. It varies from 180°C at low mass flux to 346°C at high mass flux; but the quench temperature decreases exponentially with increasing local quality.

Figures 5.2 - 5.6 show all the resultant plots for this run series. They are the measured quench temperature vs local quality, vs mass flux and vs inlet subcooling, for a mixed combination of fixed mass flux, inlet subcooling and local quality. The effect on these parameters will be discussed later.

5.3 10,200A RUN SERIES

The length effect on the true quench temperature was studied in this special artificial cold spot test series. The artifical cold spot was made of a bundle of fine copper wire wrapped tightly around the cold spot. The

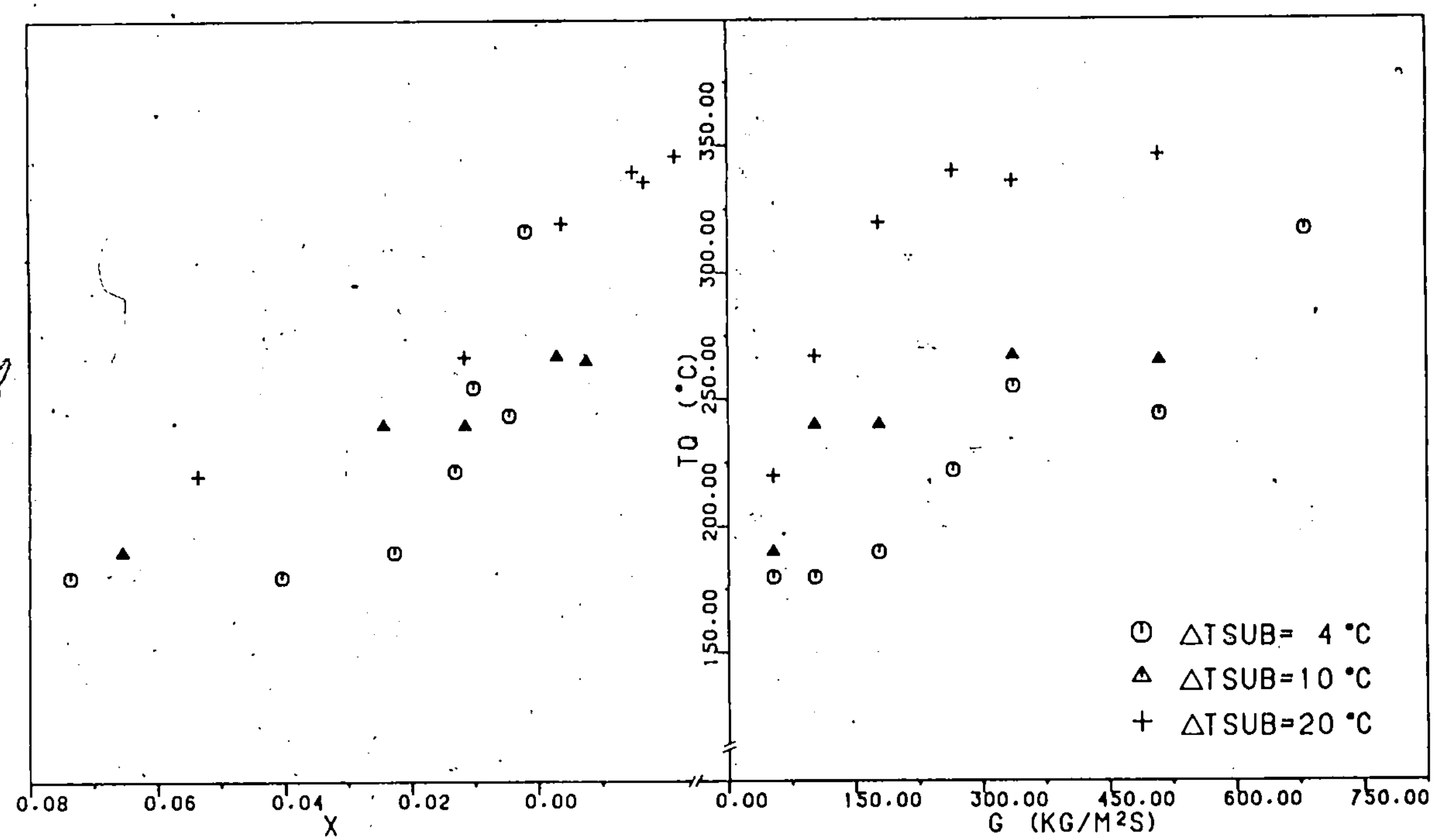

FIG. 5.2 MEASURED QUENCH TEMPERATURE VS MASS FLUX AND LOCAL QUALITY (X) FOR 10,200 RUN SERIES

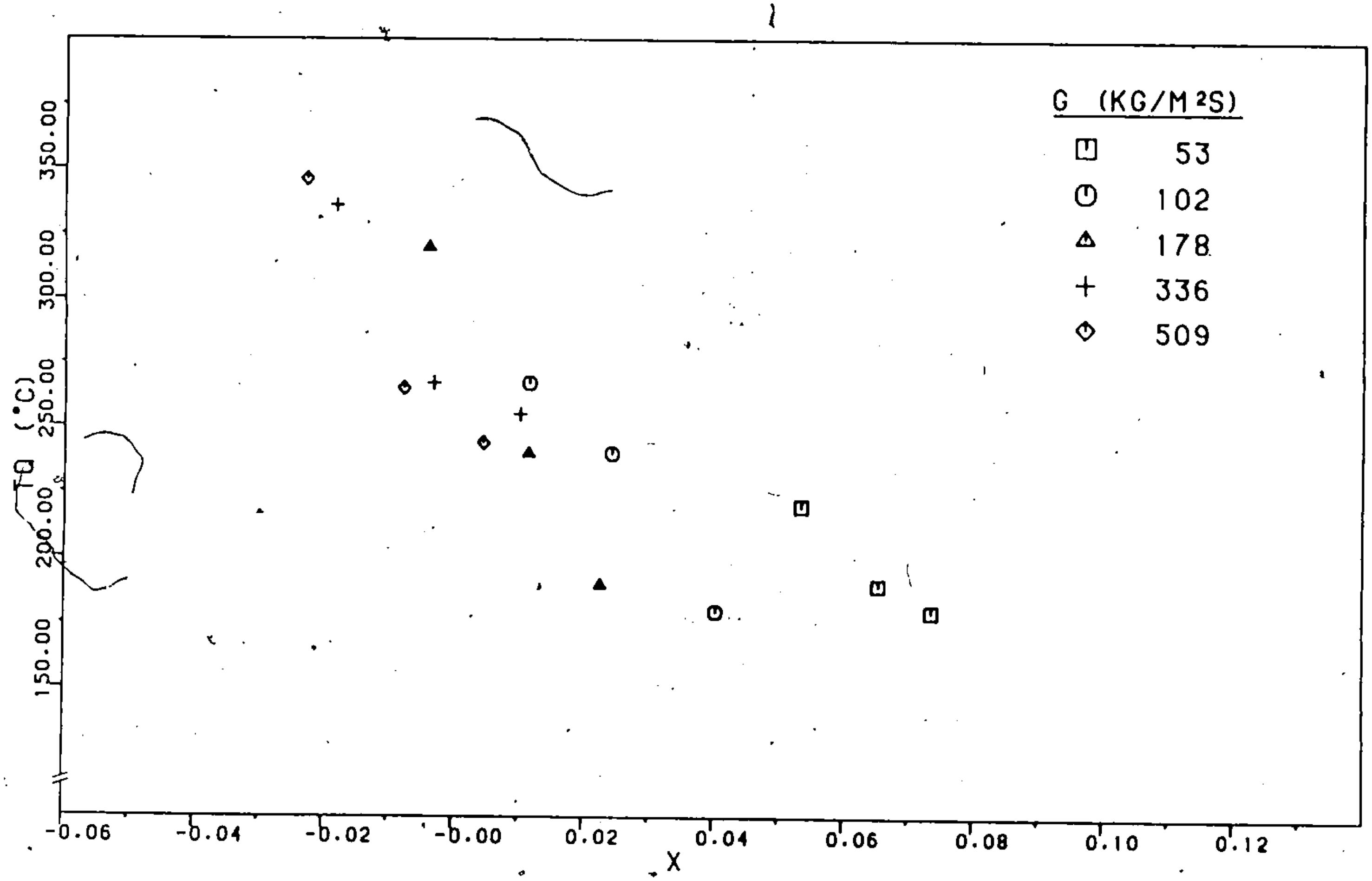

FIG. 5.3 MEASURED QUENCH TEMPERATURE VS LOCAL QUALITY FOR FIXED MASS FLUX FOR 10,200 RUN SERIES

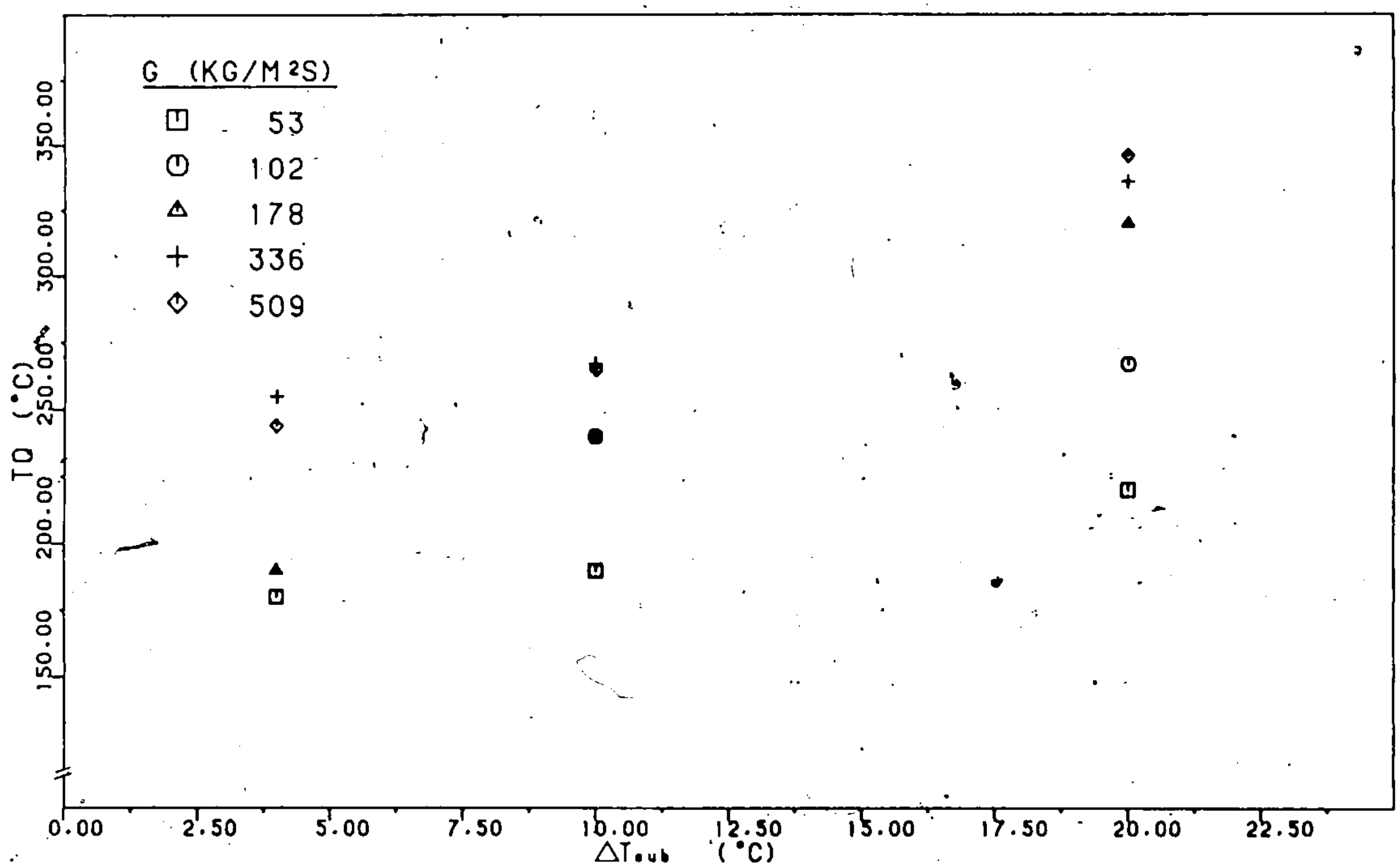

FIG. 5.4 MEASURED QUENCH TEMPERATURE VS INLET SUBCOOLING FOR FIXED MASS FLUX FOR 10,200 RUN SERIES

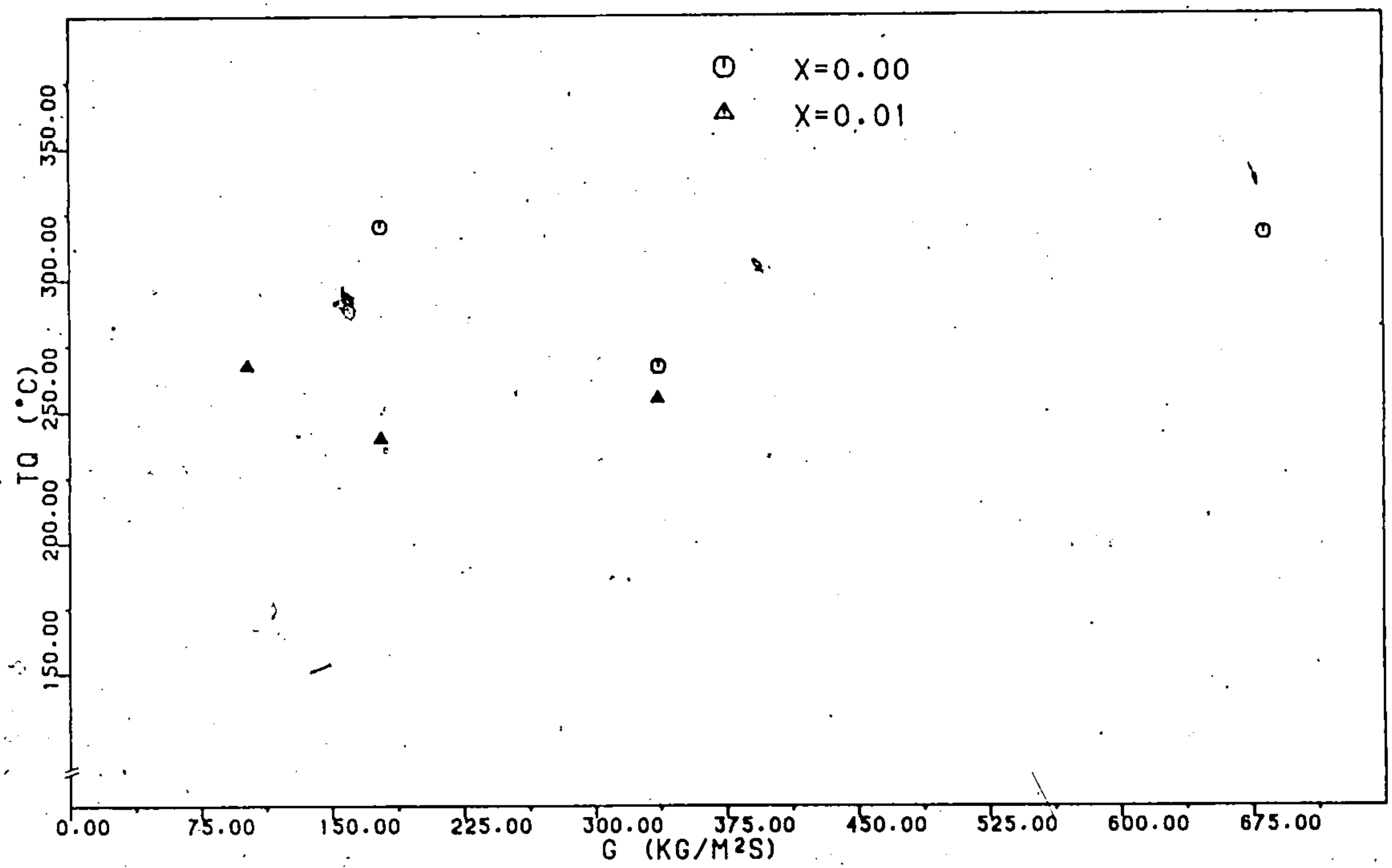

FIG. 5.5 MEASURED QUENCH TEMPERATURE VS MASS FLUX FOR FIXED LOCAL QUALITY FOR 10,200 RUN SERIES

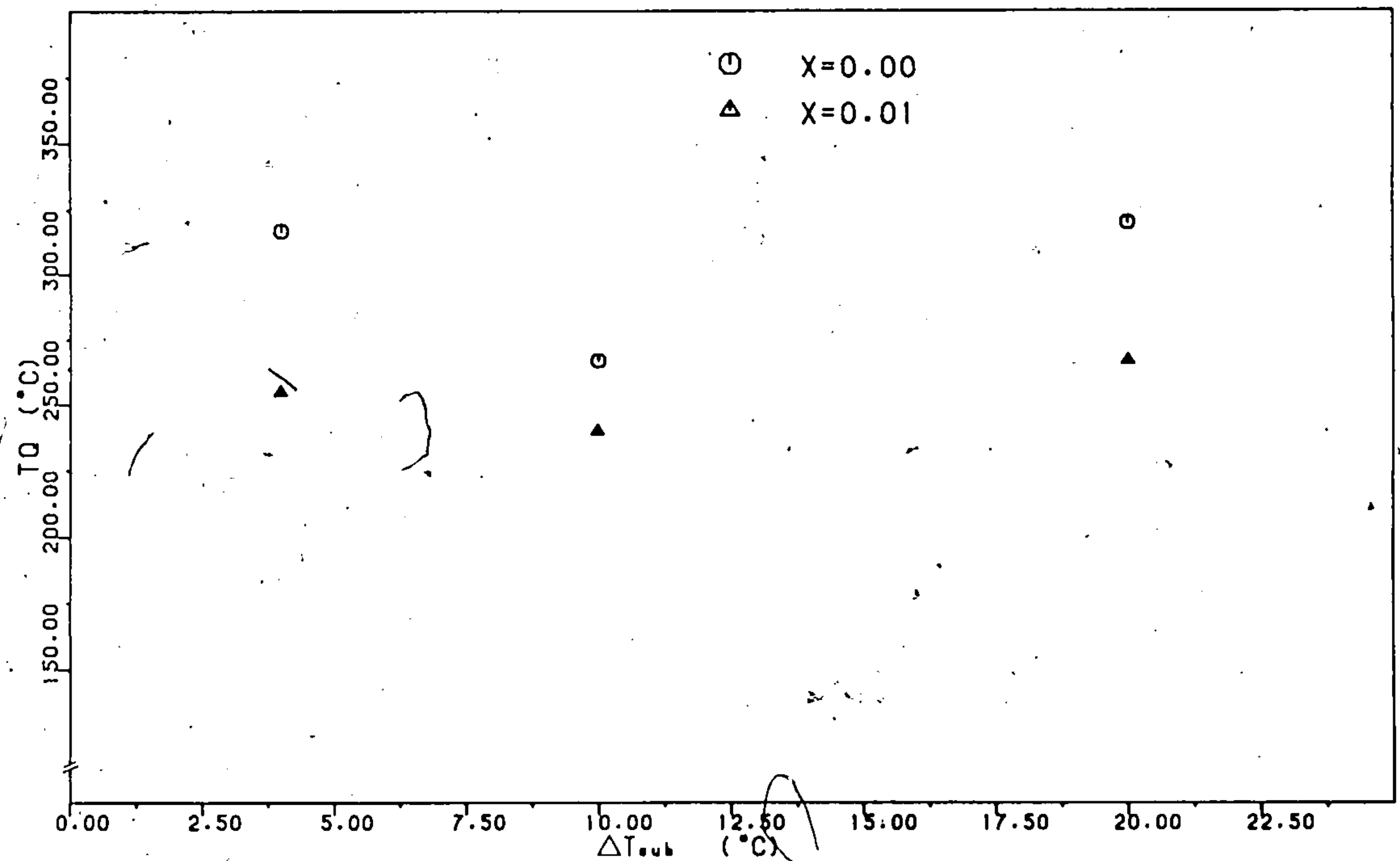

FIG. 5.6 MEASURED QUENCH TEMPERATURE VS INLET SUBCOOLING FOR FIXED LOCAL QUALITY FOR 10,200 RUN SERIES

concept of an artifical cold spot is to create a thicker portion on the test tube, at which its electric resistance is less than the rest. Consequently, the cold spot has cooler temperature than the rest, and the true quench would initiate at the cold spot with gradually reduced heat flux. True quench did occur at the cold spot, but for a rather narrow range of flow conditions. Outside this range, true quench did not occur at the cold spot.

To examine the length effect on the true quench temperature, a fixed mass flux was chosen first, and the same amount of local quality (X) was generated at both locations of true quench in the cold spot test and in the regular test by adjusting inlet subcoolings. The two measured quench temperatures were then compared. The two locations of true quench should be quite distant.

Table 4.3 lists all six successful cold spot test results. Three additional regular runs were also included for purpose of comparison. For example, in cold spot test run 10,205A, true quench occurs at 15 cm with X of 0.0351 and T_Q of 190°C. This compares with regular run 10,252, where true quench occurs at 30 cm with X of 0.0352 and T_Q of 195°C. These results indicate a very small effect on the true quench temperature particularly for quench location occurring at 15 cm away from the BHP. However, no clear conclusion can be obtained for true quench located very near to the BHP. It is possible that length effect is present at this region.

5.4 10,300 RUN SERIES

This run series is similar to the 10,200 run series except it was performed in the closed experimental loop with different system pressures.

During the experiments, the system pressure increased slightly due to vapour generation caused by the heated test section. In order to maintain a constant pressure, a remote controlled solenoid vent valve was used to release excess pressure throughout the experiments.

For a given pressure, the behaviour of the parametric trends of the true quench temperature is similar to those of 10,200 run series, except the true quench temperature is varied with pressure. Figures 5.7 - 5.22 show all the results for this series. Parametric trends are to be discussed in the next section.

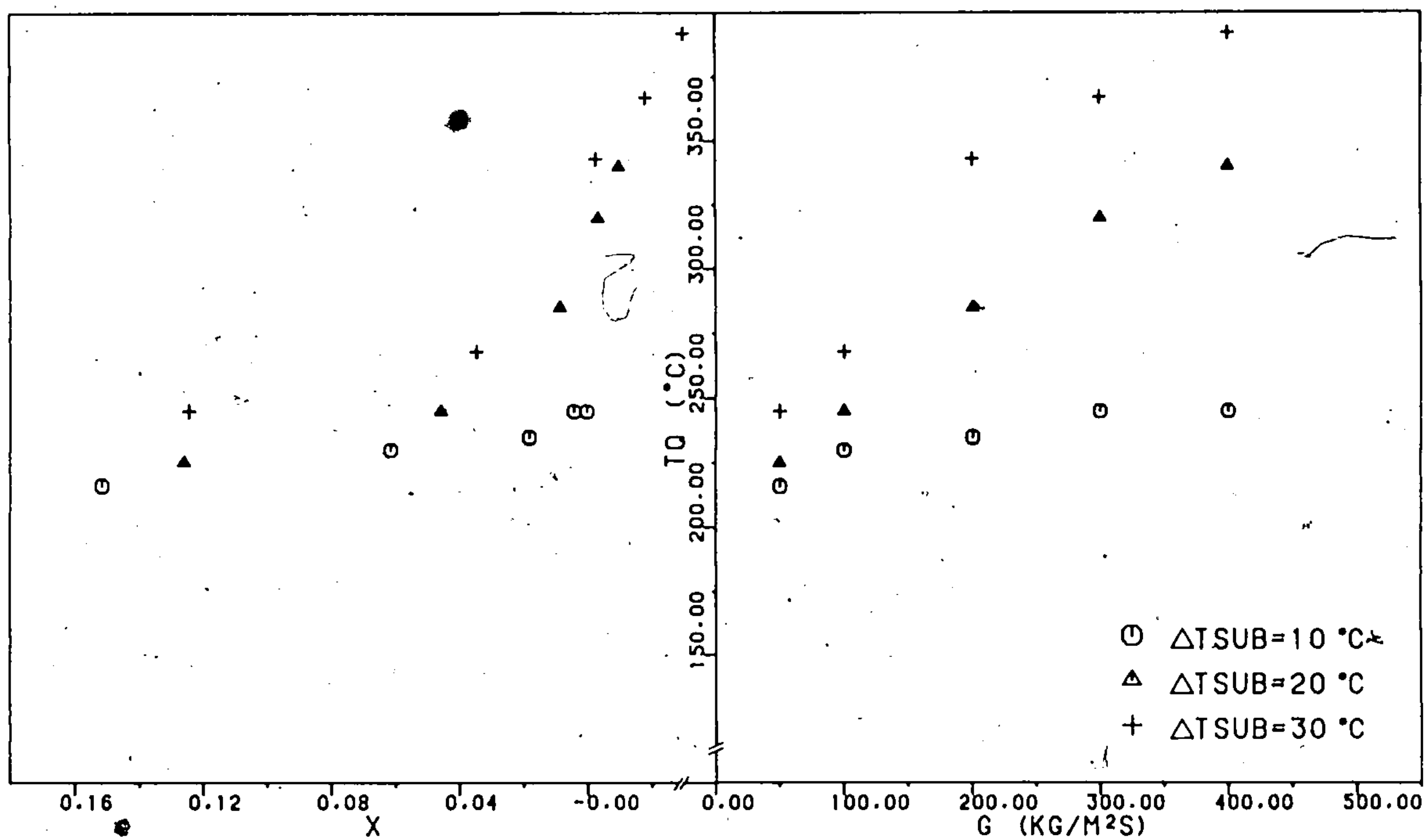

FIG. 5.7 MEASURED QUENCH TEMPERATURE VS MASS FLUX AND LOCAL QUALITY FOR 10,300 RUN SERIES AT P=206 kPa

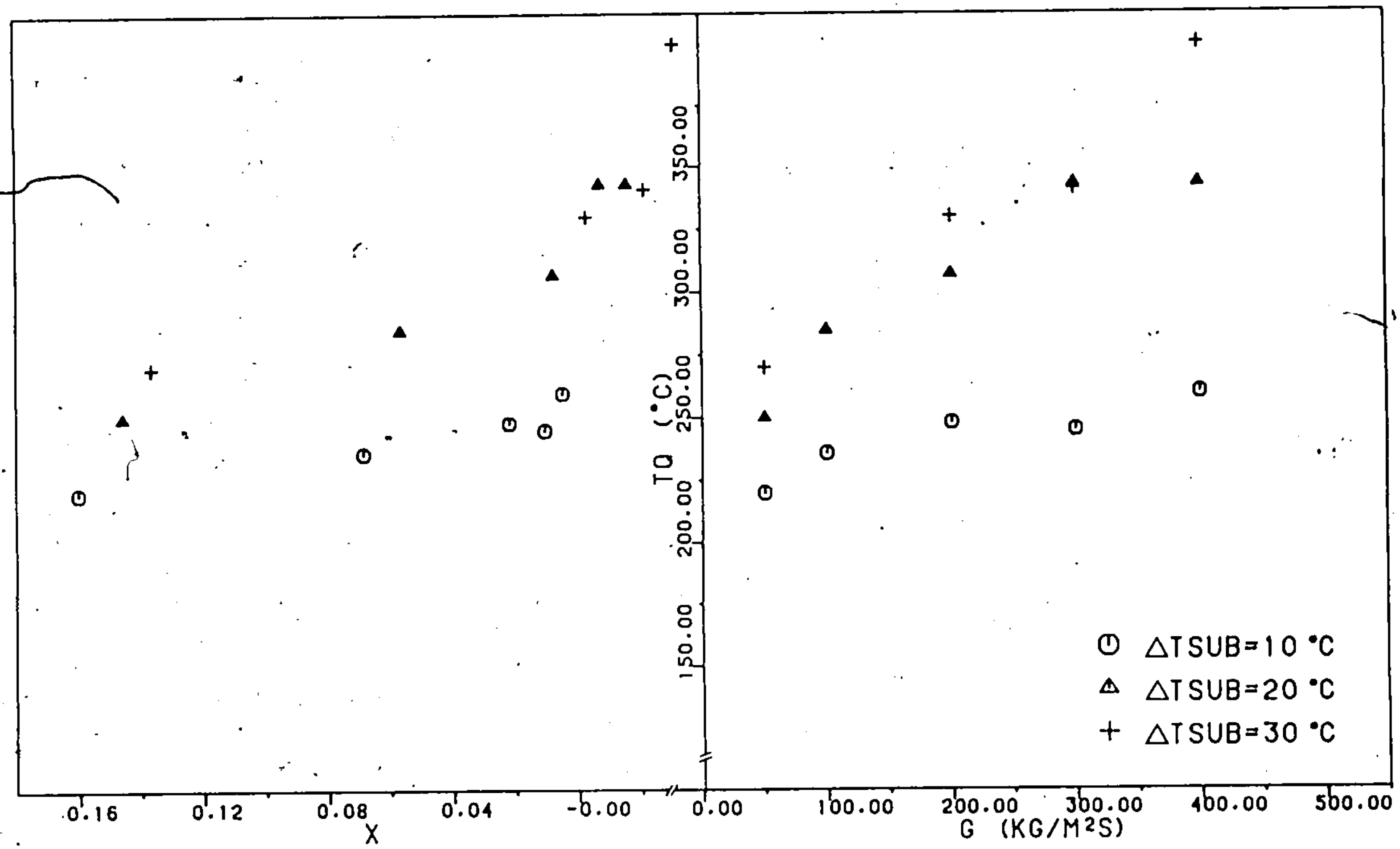

FIG. 5.8 MEASURED QUENCH TEMPERATURE VS MASS FLUX AND LOCAL QUALITY FOR 10,300 RUN SERIES AT P=344 kPa

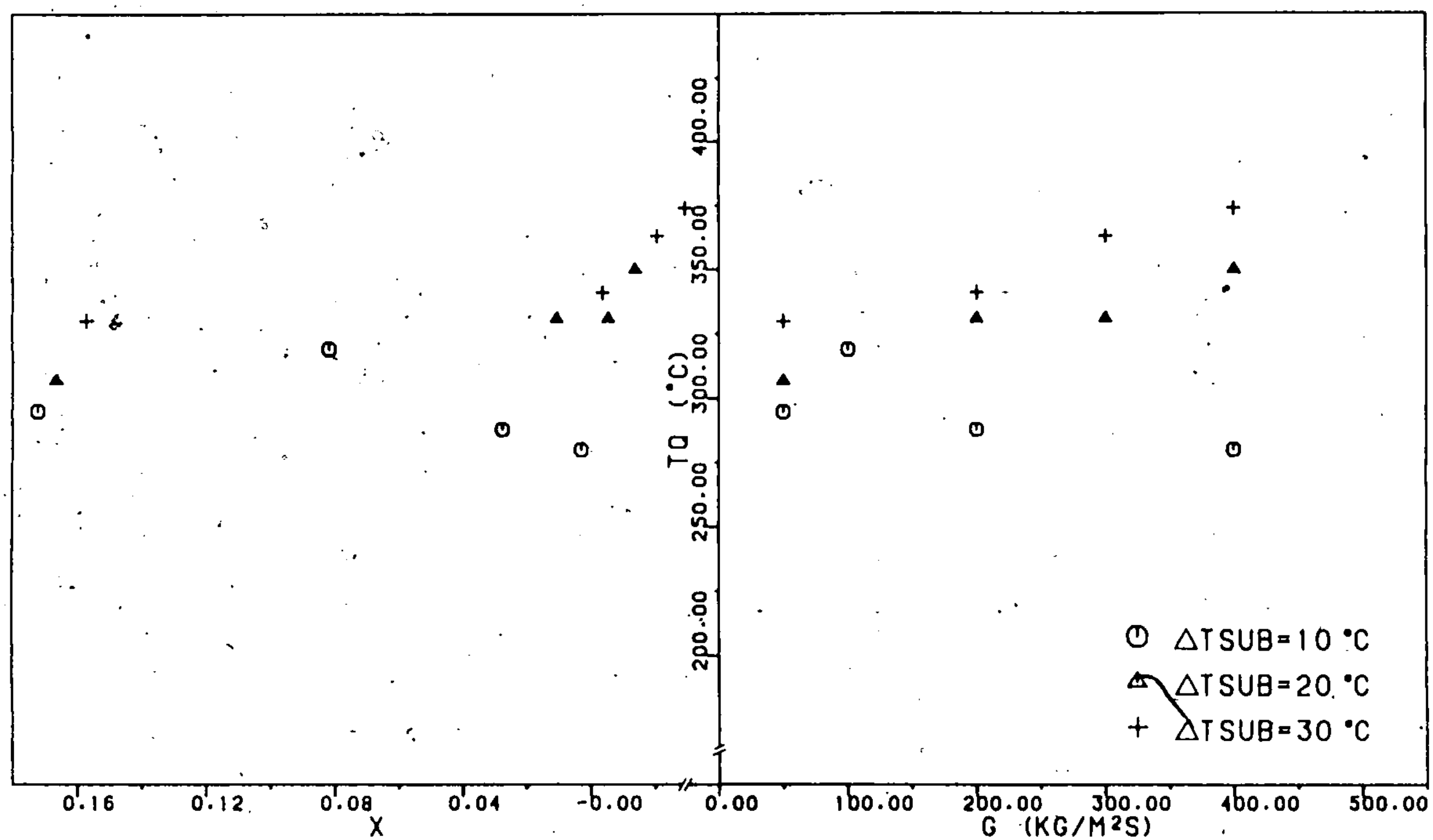

FIG. 5.9 MEASURED QUENCH TEMPERATURE VS MASS FLUX AND LOCAL QUALITY FOR 10,300 RUN SERIES AT P=550 kPa

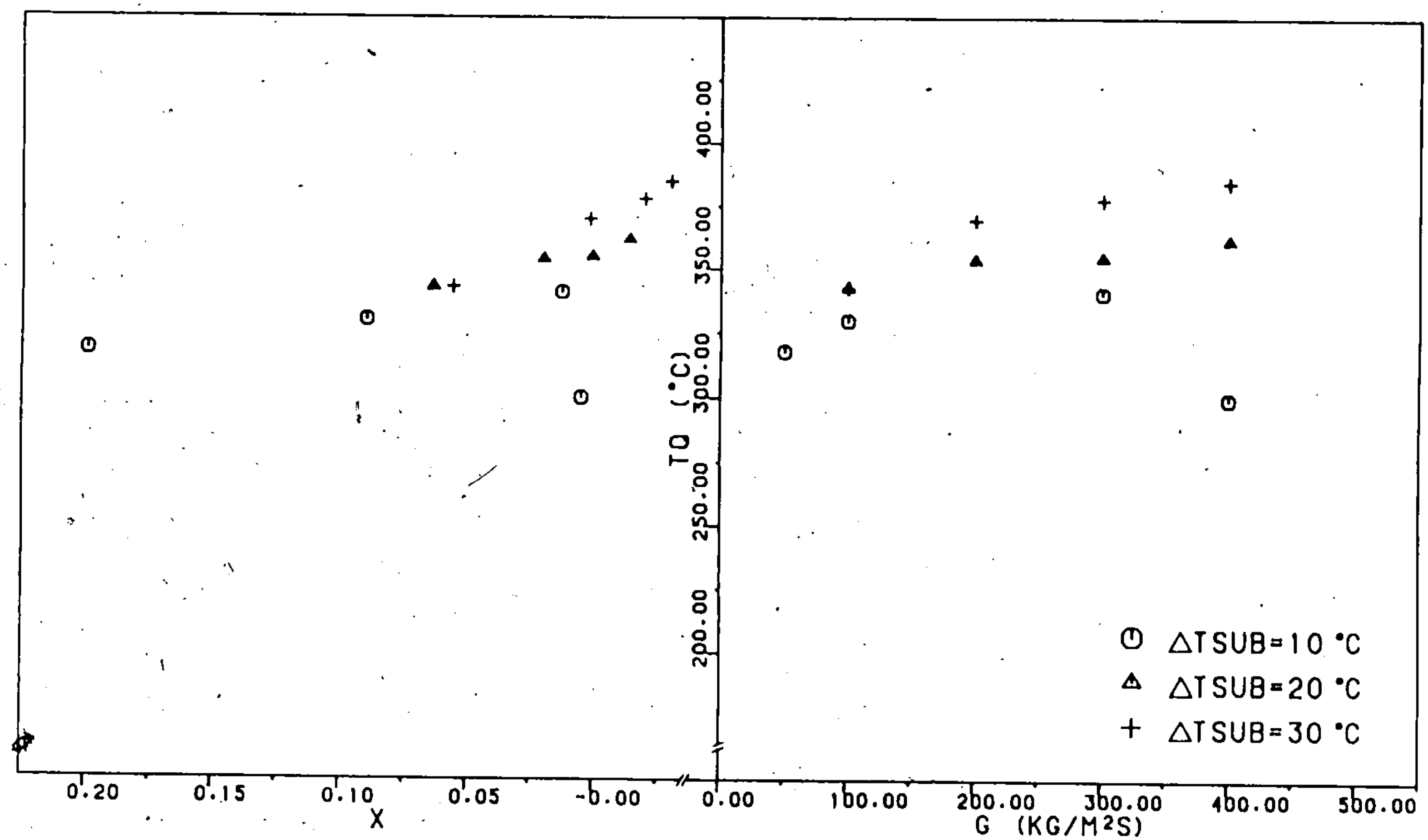

FIG. 5.10 MEASURED QUENCH TEMPERATURE VS MASS FLUX AND LOCAL QUALITY FOR 10,300 RUN SERIES AT P=687 kPa

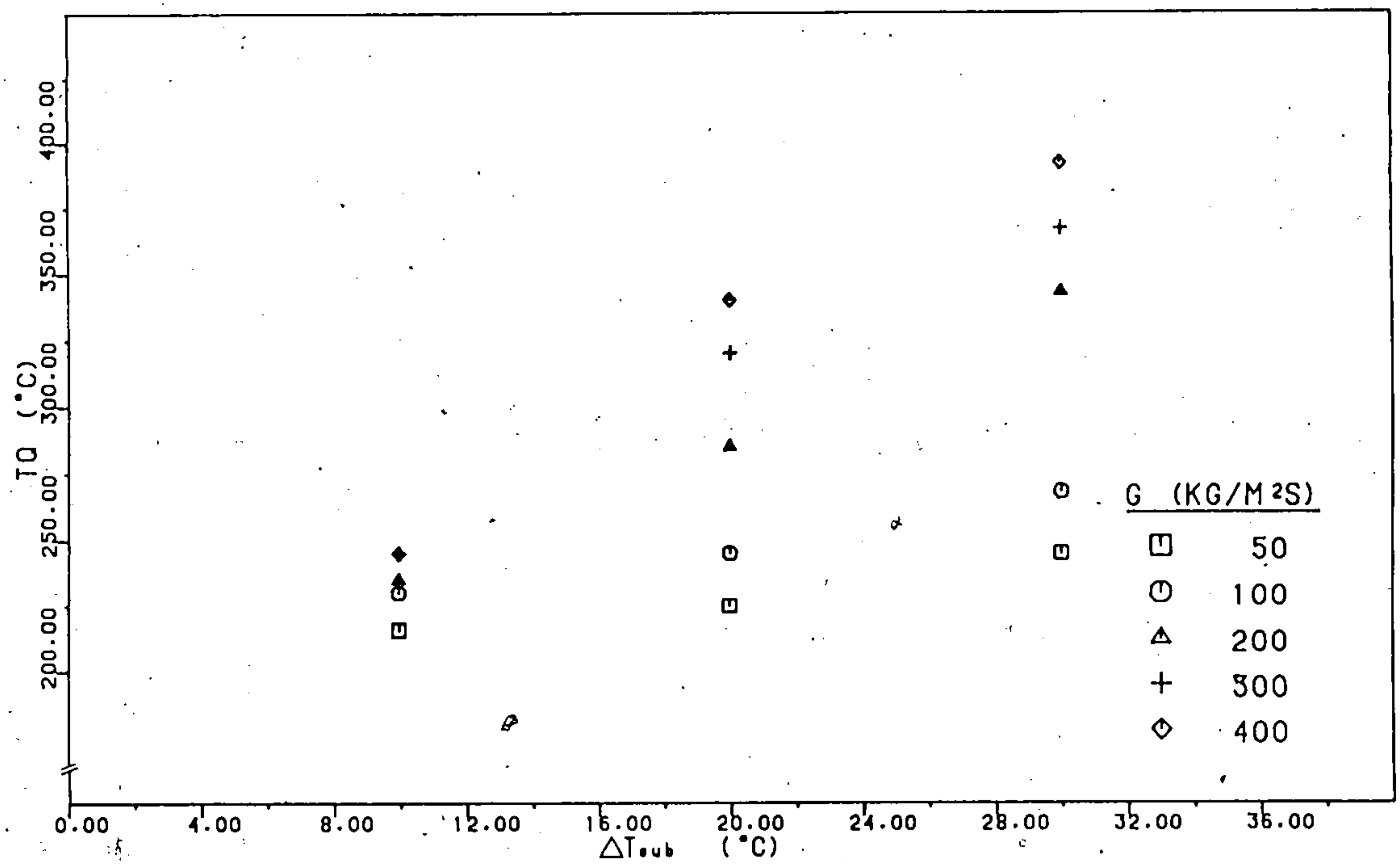

FIG. 5.11 MEASURED QUENCH TEMPERATURE VS INLET SUBCOOLING FOR FIXED MASS FLUX FOR 10,300 RUN SERIES AT P=206 kPa

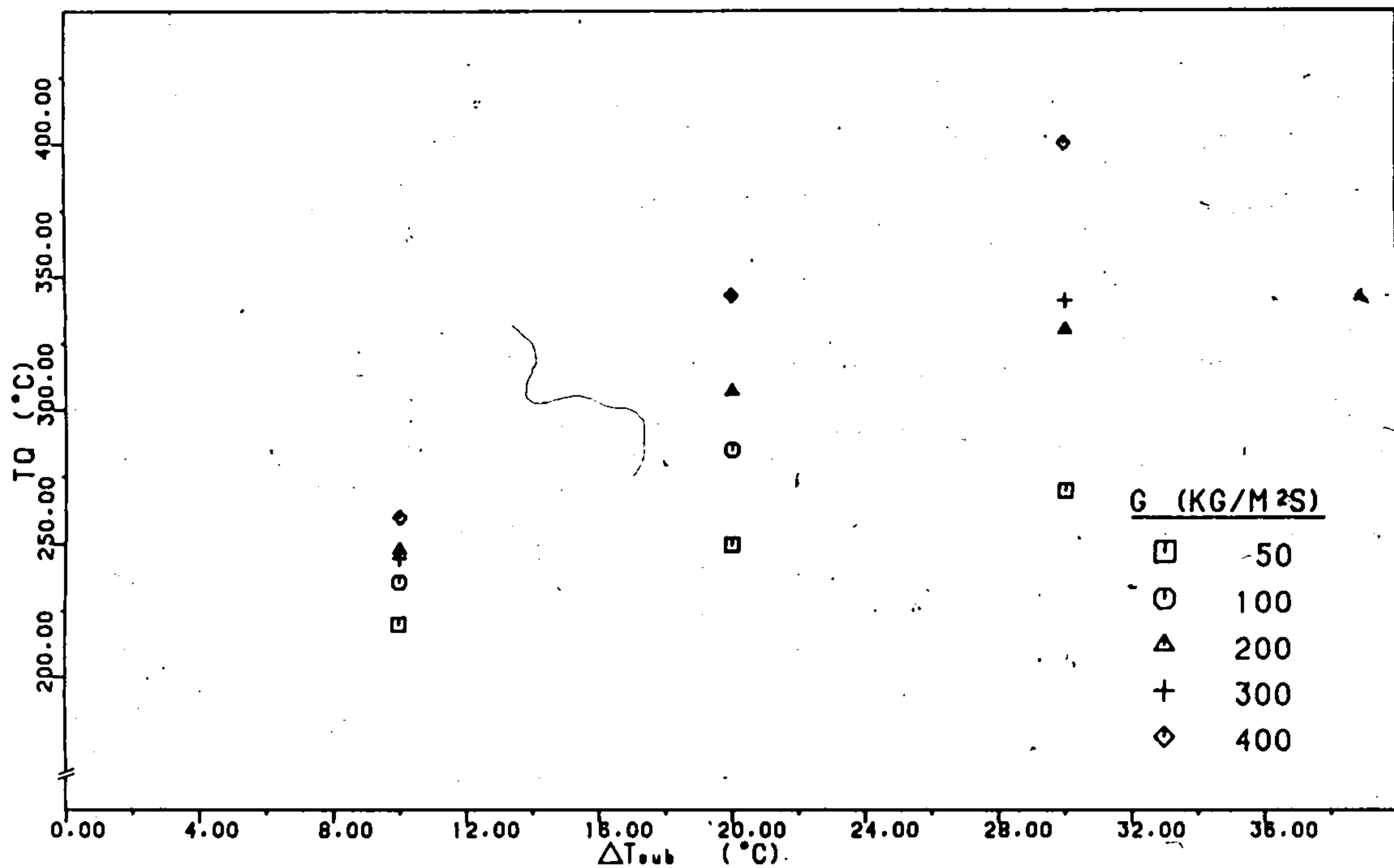

FIG. 5.12 MEASURED QUENCH TEMPERATURE VS INLET SUBCOOLING FOR FIXED MASS FLUX FOR 10,300 RUN SERIES AT P=344 kPa

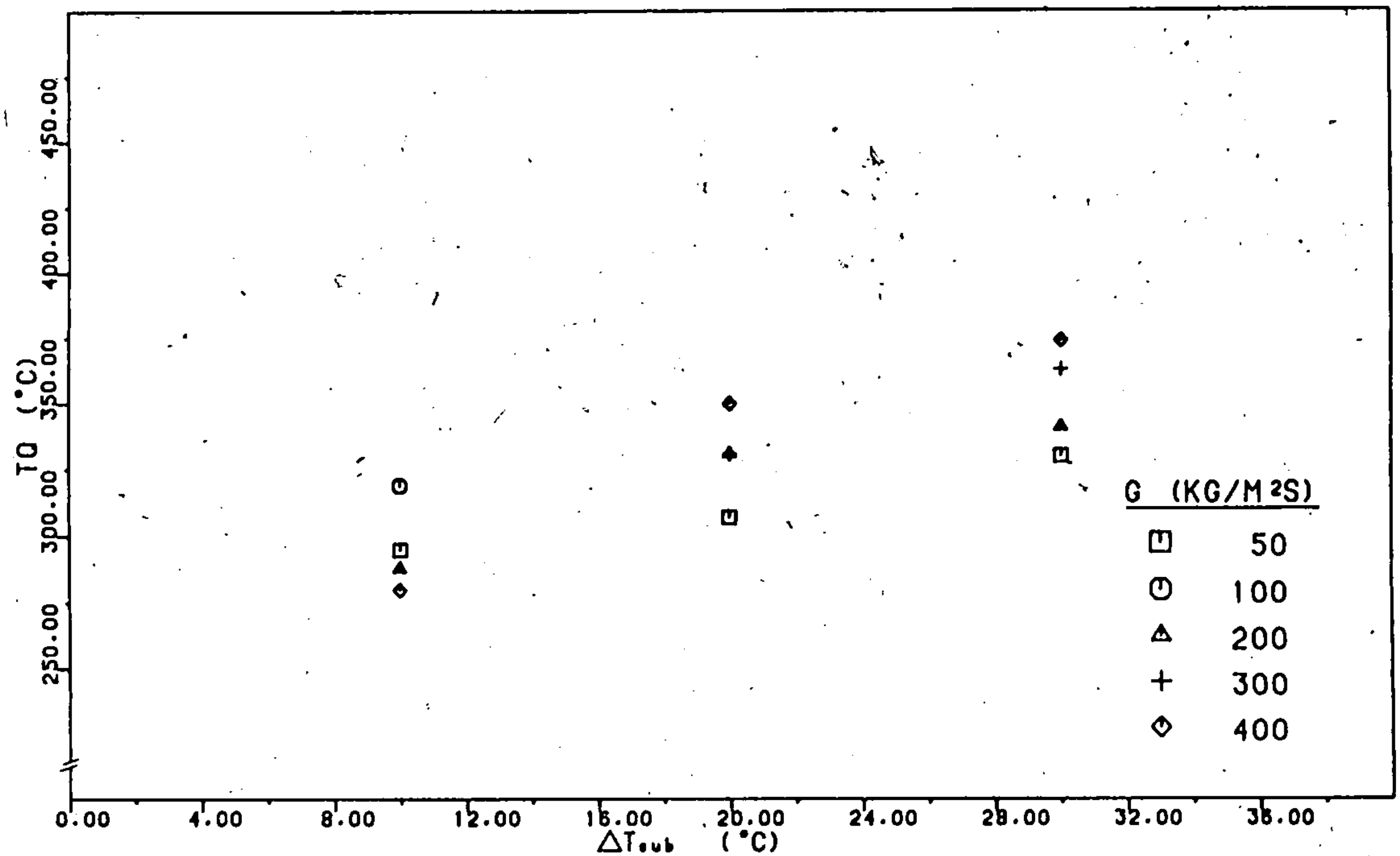

FIG. 5.13 MEASURED QUENCH TEMPERATURE VS INLET SUBCOOLING FOR FIXED MASS FLUX FOR 10,300 RUN SERIES AT P=550 kPa.

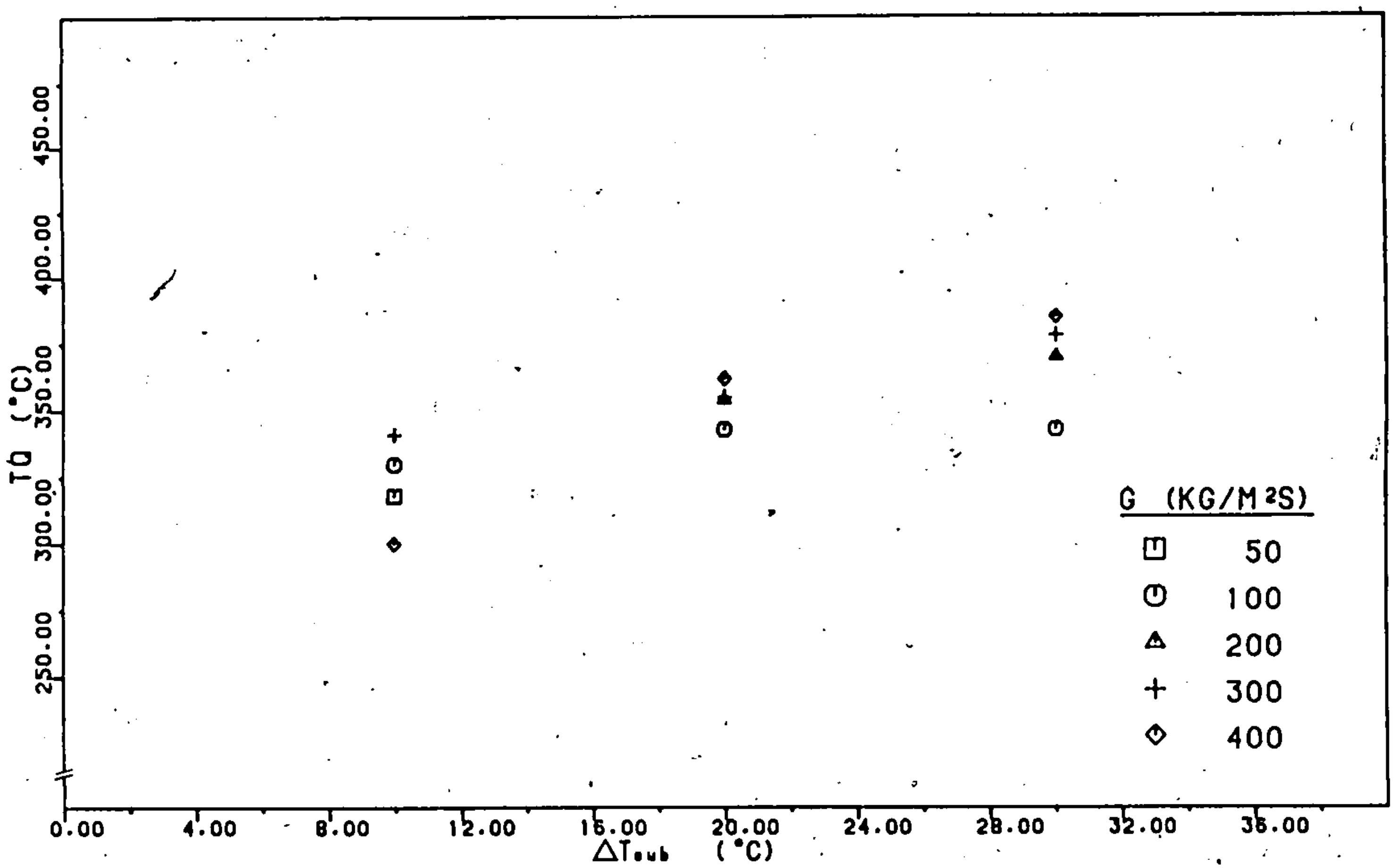

FIG. 5.14 MEASURED QUENCH TEMPERATURE VS INLET SUBCOOLING FOR FIXED MASS FLUX FOR 10,300 RUN SERIES AT P=687 kPa

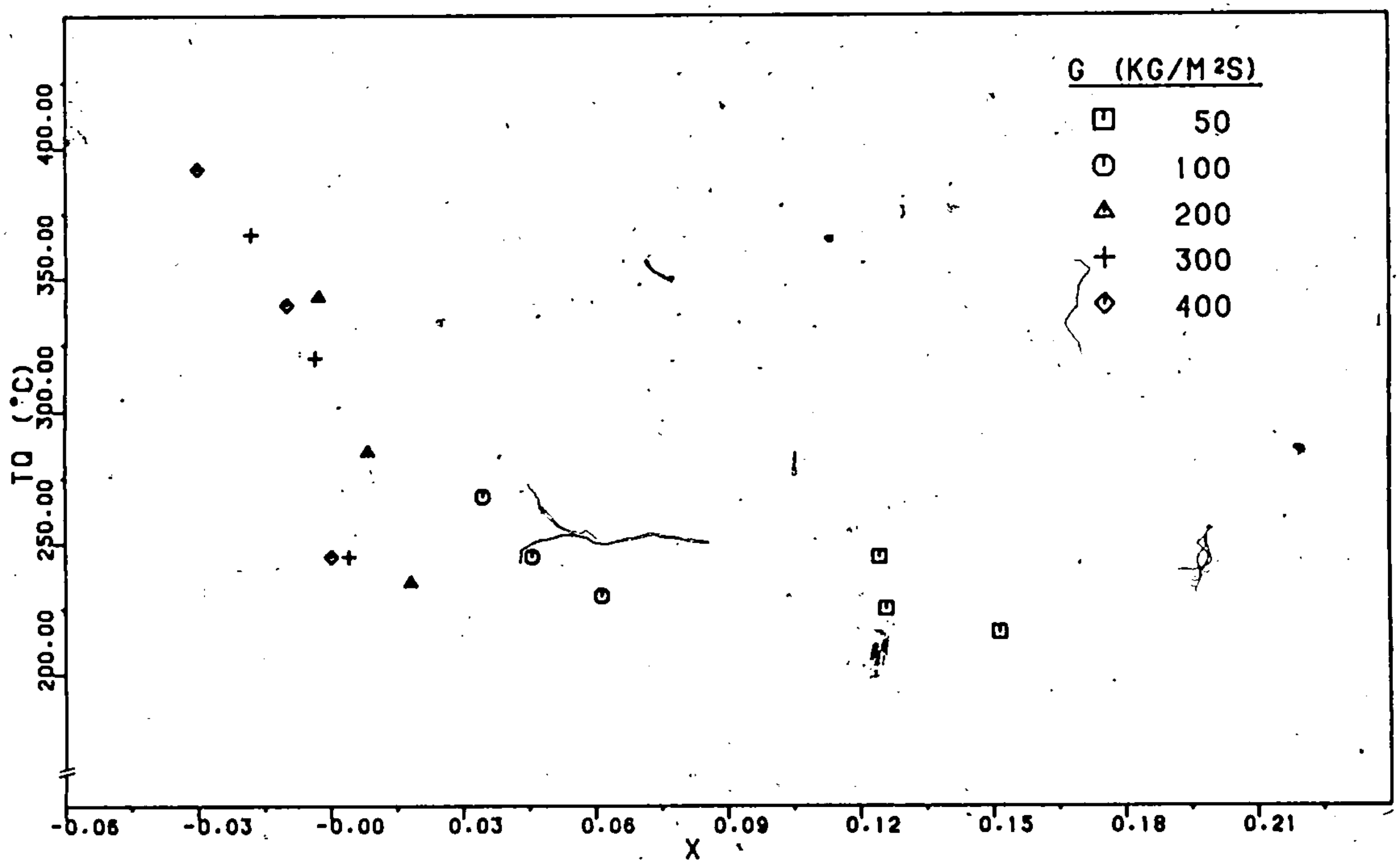

FIG. 5.15 MEASURED QUENCH TEMPERATURE VS LOCAL QUALITY FOR FIXED MASS FLUX FOR 10,300 RUN SERIES AT P=206 kPa

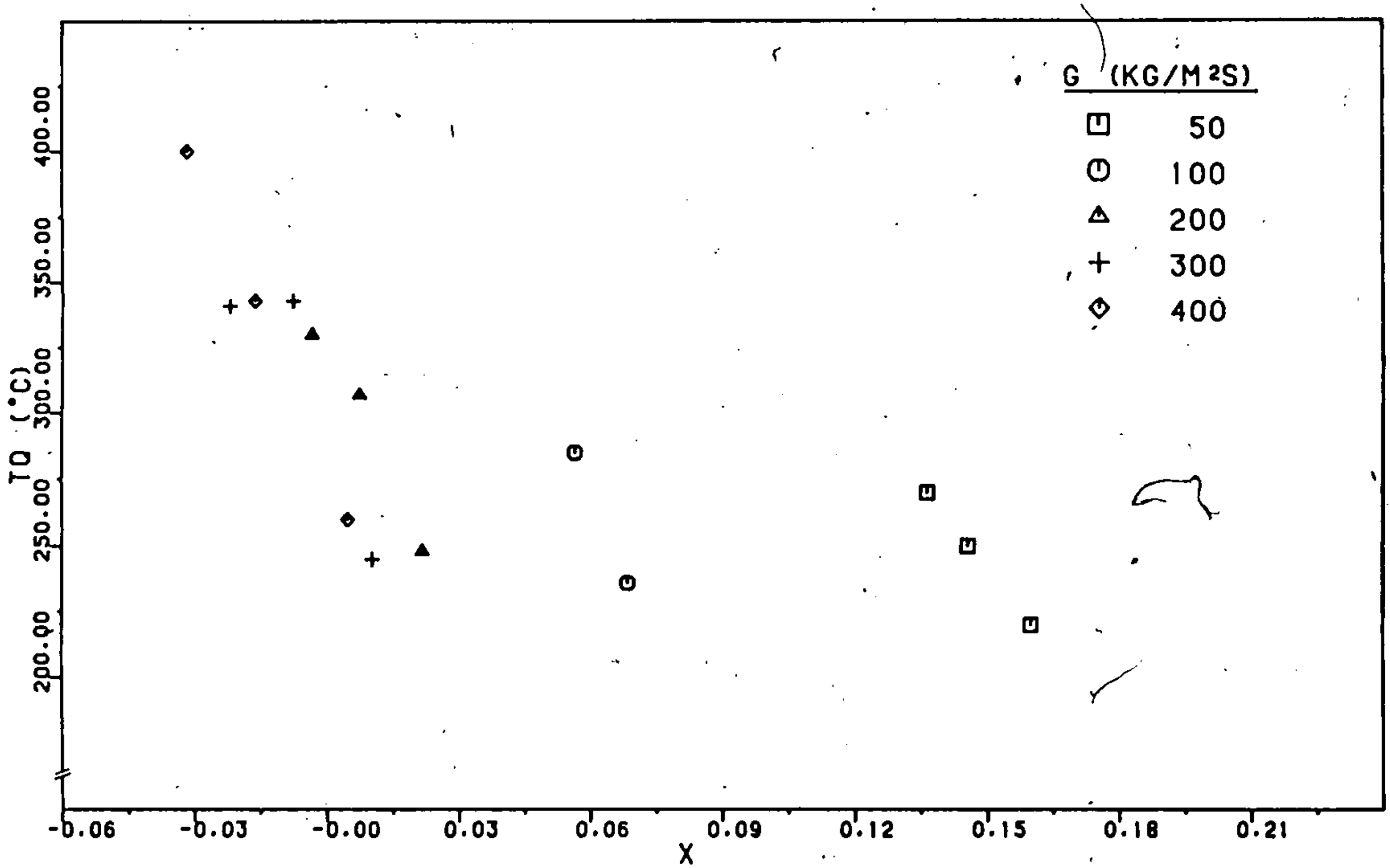

FIG. 5.16 MEASURED QUENCH TEMPERATURE VS LOCAL QUALITY FOR FIXED MASS FLUX FOR 10,300 RUN SERIES AT P=344 kPa

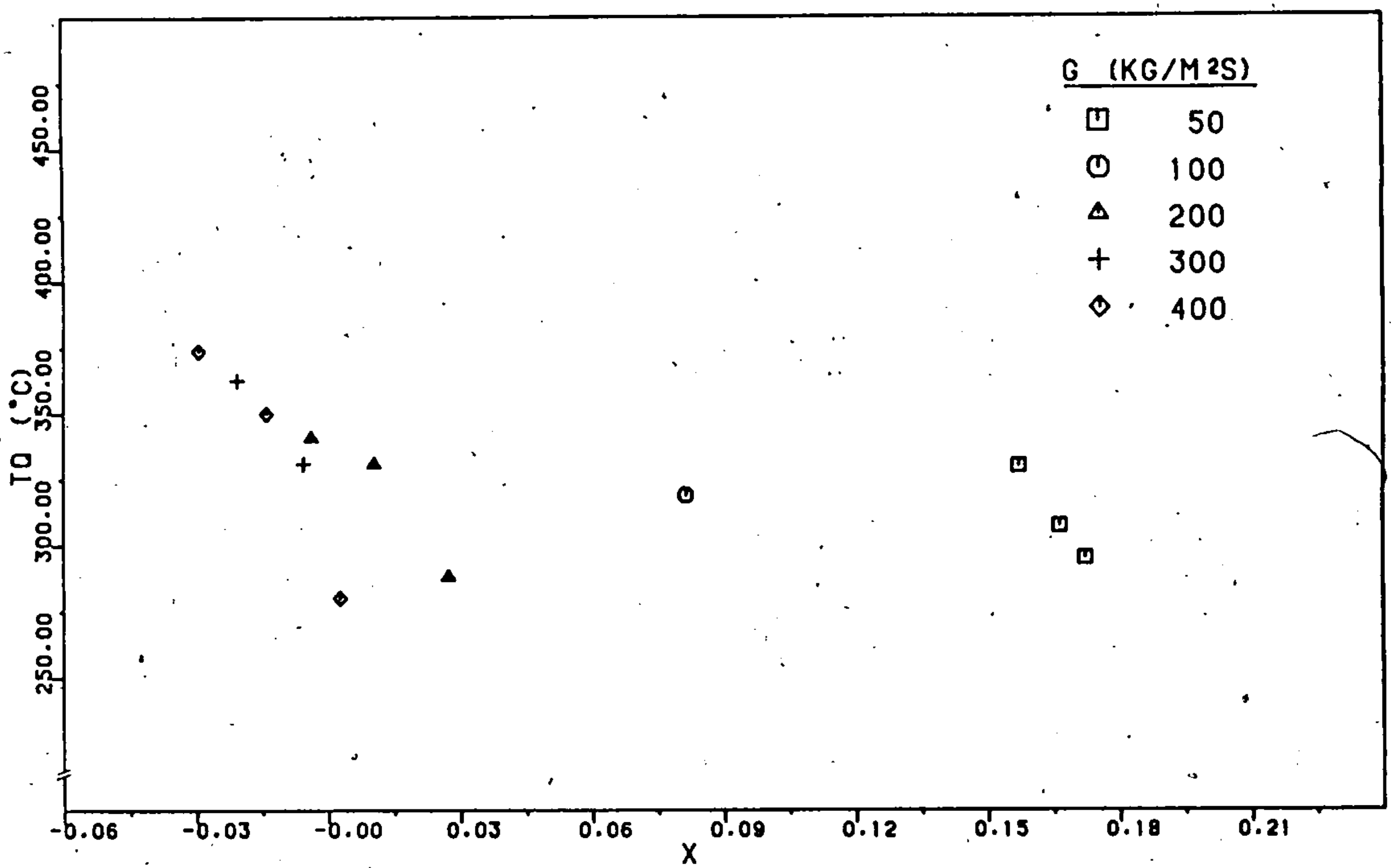

FIG. 5.17 MEASURED QUENCH TEMPERATURE VS LOCAL QUALITY FOR FIXED MASS FLUX FOR 10,300 RUN SERIES AT P=550 kPa

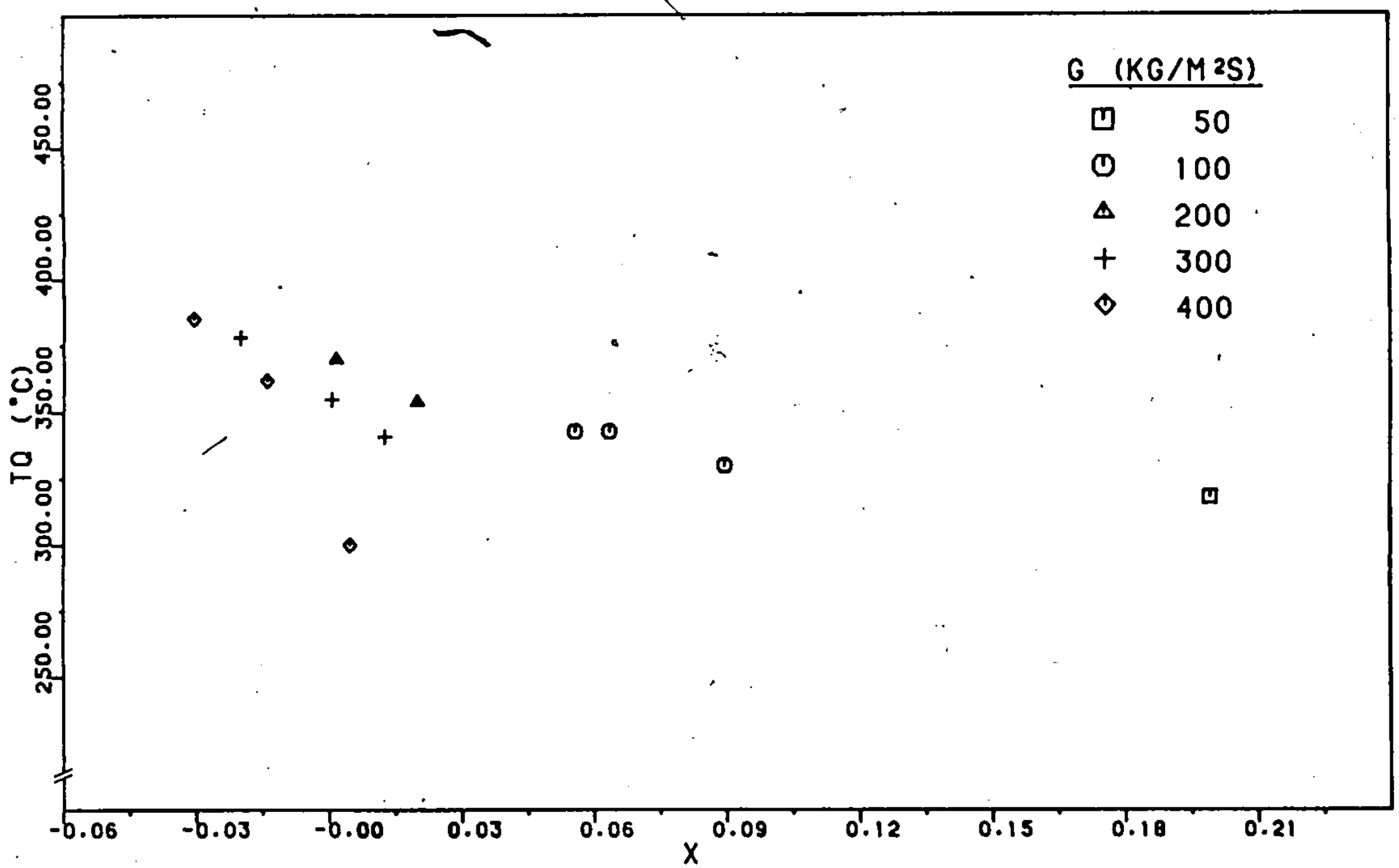

FIG. 5.18 MEASURED QUENCH TEMPERATURE VS LOCAL QUALITY FOR FIXED MASS FLUX FOR 10,300 RUN SERIES AT P=687 kPa

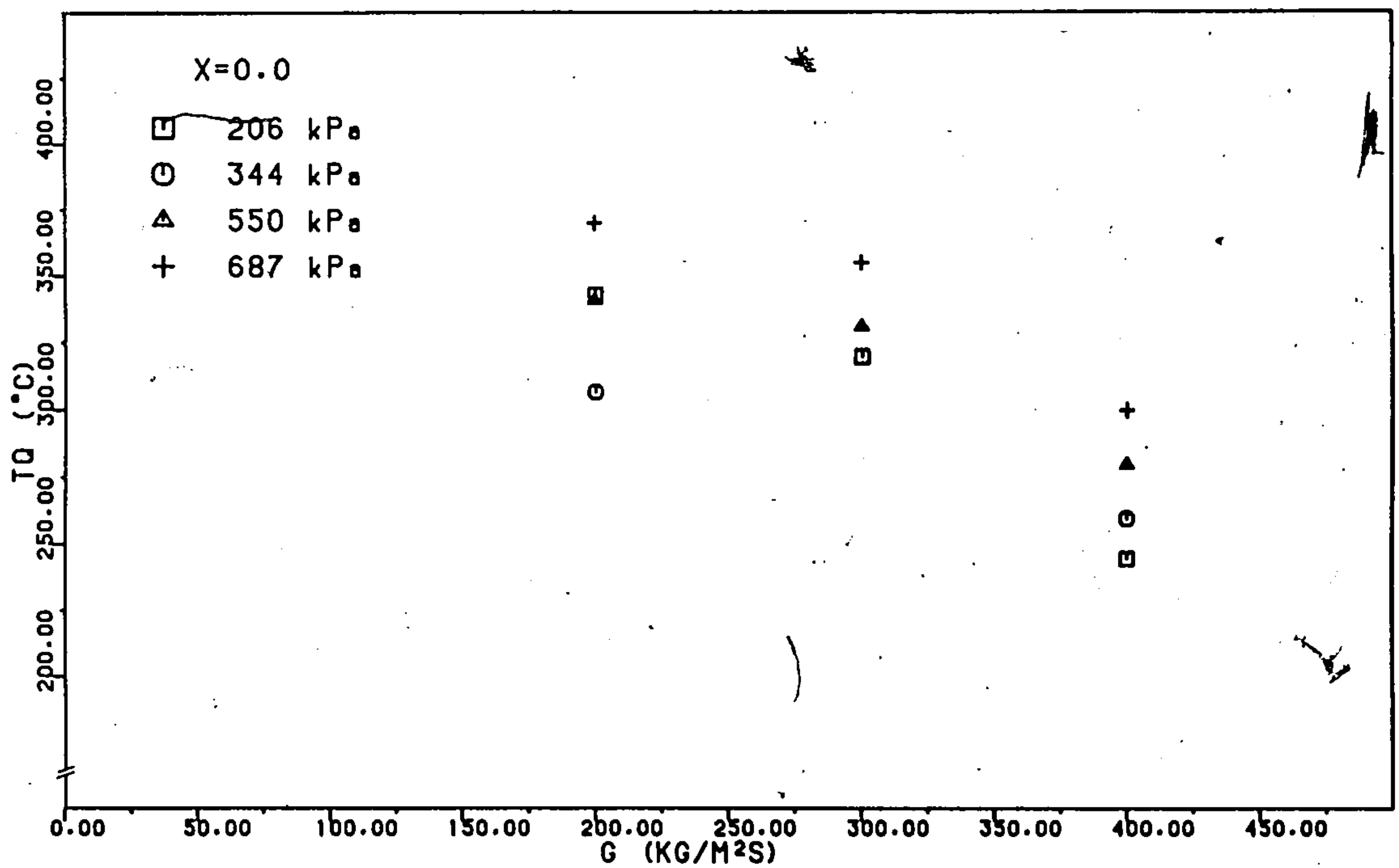

FIG. 5.19 MEASURED QUENCH TEMPERATURE VS MASS FLUX FOR FIXED LOCAL QUALITY FOR 10,300 RUN SERIES

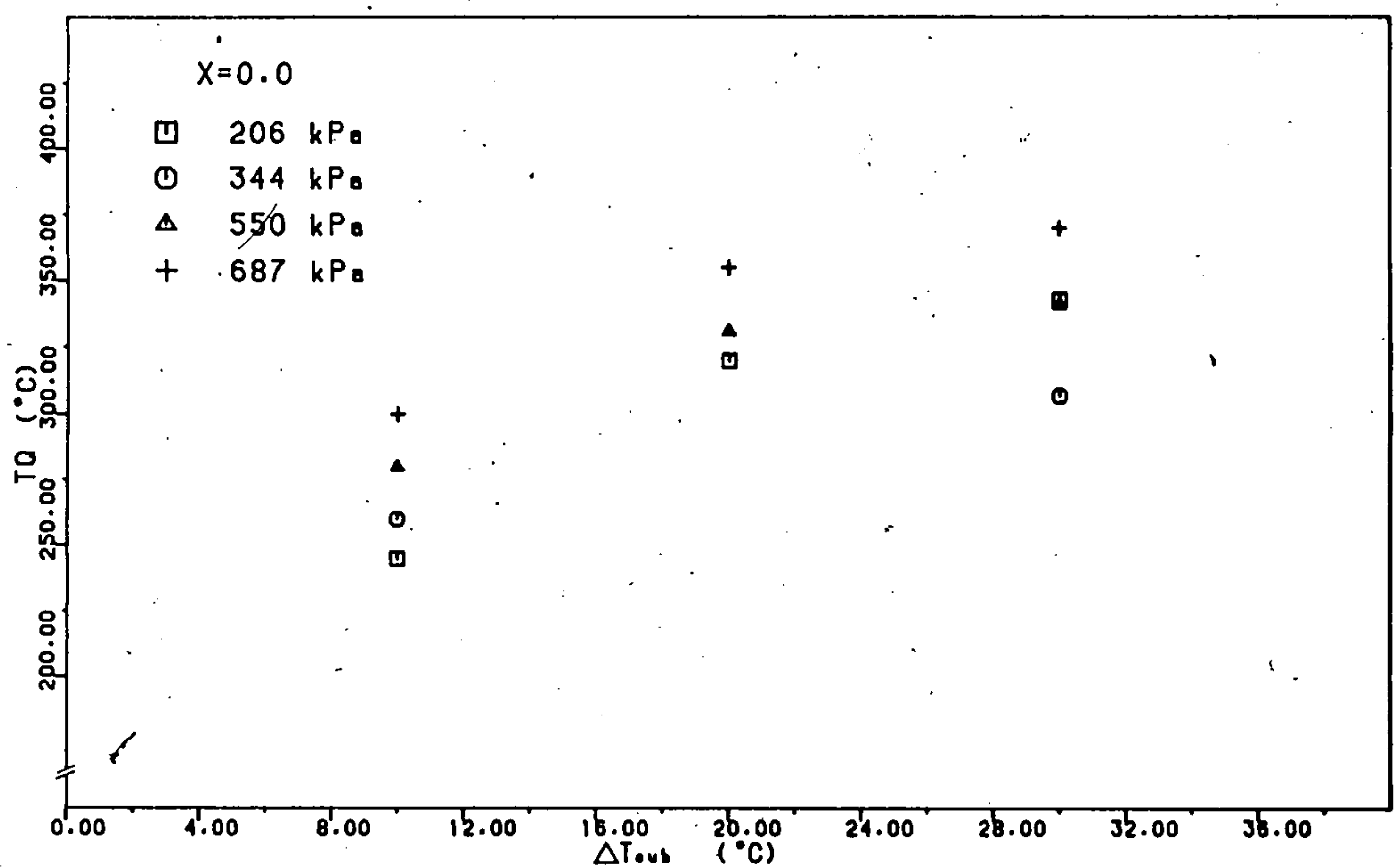

FIG. 5.20 MEASURED QUENCH TEMPERATURE VS INLET SUBCOOLING FOR FIXED LOCAL QUALITY FOR 10,300 RUN SERIES

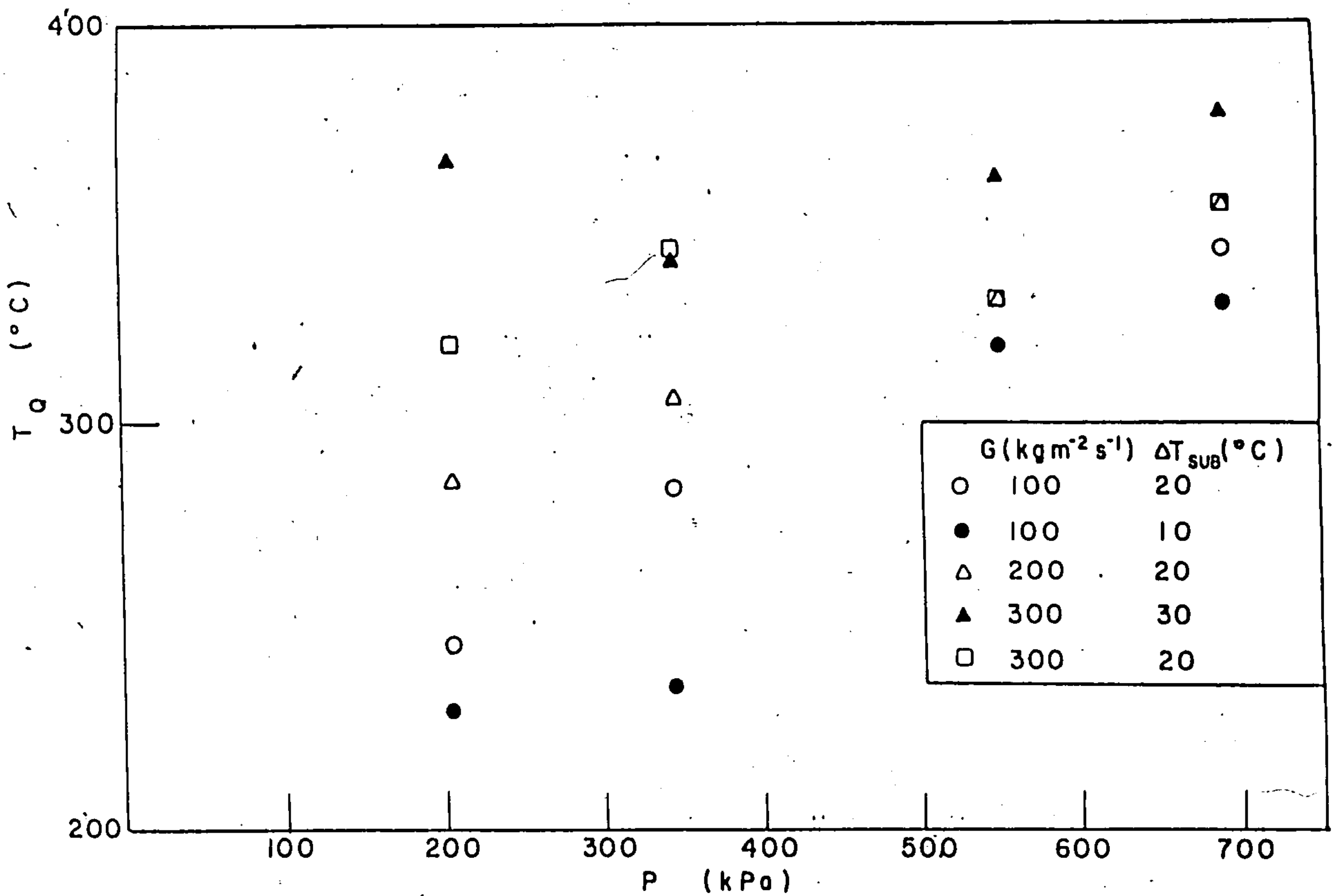

FIG. 5.21 MEASURED QUENCH TEMPERATURE VS PRESSURE FOR FIXED MASS FLUX AND INLET SUBCOOLING FOR 10,300 RUN SERIES

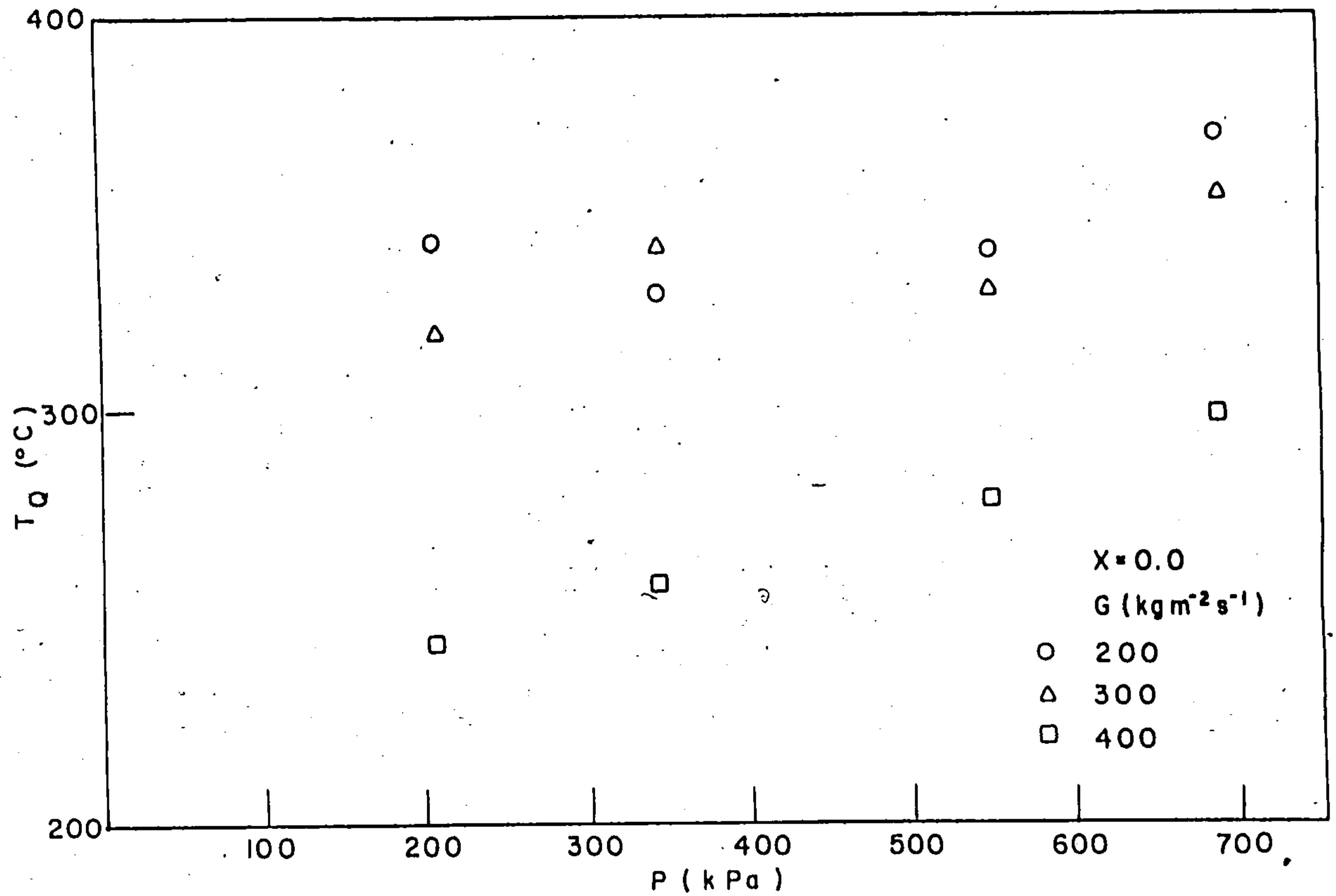

FIG. 5.22 MEASURED QUENCH TEMPERATURE VS PRESSURE FOR FIXED LOCAL QUALITY AND MASS FLUX FOR 10,300 RUN SERIES

5.5 PARAMETRIC TRENDS STUDY

5.5.1 Mass flux effect

Figures 5.7 - 5.10 show the plots of measured quench temperature against mass flux for a fixed inlet subcooling. In general, the quench temperature increases with mass flux. It is expected that higher mass flux improves convective heat transfer between the wall and the fluid. Hence, rewet can occur at a higher temperature.

When studing the effect of the quench temperature vs mass flux for a fixed local quality as described in Fig. 5.5, the quench temperature decreases initially, then increases with mass flux for atmospheric pressure. This can be explained by the following. In order to maintain a constant local quality (x), inlet subcooling has to decrease as mass flux increases. Since increasing mass flux and associated decreasing inlet subcooling have an opposite effect on the quench temperature, the resulting trend of the quench temperature vs mass flux is a net effect of two opposing factors. As for a slightly elevated pressure, the quench temperature decreases continuously with mass flux as shown in Fig. 5.19. It is believed that the mass flux range is not sufficiently large to see the complete trend. Therefore, no definite trend can be established for the mass flux effect on the true quench temperature for a fixed local quality.

5.5.2 Inlet subcooling effect

The effect of inlet subcooling for the quench temperature at a fixed mass flux is shown in Fig. 5.11 - 5.14. A quench temperature increase with inlet subcooling is observed. Usually, higher inlet subcooling enhances heat transfer resulting in a higher quench temperature.

Figure 5.6 shows the quench temperature vs inlet subcooling at a fixed local quality for atmospheric pressure. The quench temperature first decreases and then increases with inlet subcooling. This trend can be explained by the similar argument for the mass flux effect: the trend represents a net effect of two opposite factors, i.e., increasing mass flux and associated decreasing inlet subcooling. However, in Fig. 5.20 the quench temperature increases continuously with inlet subcooling for a given elevated pressure and local quality. It is believed that inlet subcooling is not low enough to see the decreasing portion.

5.5.3 Quality effect

One simple conclusion can be drawn for this effect, i.e., the quench temperature always decreases with increasing local quality. Figures 5.15 - 5.18 illustrate the quality effect. Higher quality is accompanied by more vapour. As a result, heat transfer becomes less effective; hence, the lower quench temperature is expected.

5.5.4 Pressure effect

The measured quench temperature has been plotted against pressure. Figure 5.21 is a plot for a given set of mass flux and inlet subcooling, and Fig. 5.22 is for a fixed mass flux and quality. Generally, the quench temperature increases with pressure except for higher mass flux and inlet subcooling, where the quench temperature is not very sensitive with pressure, but the slightly increasing trend can still be observed.

Increasing pressure has the net effect of promoting heat transfer in the pressure range of present experiments. It is due to the fact that the experimental pressures are well below 4 MPa (see section 2.6.3).

5.6 GENERAL DISCUSSION

Due to a limited number of thermocouples installed in the test section, there is an uncertainty about the actual location of true quench. If true quench is detected at a given thermocouple station, the true quench could actually occur anywhere between the half distance with the neighbouring thermocouple station in the upstream direction and the half distance with the neighbouring thermocouple station in the downstream direction.

A successful run was defined by spontaneously collapse of vapour film, i.e., impulse cooling collapse, or sometimes dispersed flow rewet for the case of small mass flux and small inlet subcooling. Normally, no experimental run is accepted as a successful run when true quench is detected very near the bottom hot patch, (eg., at thermocouple station located at 1 cm from the BHP). In this case, it is possible that true quench initiates at BHP. However, for some runs when the true quench is detected at the same location, the data may be accepted if the location of true quench temperature follows an expected trend.

After true quench occurs, the quench front propagates in both upstream and downstream directions. The two neighbouring thermocouples of the true quench thermocouple register slightly higher quench temperatures.

This is referred to as the apparent quench temperature which is under a strong influence of axial conduction. Figures 5.23 and 5.24 indicate the true quench temperature, the apparent quench temperature and the wall temperature at various locations at time of true quench.

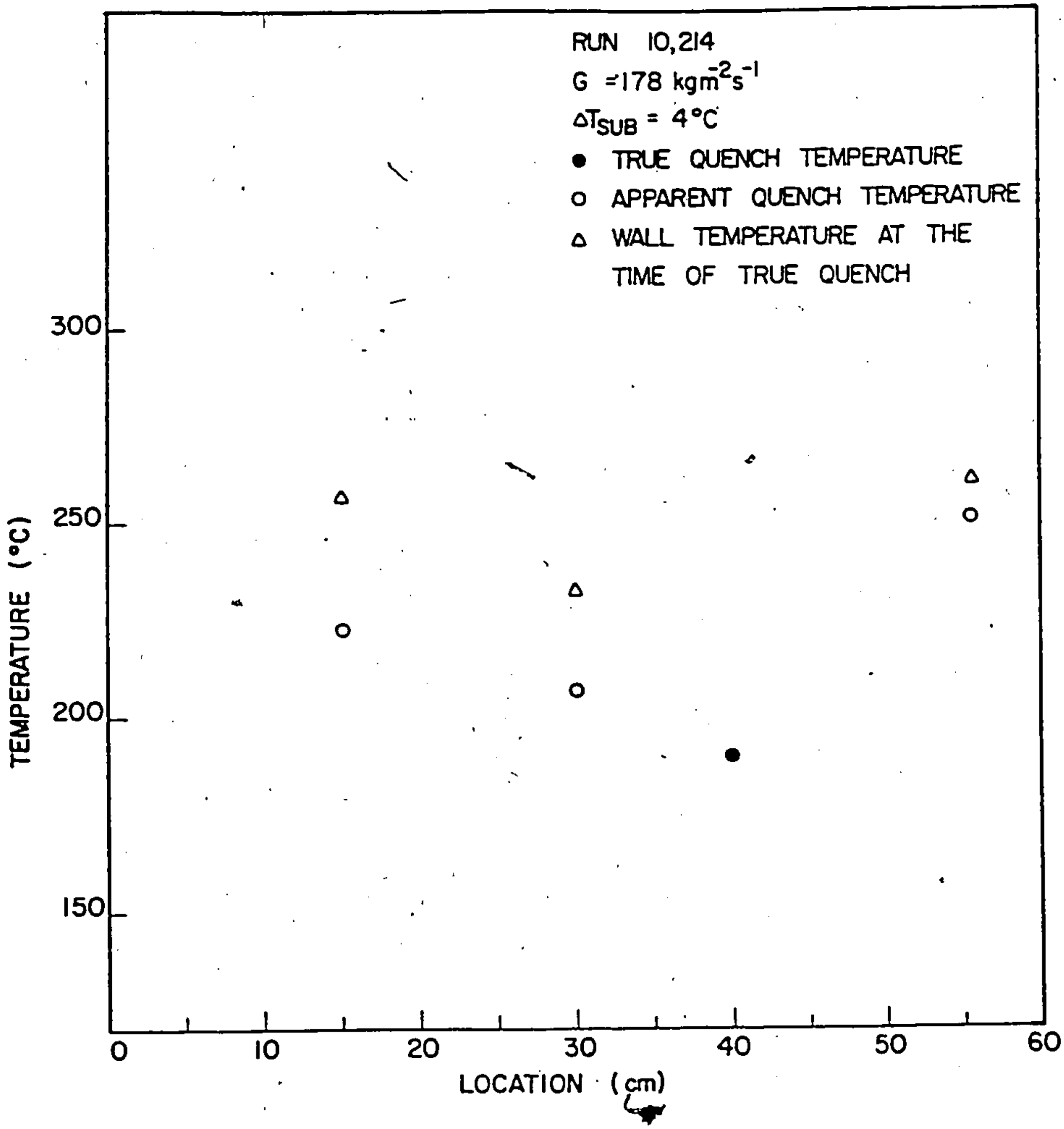

FIG. 5.23 TRUE QUENCH TEMPERATURE AND APPARENT QUENCH TEMPERATURES AT VARIOUS LOCATION FOR RUN 10,214

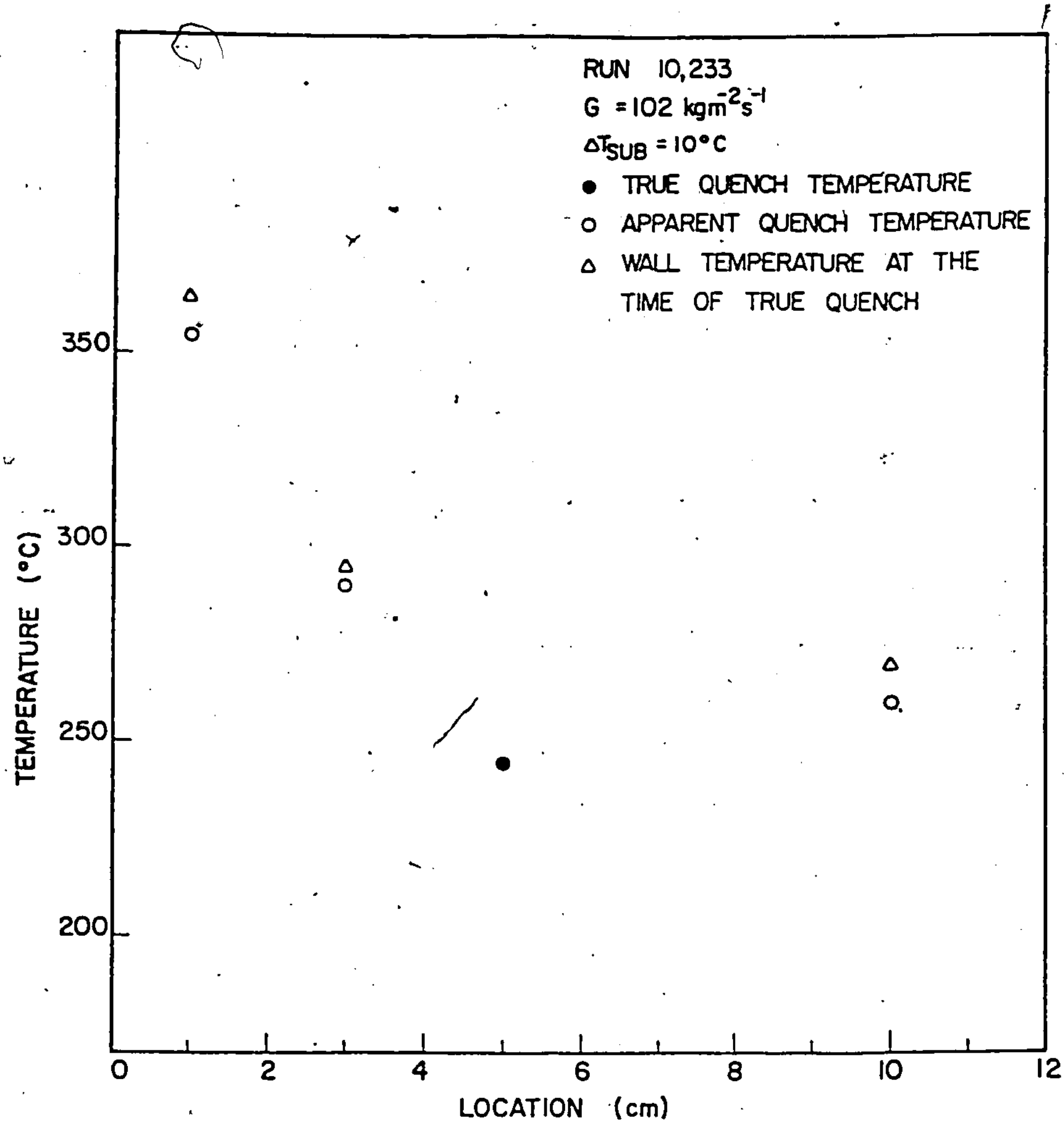

FIG. 5.24 TRUE QUENCH TEMPERATURE AND APPARENT QUENCH TEMPERATURES AT VARIOUS LOCATION FOR RUN 10,233

5.7 CORRELATION AND COMPARISON

After the study of effects of parameters, an empiricial correlation of the true quench temperature as a function of pressure, mass flux and inlet subcooling was derived as follows:

$$T_Q = 145.98 + 0.1347\ P + 0.1605\ G + 3.5069\ \Delta T_{sub} \qquad (5.1)$$

T_Q = true quench temperature in °C

P = pressure in kPa

G = mass flux in kg/m^{2}s

ΔT_{sub} = inlet subcooling in °C

The coefficients of Eq.5.1 were obtained from 10,300 run series with a total of 54 data points using the SPSS statistical package (Appendix F). The root mean square error of the correlation is 7.75%. The comparison between the correlation and the experimental data is shown in Fig. 5.25 to 5.30.

An attempt was made to correlate the true quench temperature based on local quality, mass flux and pressure.

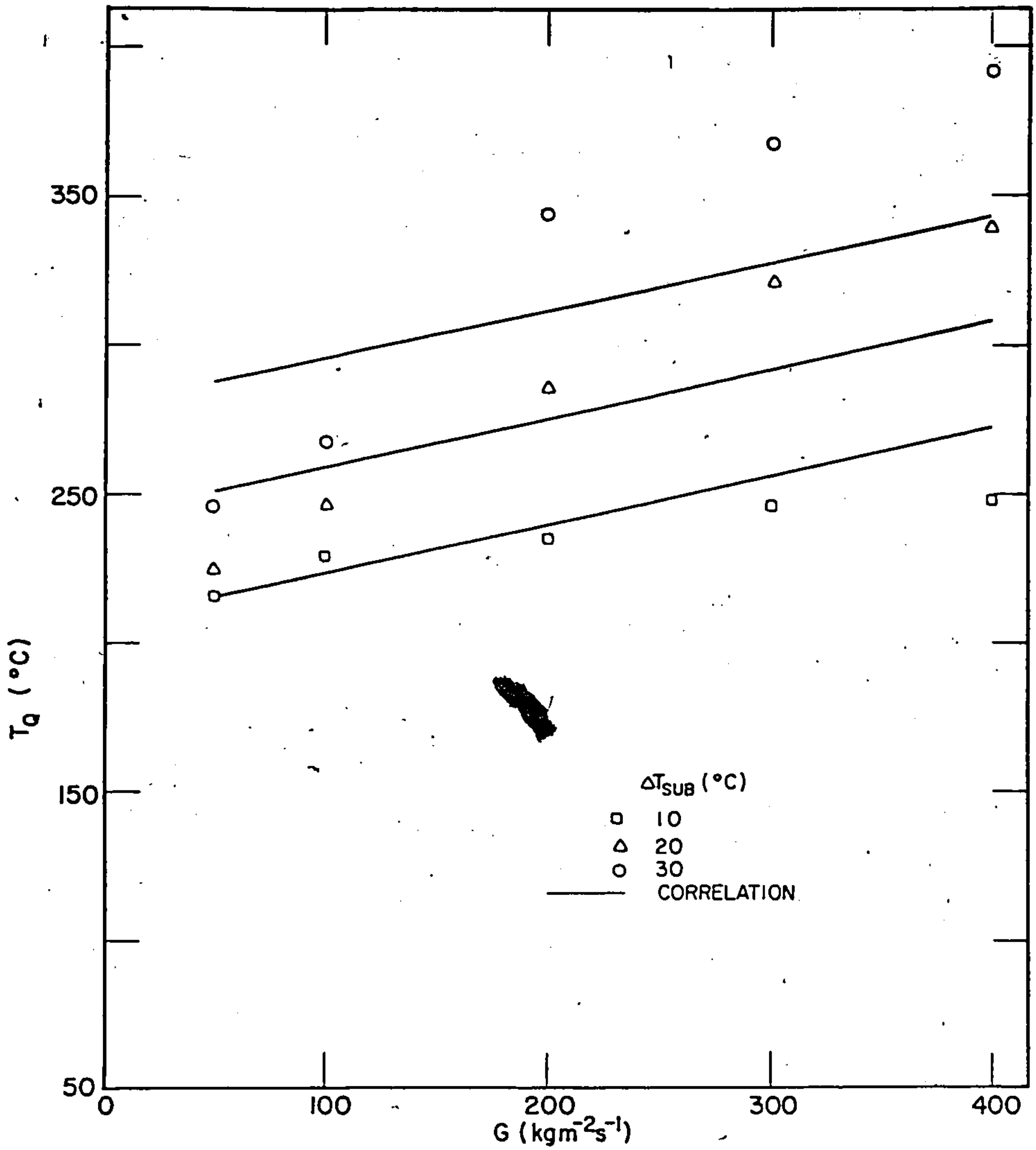

FIG. 5.25 COMPARISON OF CORRELATION WITH EXPERIMENTAL DATA FROM 10,300 RUN SERIES AT P=206 kPa

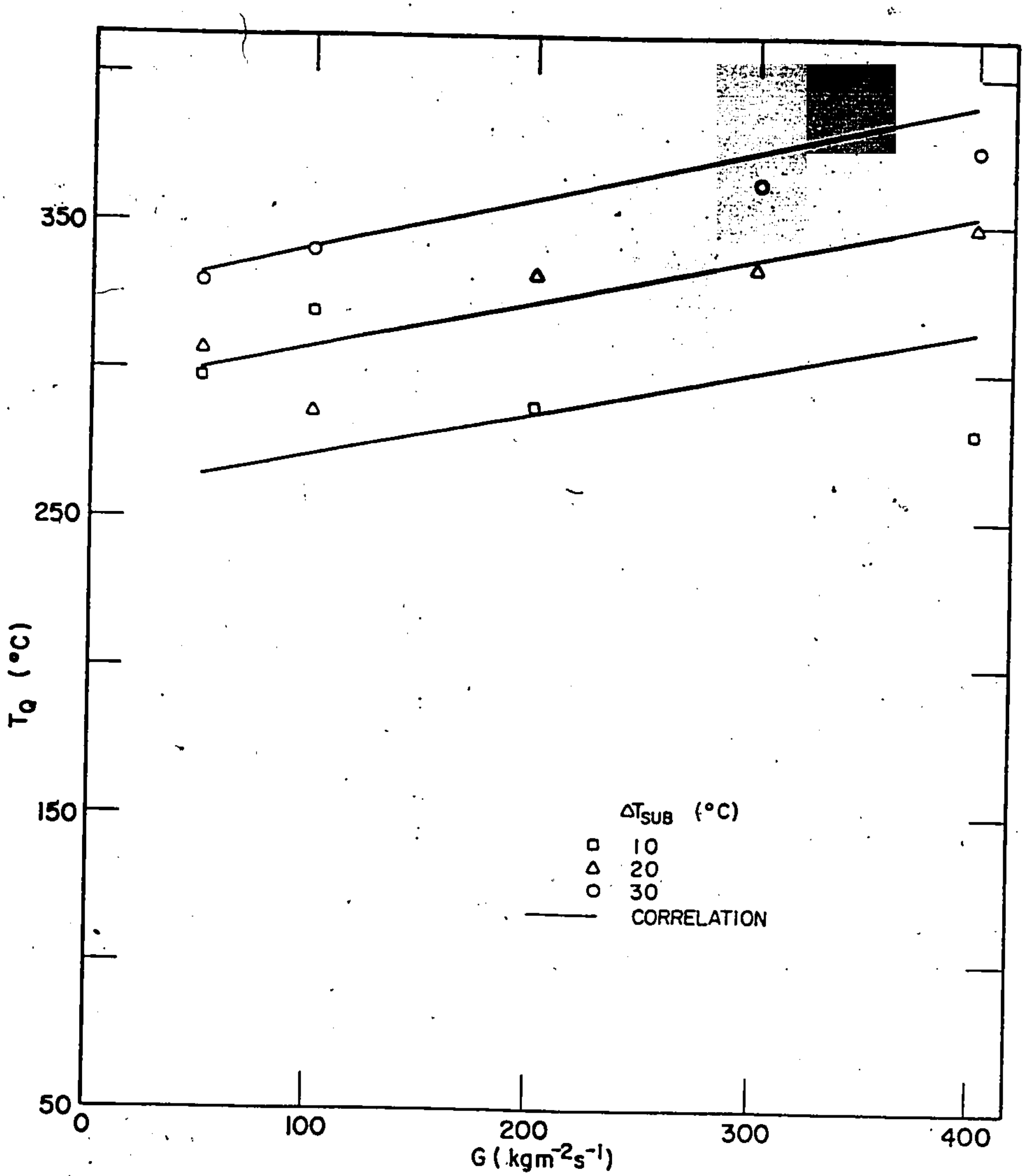

FIG. 5.26 COMPARISON OF CORRELATION WITH EXPERIMENTAL DATA FROM 10,300 RUN SERIES AT P=550 kPa

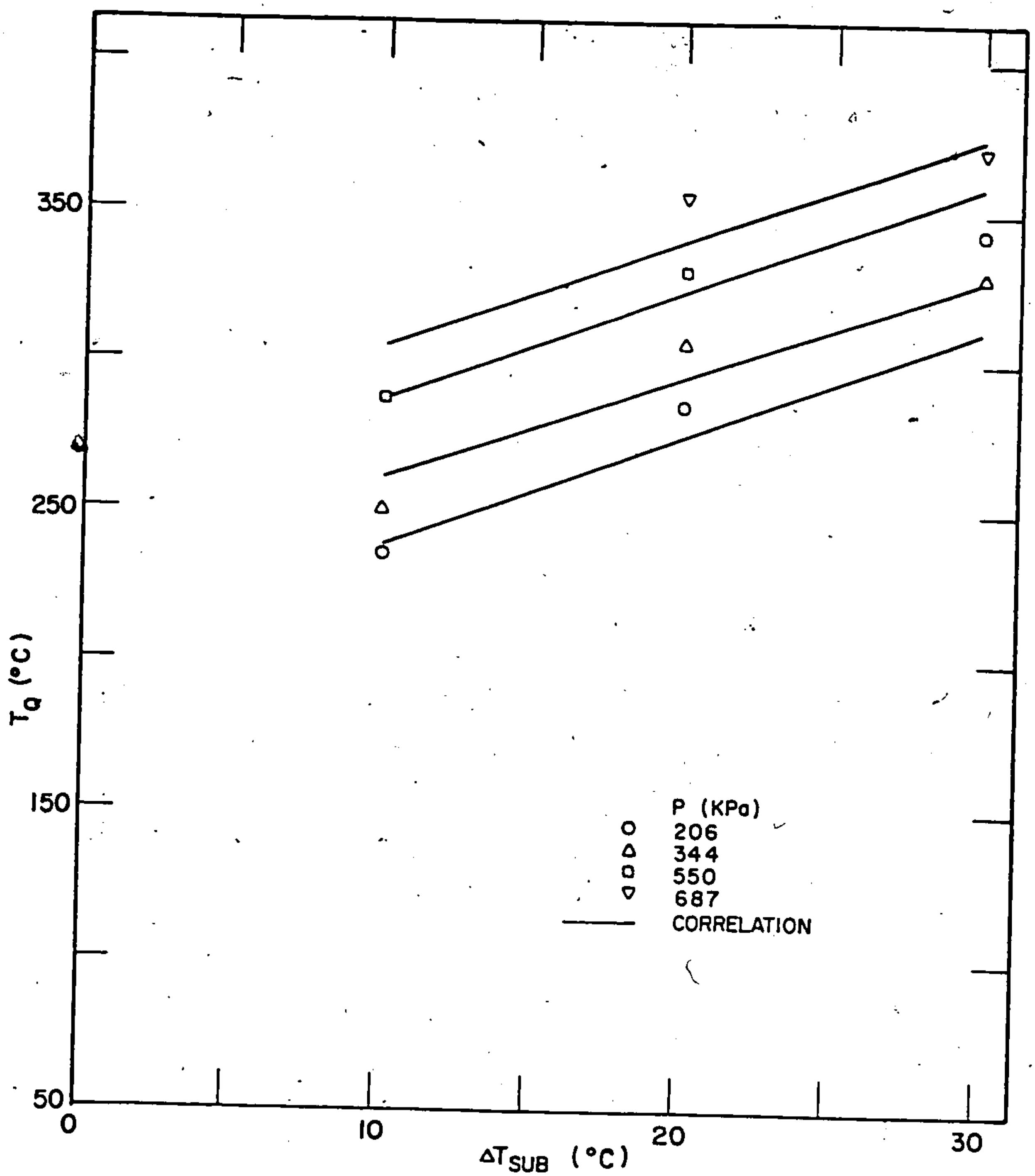

FIG. 5.27 COMPARISON OF CORRELATION WITH EXPERIMENTAL DATA FROM 10,300 RUN SERIES AT G=200 $kgm^{-2}s^{-1}$

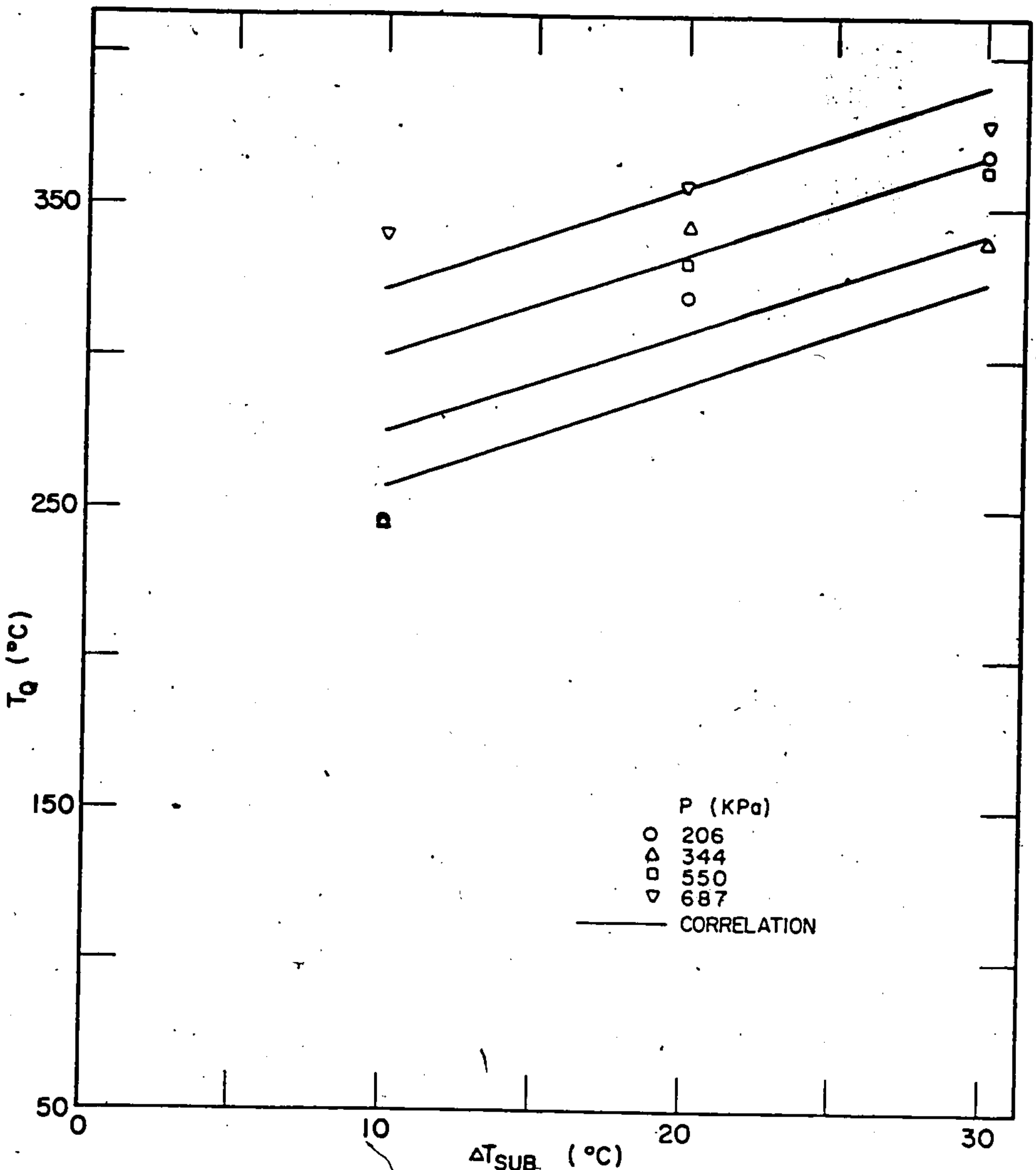

FIG. 5.28 COMPARISON OF CORRELATION WITH EXPERIMENTAL DATA FROM 10,300 RUN SERIES AT $G=300\ kgm^{-2}s^{-1}$

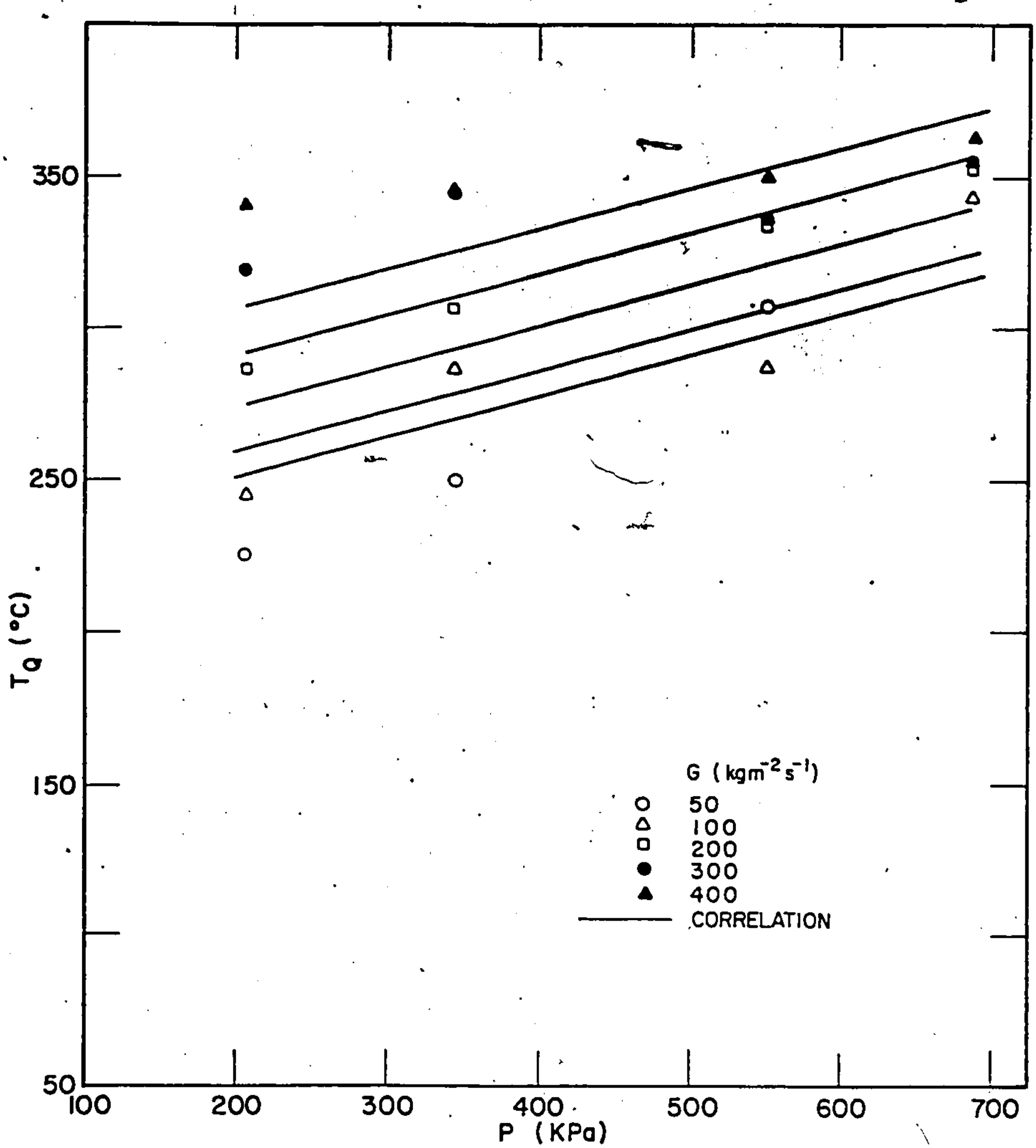

FIG. 5.29 COMPARISON OF CORRELATION WITH EXPERIMENTAL DATA FROM 10,300 RUN SERIES AT ΔT_{SUB}=20°C

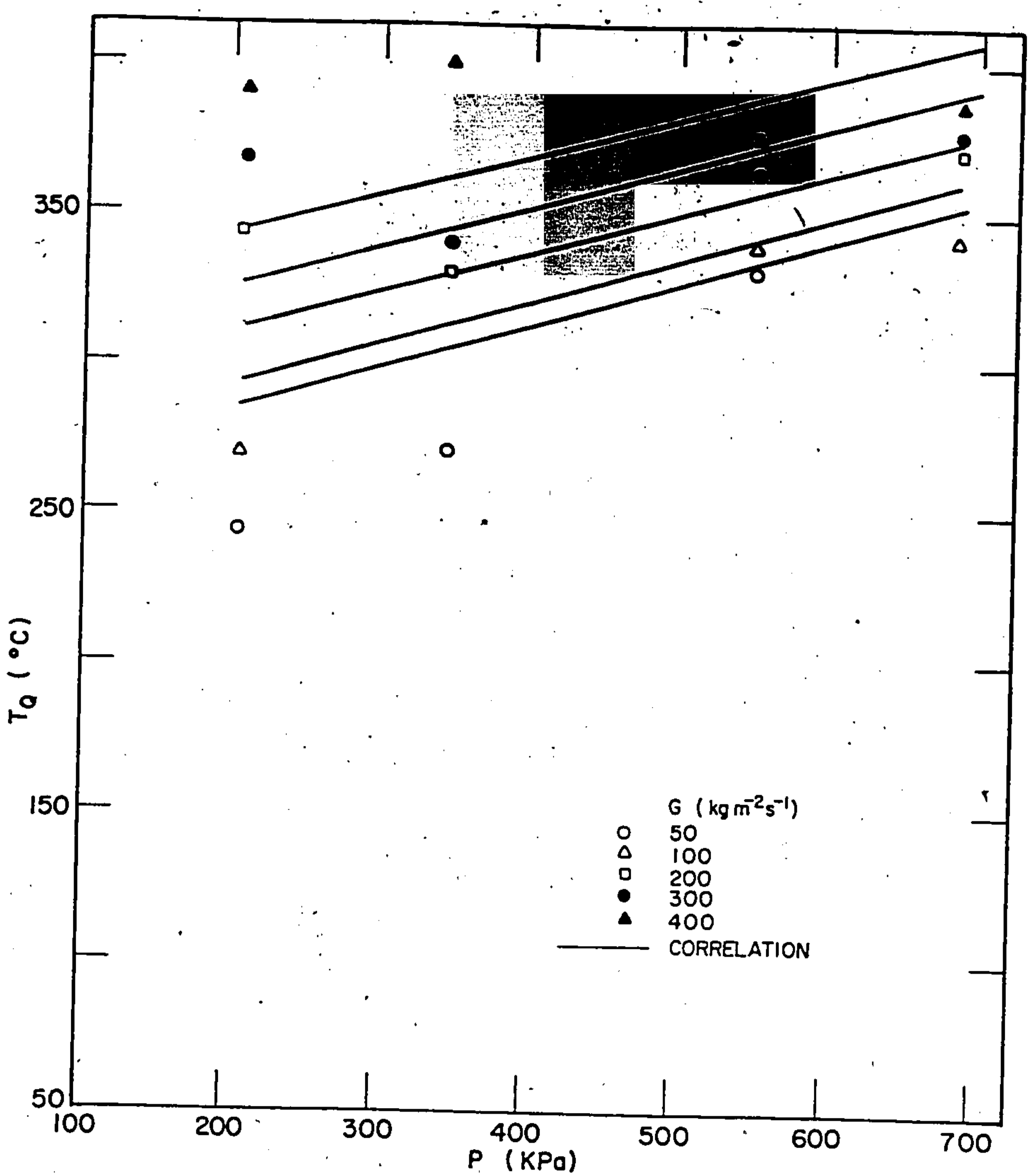

FIG. 5.30 COMPARISON OF CORRELATION WITH EXPERIMENTAL DATA FROM 10,300 RUN SERIES AT ΔT_{SUB}=30°C

Since many true quench occured very near the inlet test section, the entrance effect is very strong. Therefore, the correlation based on local quality, mass flux and pressure is not very successful.

In the literature, there is very little work published on true quench temperature measurements. Fung [28] and Stewart [16] reported the first set of the true quench temperature data at atmospheric pressure and at high pressure, respectively. Their results are shown in Tables 5.1 and 5.2. While they were performing their film boiling experiments, occasionally they obtained some true quench temperature data at the termination of steady-state film boiling. Fung only obtained 12 data points from his experiments. Stewart has produced more true quench temperature data, but at much higher pressure range (2-9 MPa).

Comparing the present data with those of Fung's under similar flow conditions, the true quench temperature in the present study is about 10% lower. It is probably due to different hot patch conditions. The present experiment has a longer and hotter hot patch. Therefore, enthalpy at the exit of the bottom hot patch is higher. Higher enthalpy decreases heat transfer. Consequently, our true quench temperature is lower.

TABLE 5.1 MINIMUM FILM BOILING TEMPERATURE (FUNG)

RUN NAME	T-MIN (C)	QUALITY
A 50.605	365.	-.154800E-02
A 50.104	302.	.218500E-01
A100.207	313.	.390580E-03
C100.057	293.	.252773E-01
C100.10D	335.	.923900E-02
C100.205	335.	.187310E-02
C150.106	310.	.994483E-03
C250.205	419.	-.134619E-01
C250.303	414.	-.214547E-01
C350.205	427.	-.180936E-01
C500.206	405.	-.143072E-01
C500.206	405.	-.143072E-01

TABLE 5.2 MINIMUM FILM BOILING TEMPERATURE (STEWART)

RUN	TIME	DATE	P OUT (KPA)	P DROP (KPA)	HOTP POW (KW)	T/S POW (KW)	FLOW (KG/H)	T IN (C)	T OUT (C)	MINF TEMP (C)	MINF POWER (KW)	MINF QUAL	T/C
3311	13:00:22	07/08/80	3031.	39.	1.57	5.66	81.6	223.1	233.4	395.9	5.13	.021	16
2311	15:57:59	07/08/80	2013.	39.	1.36	3.92	67.9	200.6	210.5	378.9	3.92	.018	16
2421	12:28:07	26/09/80	2028.	44.	1.42	7.07	118.3	190.2	209.6	396.2	6.52	-.019	16
2321	16:00:58	26/09/80	2036.	41.	1.38	6.24	79.6	190.1	210.0	389.3	5.74	-.013	17
2521	15:24:03	29/09/80	1998.	50.	1.57	7.52	208.6	190.5	209.3	377.6	7.52	-.029	16
2411	15:50:27	01/10/80	2013.	44.	1.37	4.25	117.0	200.3	209.2	350.4	3.98	-.002	16
2431	11:55:56	03/10/80	2006.	47.	1.63	11.38	118.8	171.2	209.2	466.2	11.10	-.053	17
2211	12:34:19	08/10/80	2036.	39.	1.32	3.81	48.8	201.3	209.6	386.3	3.81	.034	16
2221	15:50:29	08/10/80	2028.	39.	1.34	4.93	48.0	191.1	209.9	390.4	4.61	.010	17
2121	15:26:56	09/10/80	1938.	39.	1.32	4.01	26.1	189.6	210.0	388.7	3.66	.067	16
2111	10:19:11	10/10/80	2036.	39.	1.31	3.54	26.7	200.0	210.2	383.8	3.30	.077	16
4321	14:27:40	06/08/80	3997.	39.	1.73	6.74	80.3	231.0	249.6	419.9	6.63	.011	16
3321	16:06:20	06/08/80	3016.	41.	1.64	6.93	78.7	211.4	233.2	425.1	6.72	.004	16
4331	10:32:11	25/09/80	4072.	41.	1.73	11.80	83.3	210.2	250.4	441.1	11.36	-.042	17
4311	12:15:54	25/09/80	4034.	41.	1.54	5.80	80.2	240.0	250.5	405.8	5.44	.023	16
4421	14:50:44	25/09/80	4064.	44.	1.65	8.26	116.1	229.5	250.8	424.1	7.83	-.013	16
4411	16:15:45	25/09/80	4080.	44.	1.59	6.09	117.4	240.8	250.2	397.9	5.71	.008	16
4211	14:27:50	14/10/80	3997.	39.	1.61	5.72	48.0	240.4	249.3	418.1	5.31	.064	16
4111	11:29:36	15/10/80	3936.	39.	1.48	5.15	27.6	240.4	249.5	417.3	4.82	.117	16
4121	15:16:13	15/10/80	4019.	39.	1.57	5.59	26.8	230.3	249.8	424.7	5.25	.106	16
4221	12:17:26	16/10/80	4019.	41.	1.66	6.11	48.9	230.7	249.5	426.4	6.11	.044	16
6421	13:06:04	05/08/80	5980.	39.	1.87	8.77	121.5	255.2	275.6	428.6	8.25	-.011	16
6321	15:40:17	05/08/80	6018.	39.	1.72	7.67	82.6	256.0	276.1	432.6	7.07	.006	16
6331	21:02:55	14/08/80	5972.	39.	1.96	10.97	80.9	239.7	275.5	468.8	10.97	-.013	16
6341	22:26:19	14/08/80	5912.	39.	2.11	12.60	81.3	223.1	275.8	477.9	11.53	-.069	18
6521	17:44:30	08/09/80	6018.	41.	2.02	9.44	204.9	256.3	275.4	418.6	8.55	-.028	16
6421	10:30:51	09/09/80	5972.	41.	1.90	9.18	118.8	255.8	275.5	426.1	8.48	-.006	16
6431	11:50:53	09/09/80	6010.	41.	1.95	11.91	118.6	239.9	275.7	429.1	10.98	-.056	17
6441	14:19:00	09/09/80	6033.	44.	2.23	15.04	118.0	223.5	275.8	465.7	14.25	-.091	17
8331	16:49:02	14/08/80	7993.	39.	1.75	10.18	85.6	262.4	295.5	420.4	9.00	-.048	17
8341	18:04:30	14/08/80	7910.	39.	1.94	12.60	82.5	245.0	295.6	470.8	12.48	-.080	18
8431	14:52:25	31/07/80	7993.	39.	2.13	13.38	110.7	252.5	295.7	452.0	13.38	-.060	16
8431	16:24:36	31/07/80	8008.	39.	1.95	9.97	110.7	262.4	295.8	459.1	8.80	-.050	16
8421	14:52:06	10/09/80	7986.	41.	1.75	8.06	118.3	276.4	295.7	425.0	8.06	-.013	16
8431	10:30:15	11/09/80	7978.	41.	1.90	11.65	120.2	260.3	295.6	454.6	11.05	-.054	16
8441	12:00:19	11/09/80	8001.	44.	2.07	13.89	117.9	245.6	295.4	455.0	12.96	-.091	16
8521	15:02:41	11/09/80	7986.	44.	1.92	8.39	209.5	276.4	295.3	408.7	8.39	-.035	16
8531	16:15:20	11/09/80	8001.	52.	2.09	13.97	209.2	260.5	295.2	443.8	13.25	-.077	16
8531	17:12:09	11/09/80	8008.	50.	2.13	13.36	209.4	260.6	295.1	444.7	13.10	-.077	16
8541	11:55:47	12/09/80	7986.	50.	2.43	18.36	207.0	244.8	295.5	424.1	17.90	-.125	18
8541	13:23:06	12/09/80	7963.	50.	2.18	15.94	206.1	244.8	295.1	452.5	15.60	-.121	16
8321	15:27:28	12/09/80	8054.	41.	1.83	8.40	83.1	276.4	295.8	432.8	7.99	.011	16
8221	15:42:24	16/10/80	7978.	41.	1.63	7.54	49.2	276.4	295.1	439.4	7.59	.055	16
8121	11:13:21	17/10/80	7948.	39.	1.56	6.46	28.4	274.5	295.9	433.5	6.46	.117	16
8231	15:15:09	17/10/80	8008.	41.	1.67	8.84	49.3	259.6	295.5	426.1	8.80	-.011	17
9521	12:29:11	15/09/80	9004.	47.	1.71	7.92	209.9	285.4	303.8	406.1	7.37	-.042	16
9721	15:30:06	15/09/80	9004.	55.	2.91	16.90	623.0	285.8	300.4	405.5	16.24	-.049	16
9711	17:28:55	17/09/80	8959.	55.	2.60	7.33	618.8	294.3	300.5	371.9	7.33	-.022	16
9721	10:39:39	18/09/80	9087.	55.	2.79	17.07	625.2	286.2	301.0	397.4	16.63	-.050	16
9541	12:16:35	18/09/80	9064.	50.	2.21	18.06	206.5	255.6	304.1	457.5	18.06	-.121	16
9441	15:14:51	18/09/80	9087.	44.	1.89	12.89	120.7	255.6	304.5	448.7	[illegible]	[illegible]	[illegible]

Stewart's true quench temperature correlation was formulated based on his high pressure experimental data and Fung's low pressure data. He correlated the true quench temperature as a function of pressure and quality.

$x \leq 0$, $P < 9$ MPa

$$T_{min} = 284.7 + 44.11P - 3.72P^2 - \frac{X \cdot 10^4}{2.819 + 1.22P} \tag{5.2}$$

$x > 0$, $P < 9$ MPa

$$T_{min} = 284.7 + 44.11P - 3.72P^2 \tag{5.3}$$

P = pressure in MPa

T_{min} = minimum film boiling temperature in °C

Stewart's correlation is to be used here for comparison. For example, when $P = 0.2$ MPa and $X > 0$, $T_{min} = 293.4$°C is obtained from Stewart's correlation. Under similar conditions, our true quench temperature varies from 216°C at low mass flux to 285°C at high mass flux. Obviously, our true quench temperature is not only a function of local quality and pressure, it also depends on mass flux.

It is felt that Stewart's correlation incorporated very limited experimental data at low pressure. Thus, it is impossible to show the full effect of quality and mass flux.

Chapter VI
CONCLUSIONS

The true quench temperature for water under forced convective condition inside a heated channel was investigated in this study. The information of the true quench temperature is needed to predict the onset of true quench in terms of flow coditions.

The true quench temperature has a direct application in the post-dryout study under LOCA conditions, more specifically, in a sub-channel analysis. The other applications include the design of water-tube boilers, pipe stills, refrigeration equipment, evaporators and many other major items in chemical and power plants. Whenever dryout occurs in a system, the true quench temperature phenomenon can be applied during the rewetting process.

Below is the summary of this study:

1. The true quench temperature is defined as the quench temperature at the onset of rewetting in a flow channel. It has two important features: (a) the onset of rewetting can occur anywhere along the flow channel and (b) axial conduction is absent. The true

quench temperature based on this study is a function of flow parameters.

2. In general, the true quench temperature increases with mass flux, inlet subcooling and pressure, but decreases with increasing quality.
3. An empirical correlation for the true quench temperature as a function of mass flux, pressure and inlet subcooling was formulated. The comparison between the correlation and the experimental data shows fair agreement.
4. When comparing Stewart's correlation with the present data, his true quench temperature appears to be higher under similar flow conditions. It is believed that his correlation incorporated very limited low pressure data and does not show the full effect of quality and mass flux.
5. The true quench temperature is always lower than the apparent quench temperature.
6. The true quench location tends to move toward the bottom hot patch as mass flux and inlet subcooling increase.
7. A thicker test tube requires more power for heating; therefore the true quench location is pushed toward in the downstream direction.

8. Based on preliminary artifical cold spot tests, the length effect on the quench temperature is minimal, except when quench occurs very near the bottom hot patch.
9. The local quality at the true quench location is strongly influenced by the film boiling heat flux of the bottom hot patch.
10. A properly functioning hot patch is strongly dependent on the method of soldering. An improper soldering process may cause the failure of the performance of the hot patch, i.e., the quench front initiates from the hot patch.
11. The measurements of the true quench temperature at slightly higher pressure (greater than 100 psia) are in progress at the present time. A new correlation will be formulated using the new experimental data and the data obtained from the present investigation along with those of Stewart's high pressure data.

BIBLIOGRAPHY

1. Hsu, Y.Y. and Graham, R.W., Transport Processes in Boiling and Two-Phase System, McGraw Hill, 1976.

2. Greoneveld, D.C., "Heat Transfer Problems in Nuclear Power Reactors", Lecture notes presented at University of Ottawa, May, 1975.

3. Elias, E. and Chambre, P., "Inverted-annular Film Boiling Heat Transfer from Vertical Surfaces", Nuclear Engineering and Design, vol 64, pp 249-257, 1981.

4. Goodman, J. and Elias, E., Trans ANS 28, 1978.

5. Chi, J.W.H., "Slug Flow and Film Boiling of Hydrogen", ASME, 65-WA/HT-32, 1965.

6. Kalinin, E.K. et al, "Heat Transfer in Tubes with Rod Regime in the case of Flow Boiling of a Subcooled Liquid", Cocurrent Gas-Liquid Flow, Plenum, New York, 1969.

7. Groeneveld, D.C., "Heat Transfer Phenomena Related to the Boiling Crisis", Lecture notes on ISPRA course, May, 1980.

8. Hewitt, G.F. and Roberts, D.N., "Studies of Two-phase Flow Patterns by Simultaneous X-ray and Flash Photography", AERE-M 2159, HMSO, 1969.

9. Collier, J.G., Convective Boiling and Condensation, McGraw Hill, 1981.

10. Berenson, P.J., "Experiments on Pool-Boiling Heat Transfer", International Journal of Heat and Mass Transfer, Vol 5, pp 985-999, 1962.

11. Groeneveld, D.C., "Prediction Methods for Post-CHF Heat Transfer and Superheated Steam Cooling Suitable for Reactor Accident Analysis", Centre d'Etudes Nucleaires de Grenoble Report, May, 1982.

12. Iloeje, O.C., Plummer, D.N., Griffith, P., Rohsenow, W.M., "An Investigation of the Collapse and Surface Rewet in Film Boiling in Forced Vertical Flow", ASME paper, 73-WA/HT-20, 1973.

13. Kalinin, E.K. et al, "Investigation of the Crisis of Film Boiling in Channels", Paper Presented at the Winter Annual Meeting of ASME, 1969.

14. Cheng, S.C. et al, "Transition Boiling Heat Transfer in Forced Vertical Flow", Final Report, June 81-June 82, ANL Contract 31-109-38-5503.

15. Cheng, S.C. et al, "Transition Boiling Heat Transfer in Forced Vertical Flow", Quarter Report No. 23, July-Sept 1982, ANL Contract 31-109-38-5503.

16. Stewart, J.C., "Low Quality Film Boiling at Intermediate and Elevated Pressure", M.A.Sc. Thesis, University of Ottawa, 1981.

17. Simom, F.F. and Simomeau, R.J., "Transition from Film to Nucleate Boiling in Vertical Forced Flow", ASME Paper, 69-HT-26, 1969.

18. Spieglar, P. et al, "Onset of Stable Film Boiling and the Foam Limit", International Journal of Heat and Mass Transfer, Vol. 6, pp. 987-994, 1963.

19. Berenson, P.J., "Film Boiling Heat Transfer from a Horizontal Surface", Journal of Heat Transfer, Vol. 83, pp 351-358, 1961.

20. Plummer, D.N. Iloeje, O.C., Griffith, P. and Rohsenow, W.M., "A Study of Post Critical Heat Flux Transfer in a Forced Convection System", MIT Report, 1975.

21. Cheng, S.C., Ng, W.W.L. and Heng, K.T., "Measurement of Boiling Curves of Subcooled Water under Forced Convective Conditions", International Journal of Heat and Mass Transfer, Vol. 21, pp 1385-1392, 1978.

22. Comeau, J.G., "A Review of the Leidenfrost Phenomenon", M.Eng. Project, University of Ottawa, 1978.

23. Groeneveld, D.C. and Fung, K.K., "Forced Convective Transition Boiling: Review of Literature and Comparison of Prediction Methods", AECL-5543, 1976.

24. Stewart, J.C. and Groeneveld, D.C., "Low Quality and Subcooled Film Boiling of Water at Elevated Pressures", Nuclear Engineering and Design, Vol, 68, 1982.

25. Ragheb, H.S. and Cheng, S.C., "Observations in Transition Boiling of Subcooled Water under Forced Convective Conditions", International Journal of Heat and Mass Transfer, Vol 24, No.7, pp 1127-1137, 1981.

26. Cheng, S.C., Heng, K.T. and Ng, W., "A Technique to Construct a Boiling Curve from Quenching Data considering Heat Loss", International Journal of Multiphase Flow, Vol.3, pp 495-499, 1977.

27. IBM System/360 Continuous System Modeling Program User's Manual Program, No.360 A-CX-16X, 1972.

28. Fung, K.K., "Subcooled and Low Quality Film Boiling of Water in Vertical Flow at Atmospheric Pressure", Ph.D. Thesis, University of Ottawa, 1981.

Appendix A

HEAT LOSSES TEST

In the present experiments, the heat losses are mainly incurred at the copper connecting cables. For simplicity, it was assumed that one half of total losses going to the lower cable by conduction, and the other half to the upper cable [16]. This assumption also implies that the heat losses from the remainder of the test section through the insulation are negligible.

Heat losses tests were performed at the no-flow condition. The bottom and top hot patch were set at experimental temperatures, the direct power level and the average wall temperature were recorded by the Fluke datalogger. The test was repeated at different average wall temperature. Figure A.1 shows the result of the test with heat losses vs average wall temperature.

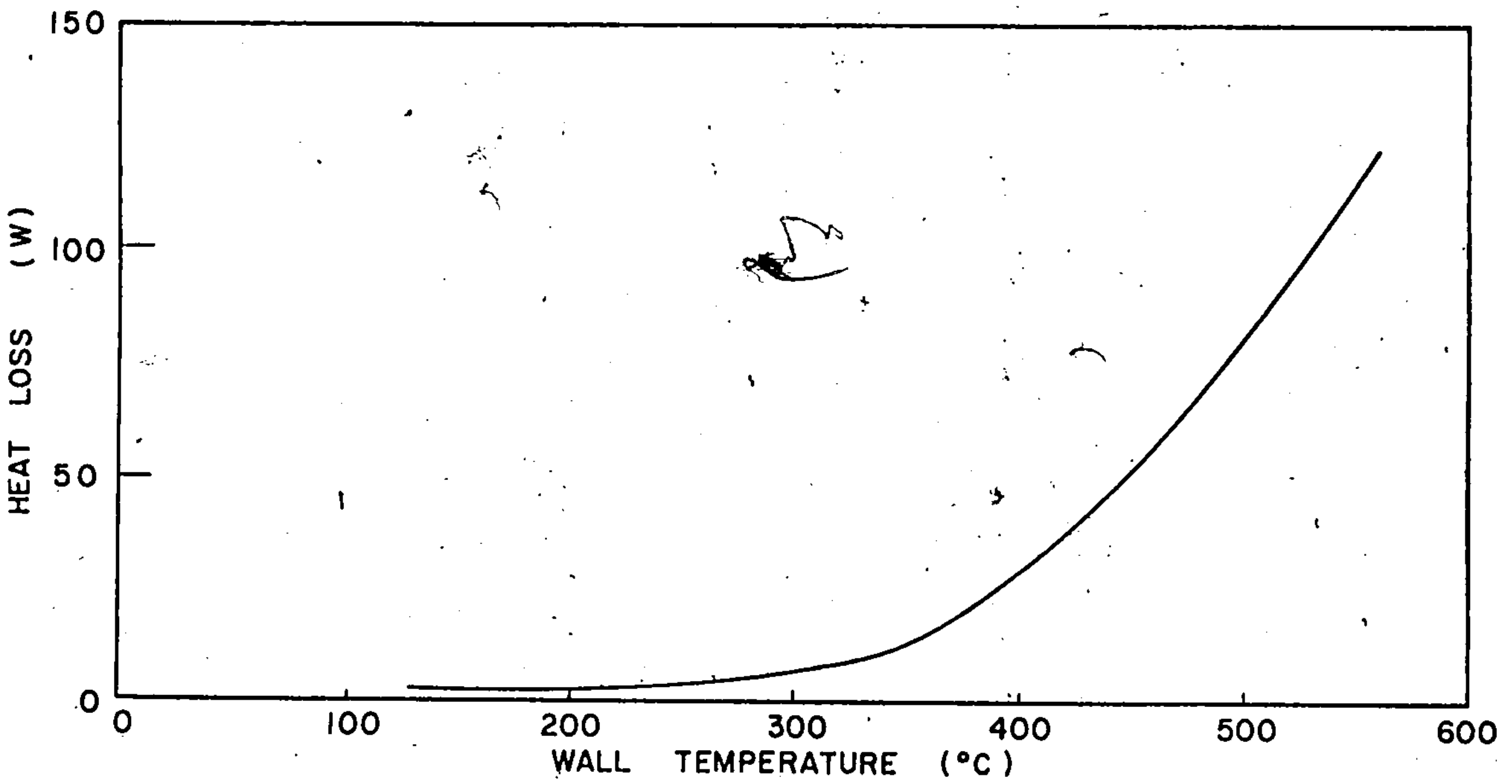

FIG. A.1 HEAT LOSSES VS AVERAGE WALL TEMPERATURE FOR 10,300 RUN SERIES

Appendix B

COOLDOWN TEST OF THE BOTTOM HOT PATCH

After each successful quench run, a separate cooldown test of the bottom hot patch followed. The temperature history of the bottom hot patch was used to evaluate the film boiling heat flux of the bottom hot patch by applying Cheng's model [26].

During the test, the temperature of the bottom hot patch was set slightly higher than at the true quench temperature experiments. Power for direct heating and the flow parameters were set at the same value as that of the true quench conditions. At the beginning of the cooldown test, the power of the bottom hot patch was turned off. The data thermocouple T.C.1 (Fig. 3.3) was recorded by the Fluke datalogger with every two-second interval.

The cooldown test terminated as the temperature of the bottom hot patch dropped to about 50°C below the true quench temperature experiments.

Appendix C

MATHEMATICAL METHOD FOR DETERMINATING FILM BOILING HEAT FLUX

The heat transfer from the bottom hot patch to the fluid between time 0 to t is assumed equal to the change in heat content (Q) inside the cylindrical block, minus heat loss through the outer wall during the same time interval. Q can be expressed as:

$$Q(t) = \rho c_p L \int_{r_{in}}^{r_{out}} 2\pi r T(r,t) dr \qquad (C.1)$$

where L represents the length of the bottom hot patch. The function T(r,t) is obtained as the solution to the one-dimensional Fourier equation on cylindrical co-ordinates:

$$\frac{\partial T}{\partial t} = \alpha\left(\frac{\partial^2 T}{\partial r^2} + \frac{1}{r}\frac{\partial T}{\partial r}\right) \qquad (C.2)$$

and is subject to the following initial and boundary conditions:

1. $T = T(r,0)$ ... In general. (C.3)
2. $T(r_o,t) = T_o$ ... r_o and T_o are the location and recordings of the data thermocouple respectively. (C.4)
3. $$-k \left.\frac{\partial T}{\partial r}\right)_{r=r_{out}} = h\ (T_n - T_{amb}) \qquad (C.5)$$

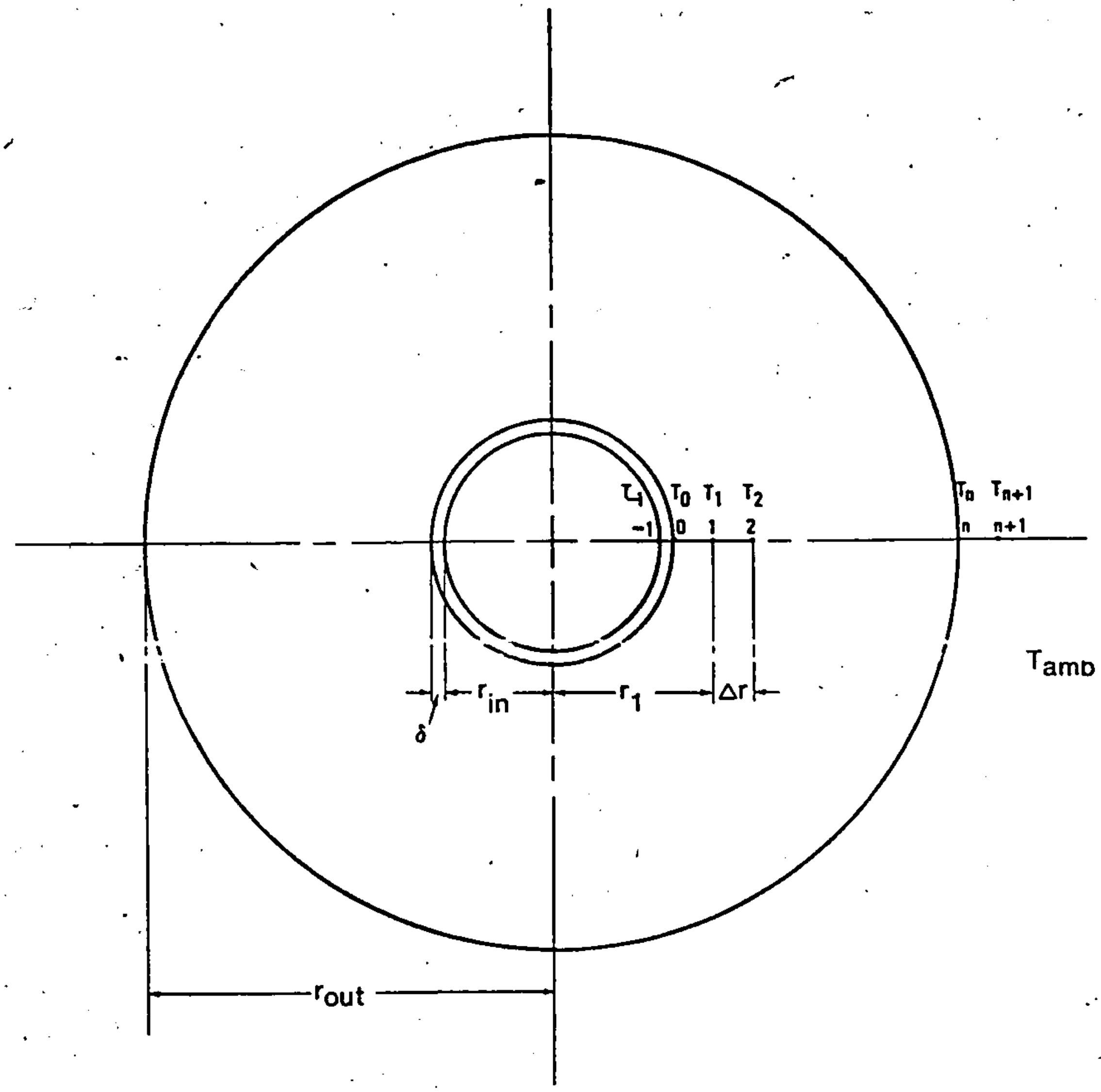

FIG. C.1 NODAL POINTS DISTRIBUTION

h is the heat transfer coefficient at the outer wall

The solution of Eq.(C.2) can be obtained by reducing it to a system of linear first-order differential equations in t. This is achieved by discretizing along the r-direction using the approximation:

$$\left.\frac{\partial T}{\partial r}\right|_{r=r_i} = \frac{T_{i+1}(t) - T_{i-1}(t)}{2\,\Delta r} \tag{C.6}$$

and

$$\left.\frac{\partial^2 T}{\partial r^2}\right|_{r=r_i} = \frac{T_{i-1}(t) - 2T_i(t) + T_{i+1}(t)}{(\Delta r)^2} \tag{C.7}$$

where $T_i(t)$ represents the temperature at the i^{th} nodal point

$$(1 \leq i \leq n+1) \text{ and } \Delta r = [r_{out} - (r_{in} + \delta)] / n$$

Using Eqs.(C.6) and (C.7) along with initial and boundary conditions, the following system of equations can be inferred from Eq.(C.2).

$$\frac{\partial T_i}{\partial t} = \alpha\left[\frac{T_{i-1} - 2T_i + T_{i+1}}{(\Delta r)^2}\right] + \frac{\alpha}{r_i}\left[\frac{T_{i+1} - T_{i-1}}{2\,\Delta r}\right] \tag{C.8}$$

$$1 \leq i \leq n$$

where

$$r_i = r_{in} + \delta + i\,\Delta r$$

and

$$\frac{-k}{2}\left(\frac{T_n - T_{n-1}}{\Delta r} + \frac{T_{n+1} - T_n}{\Delta r}\right) = h\,(T_n - T_{amb}) \qquad \text{(C.9)}$$

Eq.(C.9) is a direct consequence of Eq.(C.5). Furthermore, T_{n+1} in Eq.(C.8) can be eliminated by using Eq.(C.9).

Eq.(C.8) contains a system of n equations with n unknowns in T_i and are readily solved. Once T_1 up to T_n have been solved and dT_0/dt determined experimentally, the inner wall temperature T_{-1} can then be calculated in the following Fourier equation based on the nodal point i=0.

$$\frac{[r_o^2 - (r_o - \delta/2)^2]\,\rho_t c_t + [(r_o + \Delta r/2)^2 - r_o^2]\,\rho_c c_c}{(r_o + \Delta r/2)^2 - (r_o - \delta/2)^2}\,\frac{dT_o}{dt}$$

$$= \frac{k_c(T_1 - T_o)/\Delta r - k_t(T_o - T_{-1})/\delta}{(\Delta r + \delta)/2} + \frac{1}{2r_o}\left[\frac{k_c(T_1 - T_o)}{\Delta r} + \frac{k_t(T_o - T_{-1})}{\delta}\right] \qquad \text{(C.10)}$$

Eq.(C.1) expressed in terms of summation, becomes

$$Q = 2\pi\delta\rho_t c_t L\,[0.5T_{-1} r_{in} + 0.5T_o(r_{in} + \delta)]$$

$$+\, 2\pi\Delta r\rho_c c_c L\,[0.5T_o(r_{in} + \delta) + \sum_{i=1}^{n-1} T_i r_i + 0.5T_n r_n] \qquad \text{(C.11)}$$

The expression of net heat transfer to the fluid, q, in terms of Q and heat loss is:

$$q = \frac{-dQ}{dt} / A_{in} - h\, A_{out} \left(T_n - T_{amb} \right) / A_{in}$$

$$= \frac{-1}{2\pi r_{in} L} \frac{dQ}{dt} - h \frac{r_{out}}{r_{in}} \left(T_n - T_{amb} \right) \quad \text{(C.12)}$$

where A_{in} and A_{out} represent the inner and the outer test section area, respectively.

All calculations are performed via the CSMP computer package [27]. The Runge-Kutta fixed-step size method has been used in numerical integration with selection of n=8 and Δt=0.1 second and its convergency checked. Nonlinear function generation capability of CSMP is used to generate T_o from experimental data and DERIV (derivative) module used to compute dT_o/dt from T_o and dQ/dt from Q. A complete program has been established starting with thermocouple recordings (temperature vs time) as input, and at the end, q vs the wall temperature printed and plotted (see Appendix E for a sample program).

The heat transfer coefficient h at the outer wall of the bottom hot patch is negligibly small. It is based on the assumption of good insulation around the hot patch.

Appendix D

SAMPLE CALCULATION OF LOCAL QUALITY

Local x at the quench location can be calculated by the following heat balance equation

$$h_{\ell} + \frac{\Delta Q}{\dot{m}} = h_f + x h_{fg} \qquad (1)$$

where ΔQ represents the heat gained from the BHP plus the heat gained from the test section due to direct heating, and minus heat losses.

Sample Calculation: Run No. 10348 (Table 4.4C)

$P = 80$ psia (550 kPa)

$T_{sat} = 156^{\circ}C$

$\Delta T_{sub} = 20^{\circ}C$

$G = 200\ kg/m^2s$

Direct heating power at quench = 1,941 W

Quench location = 5 cm from the BHP

$T_Q = 331^{\circ}C$

Test section total direct heated area inside the tube (excluding the area adjacent to both hot patches) = $2.226 \times 10^{-2} m^2$

Test section cross-sectional area inside the tube = $9.474 \times 10^{-5}\ m^2$

Test section perimeter inside the tube = 3.45×10^{-2} m

$\bar{h}_{\ell}$ (at 136°C) = 570.26 kWs/kg

h_f (at 156°C) = 656.44 kWs/kg

h_{fg} (at 156°C) = 2,096.7 kWs/kg

H.F. (BHP) = 5.13×10^5 W/m² (from a separate cooldown experiment for the BHP to determine the film boiling heat flux at temperature of 700°C)

$\dot{m}$ = G · Test section cross-sectional area

= $200 \cdot 9.474 \times 10^{-5}$

= 1.895×10^{-2} kg/s

Heat gained from the BHP

= H.F. (BHP) · BHP heated area inside the tube

= $5.13 \times 10^5 \cdot 3.45 \times 10^{-2} \cdot (0.105)$

= 1,859 W

$$\text{H.F. (test section)} = \frac{\text{Direct heating power at quench}}{\text{Test section total direct heated area}}$$

$$= \frac{1{,}941}{2.226 \times 10^{-2}}$$

$$= 8.72 \times 10^4 \text{ W/m}^2$$

Heat gained from the test section due to direct heating

= H.F. (test section) · Test section directed heated area inside the tube from the inlet to the quench location

= $8.72 \times 10^4 \cdot 3.42 \times 10^{-2} (0.015 + 0.05)$

= 196 W

Heat losses = 8 W (from a separate heat loss test at quench conditions except no flow passing through)

Now, Eq. (1) can be rearranged

$$x = (h_\ell + \frac{\Delta Q}{\dot{m}} - h_f)\frac{1}{h_{fg}}$$

$$= [\ 570.26 + \frac{1,859 + 196 - 4}{1000\ (1.895 \times 10^{-2})} - 656.44\ ]\ \frac{1}{2,096.7}$$

$$= 0.0105.$$

Appendix E

CONTINUOUS SYSTEM MODELING PROGRAM

****CONTINUOUS SYSTEM MODELING PROGRAM****

PROBLEM INPUT STATEMENTS

```
/      DIMENSION R(30)
 FIXED NPOINT
 FIXED IK
 FIXED IT
 PARAM CK=379.069,CSP=385.186,CRHO=8938.323
 PARAM SK=17.31,SSP=460.570,SRHO=7816.784
 INITIAL
 IK=10
 DELZ=(21.0/(64.0*12.0))*0.3048
 X=1.0
Z=1.0
CALPHA=(1.0/0.23)*2.581E-05
*
*
*
TIN1=749.2
TIN2=748.2
DT=1.0
 T23=TIN1
 DT3 =DT
 DTDT23=(TIN2-TIN1)/DT
 RIN=(0.4324/(2.0*12.0))*0.3048
 DELRO=(0.040/12.0)*0.3048
 RO=RIN+DELRO
 L=(4.0/12.0)*0.3048
 DELR=(ROUT-RIN-DELRO)/NPOINT
  DRSQ=DELR**2
 CKDR=DELR*CK
 SKDRO=SK*DELRO
CROSP=CRHO*CSP
SROSP=SRHO*SSP
 ROUT=(3.50/(2.0*12.0))*0.3048
 NPOINT=8
 DL=(RO+DELR/2.0)**2-(RO-DELRO/2.0)**2
 C1=((RO**2-(RO-DELRO/2.0)**2)*SROSP+((RO+DELR /2.0)**2-RO**2)
    *CROSP)/DL
 C2=2.0/((DELR+DELRO)*DELR)+1.0/(2.0*RO*DELR)
 C3=1.0/(2.0*RO*DELRO)-2.0/((DELR+DELRO)*DELRO)
 IC33=T23
 IC43=T23
 IC53=T23
 IC63=T23
 IC73=T23
 IC83=T23
 IC93=T23
 ICA3=T23
 COEFFN=1.0/(2.0*3.14159*RIN)
 NOSORT
 DO 1 N=1,NPOINT
 R(N)=RO+N*DELR
 1 CONTINUE
**
```

```
**
**************************  *******  ***  ***  *********  ******
****************************************************************
*********************      10101        ************************
FUNCTION THISC=0,749.2,1,748.2,3,747.0,5,745.8,7,744.2,9,742.5,...
11,740.9,13,739.1,15,737.5,17,735.9,19,733.8,21,732.1,23,730.3,...
25,728.1,27,726.4,29,724.8,31,722.6,33,721.1,35,719.5,37,717.3,...
39,715.8,41,713.9,43,712.0,45,710.5,47,708.6,49,706.8,51,705.0,...
53,702.8,55,701.2,57,699.7,59,697.6,61,696.1,63,694.3,65,692.5,...
67,691.0,69,689.3,71,687.5,73,685.7,75,683.9,77,682.2,79,680.6,...
84,676.3,89,671.7.94,667.7,99,663.8,104,659.5,109,655.3
DYNAMIC
**
**
T23=NLFGEN(THISC,TIME)
**
**
**
**
**
****************************************************************
****************************************************************
 T33=INTGRL(IC33,DT33)
 T43=INTGRL(IC43,DT43)
 T53=INTGRL(IC53,DT53)
 T63=INTGRL(IC63,DT63)
 T73=INTGRL(IC73,DT73)
 T83=INTGRL(IC83,DT83)
 T93=INTGRL(IC93,DT93)
 TA3=T93
**
**
**
**
**        FINITE CIFF. EG'S FOR PLANE C
**
****************************************************************
 DT33 = CALPHA*(((T43-T33)-Z*(T33-T23))/DRSQ
        +((T43-T33)+Z*(T33-T23))/(2.0*DELR*R(1)))
 DT43 = CALPHA*((T33-2.0*T43+T53)/DRSQ +(T53-T33)/(2.0*DELR*R(2)))
 DT53 = CALPHA*((T43-2.0*T53+T63)/DRSQ +(T63-T43)/(2.0*DELR*R(3)))
 DT63 = CALPHA*((T53-2.0*T63+T73)/DRSQ +(T73-T53)/(2.0*DELR*R(4)))
 DT73 = CALPHA*((T63-2.0*T73+T83)/DRSQ +(T83-T63)/(2.0*DELR*R(5)))
 DT83 = CALPHA*((T73-2.0*T83+T93)/DRSQ +(T93-T73)/(2.0*DELR*R(6)))
 DT93 = CALPHA*((T83-2.0*T93+TA3)/DRSQ +(TA3-T83)/(2.0*DELR*R(7)))
**
**        TO CALCULATE T13
**
 DT23=DERIV(DTDT23,T23)
 T13 = T23 - (C1*DT23-C2*CK*Z*(T33-T23))/(C3*SK)
**
**        TO CALCULATE HEAT FLUX -- PLANE C
**
 HCONTC = 2.0*3.14159*DELZ*((T13*RIN+T23*(RIN+DELRO))*DELRO*SROSP/2.0..
        +(0.5*T23*(RIN+DELRO)+T33*R(1)+T43*R(2)+T53*R(3)+T63*R(4)     ..
        +T73*R(5)+T83*R(6)+T93*R(7)+TA3*R(8)*0.5)*DELR*CROSP)
**
 HTCS=DERIV(0.0,HCONTC)
 HT = -HTCS*COEFFN/DELZ
 CPLOT=HT    /150000.
 HT3=SK*(T23-T13)/DELRO
PLOT3=HT3/150000.
 IT =TIME
 METHOD RKSFX
```

```
NOSORT
      IF(IT.NE.IK) GO TO 98
      WRITE(6,96)TIME
      WRITE(6,93) T13,T23,T33,T43,T53,T63,T73,T83,T93,TA3
      WRITE(6,80) TZ
IK=IK+7
80    FORMAT(20X,F5.1)
93    FORMAT(1X,'PLANE C ',10(F 5.1,5X),/)
99    FORMAT(2F5.1)
96    FORMAT(30X,'TEMPERATURE DISTRIBUTION AT TIME =  ',F5.1,//)
98    CONTINUE
SORT
TWALL=T13
TMSURE=T23
TIMER FINTIM=109.00,DELT=0.1,PRDEL= 7.0,OUTDEL=0.5
LABEL  PLANE  C
PRTPLT HT (TMSURE)
CRSPLT TWALL(HT)
END
STOP
```

PLANE C

PAGE 1

Heat Flux vs. Time

MINIMUM 0.0

MAXIMUM 5.7638E 05

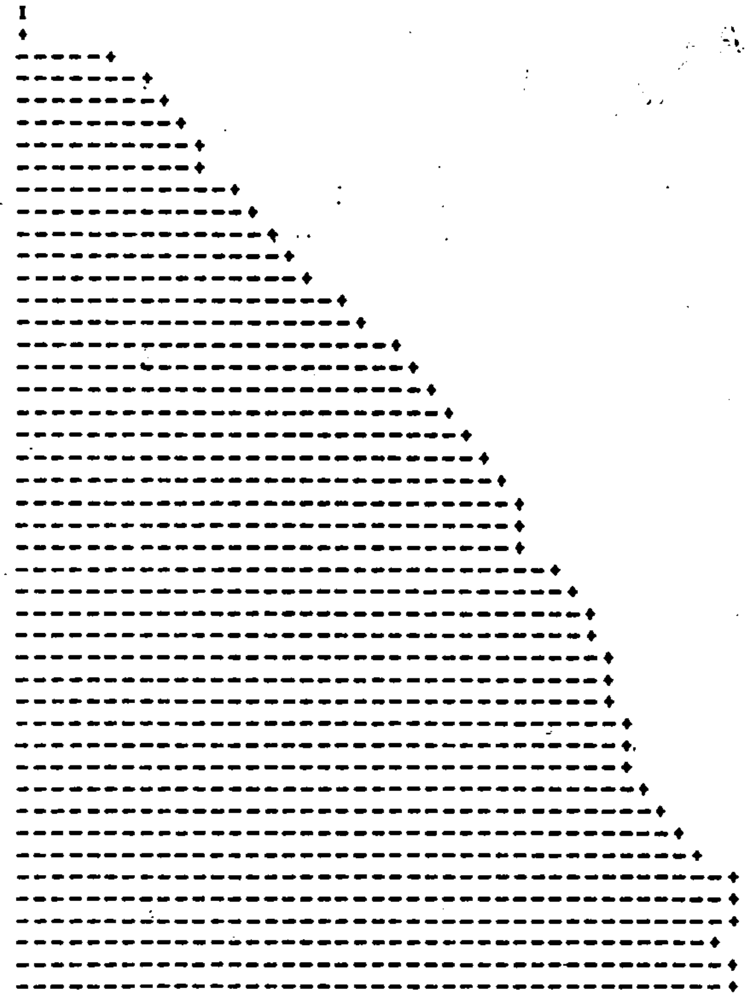

TIME	HT	TMSURE
0.0	0.0	7.4820E 02
5.0000E-01	5.8247E 04	7.4870E 02
1.0000E 00	8.7153E 04	7.4820E 02
1.5000E 00	1.0106E 05	7.4780E 02
2.0000E 00	1.1193E 05	7.4747E 02
2.5000E 00	1.1975E 05	7.4720E 02
3.0000E 00	1.1628E 05	7.4700E 02
3.5000E 00	1.4562E 05	7.4670E 02
4.0000E 00	1.5801E 05	7.4640E 02
4.5000E 00	1.6735E 05	7.4610E 02
5.0000E 00	1.7735E 05	7.4580E 02
5.5000E 00	1.9278E 05	7.4544E 02
6.0000E 00	2.1256E 05	7.4505E 02
6.5000E 00	2.2277E 05	7.4464E 02
7.0000E 00	2.4516E 05	7.4420E 02
7.5000E 00	2.5950E 05	7.4378E 02
8.0000E 00	2.6885E 05	7.4336E 02
8.5000E 00	2.8298E 05	7.4293E 02
9.0000E 00	2.9645E 05	7.4250E 02
9.5000E 00	3.0601E 05	7.4209E 02
1.0000E 01	3.1166E 05	7.4169E 02
1.0500E 01	3.2405E 05	7.4129E 02
1.1000E 01	3.2557E 05	7.4090E 02
1.1500E 01	3.3231E 05	7.4047E 02
1.2000E 01	3.5339E 05	7.4002E 02
1.2500E 01	3.6339E 05	7.3957E 02
1.3000E 01	3.7730E 05	7.3910E 02
1.3500E 01	3.7295E 05	7.3868E 02
1.4000E 01	3.8143E 05	7.3827E 02
1.4500E 01	3.8339E 05	7.3788E 02
1.5000E 01	3.8360E 05	7.3750E 02
1.5500E 01	3.9904E 05	7.3710E 02
1.6000E 01	4.0017E 05	7.3670E 02
1.6500E 01	4.0230E 05	7.3630E 02
1.7000E 01	4.0403E 05	7.3590E 02
1.7500E 01	4.2012E 05	7.3544E 02
1.8000E 01	4.3120E 05	7.3495E 02
1.8500E 01	4.4511E 05	7.3444E 02
1.9000E 01	4.6511E 05	7.3390E 02
1.9500E 01	4.6598E 05	7.3343E 02
2.0000E 01	4.6141E 05	7.3297E 02
2.0500E 01	4.5967E 05	7.3253E 02
2.1000E 01	4.6445E 05	7.3210E 02
2.1500E 01	4.6945E 05	7.3165E 02

Heat Flux vs. Time

MINIMUM 0.0 MAXIMUM 5.7638E 05

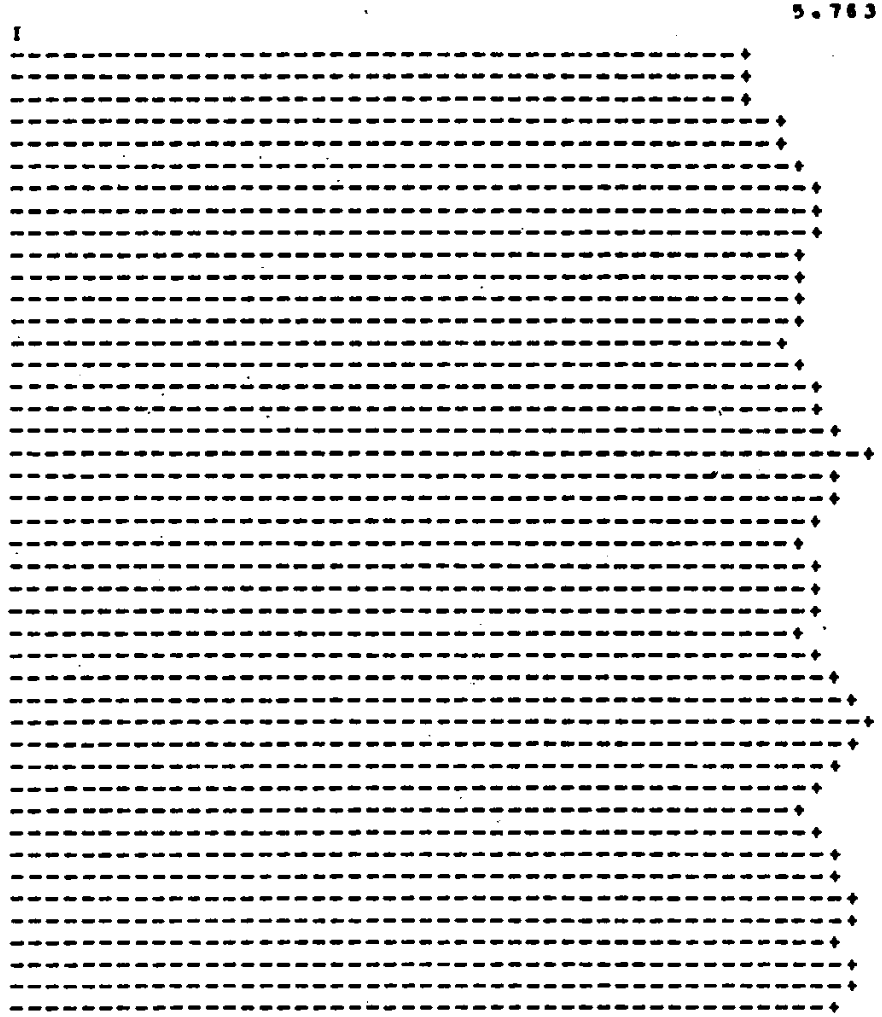

TIME	HT	TMSURE
2.2000E 01	4.7619E 05	7.3120E 02
2.2500E 01	4.7423E 05	7.3075E 02
2.3000E 01	4.7880E 05	7.3030E 02
2.3500E 01	5.0010E 05	7.2978E 02
2.4000E 01	5.0488E 05	7.2925E 02
2.4500E 01	5.1488E 05	7.2869E 02
2.5000E 01	5.2640E 05	7.2810E 02
2.5500E 01	5.1966E 05	7.2763E 02
2.6000E 01	5.2444E 05	7.2719E 02
2.6500E 01	5.1227E 05	7.2678E 02
2.7000E 01	5.1227E 05	7.2640E 02
2.7500E 01	5.1116E 05	7.2599E 02
2.8000E 01	5.1488E 05	7.2559E 02
2.8500E 01	5.0640E 05	7.2519E 02
2.9000E 01	5.1183E 05	7.2480E 02
2.9500E 01	5.2531E 05	7.2431E 02
3.0000E 01	5.2705E 05	7.2377E 02
3.0500E 01	5.4096E 05	7.2321E 02
3.1000E 01	5.5530E 05	7.2260E 02
3.1500E 01	5.4161E 05	7.2216E 02
3.2000E 01	5.4139E 05	7.2176E 02
3.2500E 01	5.2031E 05	7.2141E 02
3.3000E 01	5.1575E 05	7.2110E 02
3.3500E 01	5.2053E 05	7.2071E 02
3.4000E 01	5.1879E 05	7.2031E 02
3.4500E 01	5.1944E 05	7.1991E 02
3.5000E 01	5.1183E 05	7.1950E 02
3.5500E 01	5.2640E 05	7.1901E 02
3.6000E 01	5.3857E 05	7.1847E 02
3.6500E 01	5.4661E 05	7.1791E 02
3.7000E 01	5.5422E 05	7.1730E 02
3.7500E 01	5.4183E 05	7.1686E 02
3.8000E 01	5.4052E 05	7.1646E 02
3.8500E 01	5.2553E 05	7.1611E 02
3.9000E 01	5.1770E 05	7.1580E 02
3.9500E 01	5.2444E 05	7.1536E 02
4.0000E 01	5.3292E 05	7.1490E 02
4.0500E 01	5.4074E 05	7.1441E 02
4.1000E 01	5.4204E 05	7.1390E 02
4.1500E 01	5.4661E 05	7.1342E 02
4.2000E 01	5.3900E 05	7.1295E 02
4.2500E 01	5.4770E 05	7.1247E 02
4.3000E 01	5.5161E 05	7.1200E 02
4.3500E 01	5.4096E 05	7.1159E 02

PLANE C

PAGE 3

Heat Flux vs. Time

MINIMUM 0.0 — MAXIMUM 5.7638E 05

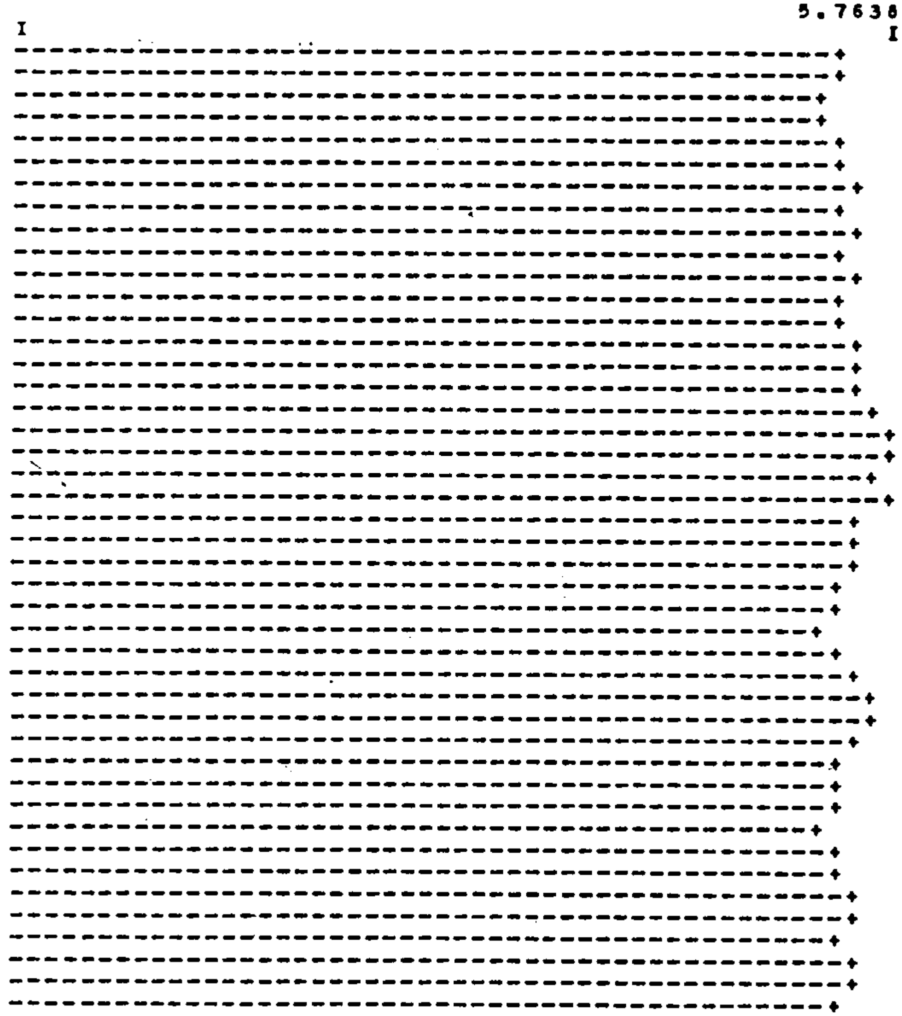

TIME	HT	TMSURE
4.4000E 01	5.3226E 05	7.1120E 02
4.4500E 01	5.3053E 05	7.1084E 02
4.5000E 01	5.2270E 05	7.1050E 02
4.5500E 01	5.2944E 05	7.1006E 02
4.6000E 01	5.3335E 05	7.0960E 02
4.6500E 01	5.3552E 05	7.0911E 02
4.7000E 01	5.4487E 05	7.0860E 02
4.7500E 01	5.3813E 05	7.0814E 02
4.8000E 01	5.4748E 05	7.0769E 02
4.8500E 01	5.3835E 05	7.0724E 02
4.9000E 01	5.4552E 05	7.0680E 02
4.9500E 01	5.4096E 05	7.0635E 02
5.0000E 01	5.4009E 05	7.0590E 02
5.0500E 01	5.4574E 05	7.0545E 02
5.1000E 01	5.4335E 05	7.0500E 02
5.1500E 01	5.5269E 05	7.0449E 02
5.2000E 01	5.6443E 05	7.0395E 02
5.2500E 01	5.6682E 05	7.0339E 02
5.3000E 01	5.7595E 05	7.0280E 02
5.3500E 01	5.6378E 05	7.0234E 02
5.4000E 01	5.6508E 05	7.0192E 02
5.4500E 01	5.4313E 05	7.0154E 02
5.5000E 01	5.4465E 05	7.0120E 02
5.5500E 01	5.4878E 05	7.0082E 02
5.6000E 01	5.3639E 05	7.0044E 02
5.6500E 01	5.3509E 05	7.0007E 02
5.7000E 01	5.2879E 05	6.9970E 02
5.7500E 01	5.3900E 05	6.9923E 02
5.8000E 01	5.4487E 05	6.9872E 02
5.8500E 01	5.5530E 05	6.9818E 02
5.9000E 01	5.6182E 05	6.9760E 02
5.9500E 01	5.4748E 05	6.9717E 02
6.0000E 01	5.3639E 05	6.9677E 02
6.0500E 01	5.4009E 05	6.9642E 02
6.1000E 01	5.3031E 05	6.9610E 02
6.1500E 01	5.2944E 05	6.9568E 02
6.2000E 01	5.3183E 05	6.9524E 02
6.2500E 01	5.4096E 05	6.9478E 02
6.3000E 01	5.4248E 05	6.9430E 02
6.3500E 01	5.4183E 05	6.9385E 02
6.4000E 01	5.3770E 05	6.9340E 02
6.4500E 01	5.4378E 05	6.9295E 02
6.5000E 01	5.4291E 05	6.9250E 02
6.5500E 01	5.3248E 05	6.9210E 02

PLANE C

PAGE 4

Heat Flux vs. Time

MINIMUM 0.0 — MAXIMUM 5.7638E 05

TIME	HT	TMSURE
6.6000E 01	5.3292E 05	6.9171E 02
6.6500E 01	5.2270E 05	6.9135E 02
6.7000E 01	5.1575E 05	6.9100E 02
6.7500E 01	5.2140E 05	6.9059E 02
6.8000E 01	5.2248E 05	6.9017E 02
6.8500E 01	5.2466E 05	6.8974E 02
6.9000E 01	5.2531E 05	6.8930E 02
6.9500E 01	5.2596E 05	6.8886E 02
7.0000E 01	5.3096E 05	6.8841E 02
7.0500E 01	5.3009E 05	6.8796E 02
7.1000E 01	5.3813E 05	6.8750E 02
7.1500E 01	5.3096E 05	6.8705E 02
7.2000E 01	5.3053E 05	6.8660E 02
7.2500E 01	5.3335E 05	6.8615E 02
7.3000E 01	5.3618E 05	6.8570E 02
7.3500E 01	5.3639E 05	6.8525E 02
7.4000E 01	5.3770E 05	6.8480E 02
7.4500E 01	5.3661E 05	6.8435E 02
7.5000E 01	5.3074E 05	6.8390E 02
7.5500E 01	5.3661E 05	6.8347E 02
7.6000E 01	5.3465E 05	6.8304E 02
7.6500E 01	5.2705E 05	6.8262E 02
7.7000E 01	5.3226E 05	6.8220E 02
7.7500E 01	5.3596E 05	6.8179E 02
7.8000E 01	5.1770E 05	6.8139E 02
7.8500E 01	5.2748E 05	6.8099E 02
7.9000E 01	5.1901E 05	6.8060E 02
7.9500E 01	5.2248E 05	6.8019E 02
8.0000E 01	5.1770E 05	6.7977E 02
8.0500E 01	5.1662E 05	6.7935E 02
8.1000E 01	5.1901E 05	6.7893E 02
8.1500E 01	5.1662E 05	6.7850E 02
8.2000E 01	5.2009E 05	6.7807E 02
8.2500E 01	5.2227E 05	6.7763E 02
8.3000E 01	5.2531E 05	6.7719E 02
8.3500E 01	5.2248E 05	6.7675E 02
8.4000E 01	5.2987E 05	6.7630E 02
8.4500E 01	5.2987E 05	6.7585E 02
8.5000E 01	5.3118E 05	6.7540E 02
8.5500E 01	5.3661E 05	6.7495E 02
8.6000E 01	5.3161E 05	6.7450E 02
8.6500E 01	5.3791E 05	6.7404E 02
8.7000E 01	5.3031E 05	6.7358E 02
8.7500E 01	5.3487E 05	6.7311E 02

PLANE C

PAGE 5

Heat Flux vs. Time

MINIMUM 0.0 I

MAXIMUM 5.7838E 05 I

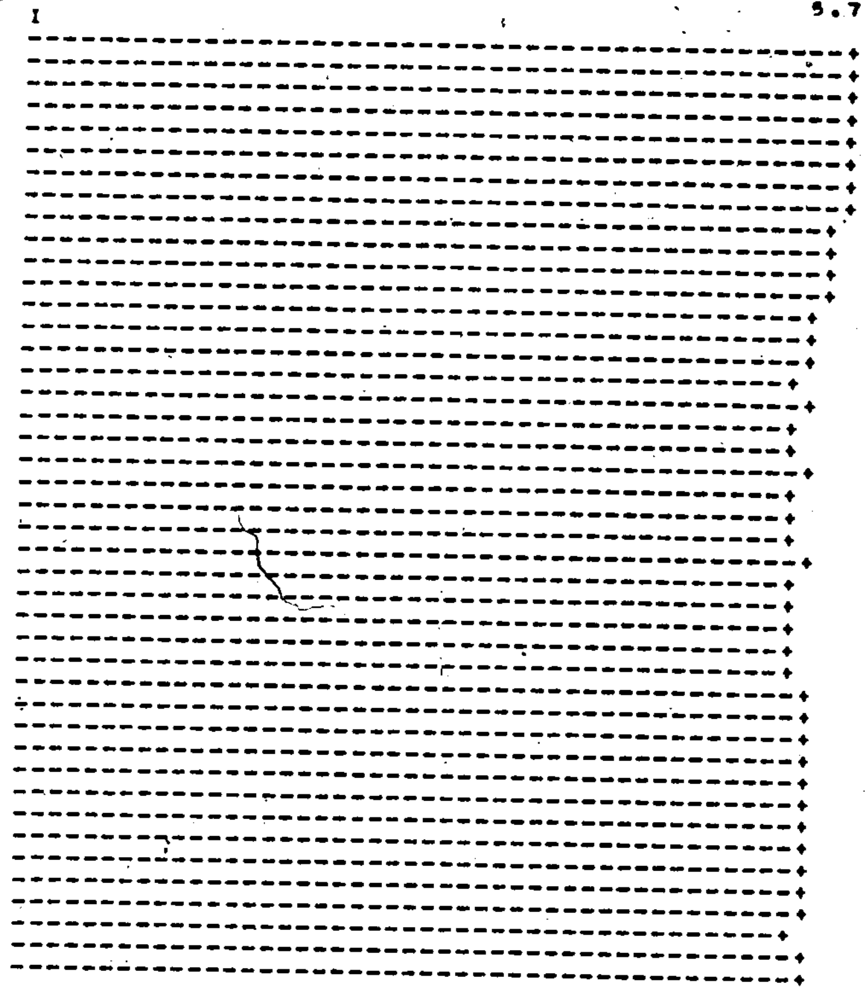

TIME	HT	TMSURE
8.8000E 01	5.3683E 05	6.7264E 02
8.8500E 01	5.3965E 05	6.7217E 02
8.9000E 01	5.3987E 05	6.7170E 02
8.9500E 01	5.3465E 05	6.7127E 02
9.0000E 01	5.3661E 05	6.7085E 02
9.0500E 01	5.3770E 05	6.7044E 02
9.1000E 01	5.3335E 05	6.7003E 02
9.1500E 01	5.3183E 05	6.6962E 02
9.2000E 01	5.2944E 05	6.6923E 02
9.2500E 01	5.3009E 05	6.6884E 02
9.3000E 01	5.2531E 05	6.6845E 02
9.3500E 01	5.1988E 05	6.6807E 02
9.4000E 01	5.1618E 05	6.6770E 02
9.4500E 01	5.1379E 05	6.6730E 02
9.5000E 01	5.1401E 05	6.6691E 02
9.5500E 01	5.0531E 05	6.6652E 02
9.6000E 01	5.0727E 05	6.6613E 02
9.6500E 01	5.0032E 05	6.6574E 02
9.7000E 01	5.0510E 05	6.6535E 02
9.7500E 01	5.1140E 05	6.6496E 02
9.8000E 01	5.0553E 05	6.6457E 02
9.8500E 01	4.9966E 05	6.6418E 02
9.9000E 01	4.9858E 05	6.6380E 02
9.9500E 01	5.0901E 05	6.6339E 02
1.0000E 02	4.9858E 05	6.6297E 02
1.0050E 02	4.9836E 05	6.6255E 02
1.0100E 02	5.0140E 05	6.6213E 02
1.0150E 02	5.0314E 05	6.6170E 02
1.0200E 02	5.0705E 05	6.6127E 02
1.0250E 02	5.0836E 05	6.6083E 02
1.0300E 02	5.0814E 05	6.6039E 02
1.0350E 02	5.1488E 05	6.5995E 02
1.0400E 02	5.1183E 05	6.5950E 02
1.0450E 02	5.1227E 05	6.5907E 02
1.0500E 02	5.0923E 05	6.5865E 02
1.0550E 02	5.1562E 05	6.5823E 02
1.0600E 02	5.1010E 05	6.5781E 02
1.0650E 02	5.1162E 05	6.5739E 02
1.0700E 02	5.1205E 05	6.5697E 02
1.0750E 02	5.1010E 05	6.5655E 02
1.0800E 02	5.0358E 05	6.5613E 02
1.0850E 02	5.1096E 05	6.5571E 02
1.0900E 02	5.0814E 05	6.5530E 02

Appendix F

SPSS PROGRAM FOR CORRELATION OF TRUE QUENCH TEMPERATURE

```
STATISTICAL PACKAGE FOR THE SOCIAL SCIENCES (SPSSG032, 1/15/75)
                          RUN NAME          MOLTIPLE REGRESSION RUN USING CARD INPUT
                          FILE NAME         PREDICTION OF QUENCHED TEMPERATURE
                          VARIABLE LIST     TQ,P,DTSUB,G
                          INPUT FORMAT      FIXED (2(F3.0,3X),F2.0,4X,F3.0)


                          N OF CASES        54
                          COMPUTE           VARA = TQ
                          COMPUTE           VARB = P
                          COMPUTE           VARC = DTSUB
                          COMPUTE           VARD = G
                          COMPUTE           CONSTANT = 145.98135
                          COMPUTE           BB = 0.13473
                          COMPUTE           BC = 3.50685
                          COMPUTE           BD = 0.18046
                          COMPUTE           PTQ = CONSTANT+BB*VARB+BC*VARC+BD*VARD
                          COMPUTE           ERROR = ((PTQ-TQ)/TQ)**2
                          PRINT FORMATS     TQ,P,DTSUB,G,PTQ(2)
                          VAR LABELS        TQ      QUENCHED TEMPERATURE/
                                            P       PRESSURE/
                                            DTSUB   SUBCOOL TEMPERATURE/
                                            G       MASS FLUX
                          LIST CASES        CASES = 54/VARIABLES = TQ,P,DTSUB,G,PTQ/
                          TRANSFORM

ITEM                 ACTUAL   MAXIMUM

VARS RECODED              0       100
VALUES RECODED            0       952
TRANSFORMATIONS          10       238
MATH OPERATORS           17      1904
LITERAL VALUES            6       193

                          READ INPUT DATA
```

MULTIPLE REGRESSION RUN USING CARD INPUT

FILE PREDICTI (CREATION DATE = 11/30/82) OF QUENCHED TEMPERATURE

CASE-N	TQ	P	DTSUB	G	PTQ
1	245.00	206.00	30.00	50.00	286.96
2	268.00	206.00	30.00	100.00	294.99
3	343.00	206.00	30.00	200.00	311.03
4	367.00	206.00	30.00	300.00	327.08
5	392.00	206.00	30.00	400.00	343.13
6	225.00	206.00	20.00	50.00	251.90
7	245.00	206.00	20.00	100.00	259.92
8	285.00	206.00	20.00	200.00	275.96
9	320.00	206.00	20.00	300.00	292.01
10	340.00	206.00	20.00	400.00	308.05
11	216.00	206.00	10.00	50.00	216.83
12	230.00	206.00	10.00	100.00	224.85
13	235.00	206.00	10.00	200.00	240.90
14	245.00	206.00	10.00	300.00	256.94
15	245.00	206.00	10.00	400.00	272.99
16	270.00	344.00	30.00	50.00	305.56
17	330.00	344.00	30.00	200.00	329.63
18	341.00	344.00	30.00	300.00	345.67
19	400.00	344.00	30.00	400.00	361.72
20	250.00	344.00	20.00	50.00	270.49
21	285.00	344.00	20.00	100.00	278.51
22	307.00	344.00	20.00	200.00	294.56
23	343.00	344.00	20.00	300.00	310.60
24	343.00	344.00	20.00	400.00	326.65
25	220.00	344.00	10.00	50.00	235.42
26	236.00	344.00	10.00	100.00	243.44
27	248.00	344.00	10.00	200.00	259.49
28	245.00	344.00	10.00	300.00	275.53
29	260.00	344.00	10.00	400.00	291.58
30	330.00	550.00	30.00	50.00	333.31
31	341.00	550.00	30.00	100.00	341.33
32	363.00	550.00	30.00	300.00	373.43
33	374.00	550.00	30.00	400.00	389.47
34	307.00	550.00	20.00	50.00	298.24
35	285.00	550.00	20.00	100.00	306.27
36	331.00	550.00	20.00	200.00	322.31
37	331.00	550.00	20.00	300.00	338.36
38	350.00	550.00	20.00	400.00	354.40
39	295.00	550.00	10.00	50.00	263.17
40	319.00	550.00	10.00	100.00	271.20
41	288.00	550.00	10.00	200.00	287.24
42	280.00	550.00	10.00	400.00	319.34
43	343.00	687.00	30.00	100.00	359.79
44	370.00	687.00	30.00	200.00	375.84
45	378.00	687.00	30.00	300.00	391.88
46	385.00	687.00	30.00	400.00	407.93
47	343.00	687.00	20.00	100.00	324.72
48	354.00	687.00	20.00	200.00	340.77
49	355.00	687.00	20.00	300.00	356.82
50	362.00	687.00	20.00	400.00	372.86
51	318.00	687.00	10.00	50.00	281.63
52	330.00	687.00	10.00	100.00	289.66
53	341.00	687.00	10.00	300.00	321.75
54	300.00	687.00	10.00	400.00	337.79

MULTIPLE REGRESSION RUN USING CARD INPUT

FILE PREDICTI (CREATION DATE = 11/30/82) OF QUENCHED TEMPERATURE

VARIABLE	MEAN	STANDARD DEV	CASES
VARA	308.3704	51.0643	54
VARB	431.4815	186.1149	54
VARC	19.8148	8.1242	54
VARD	216.6667	131.0336	54

MULTIPLE REGRESSION RUN USING CARD INPUT

FILE PREDICTI (CREATION DATE = 11/30/82) OF QUENCHED TEMPERATURE

CORRELATION COEFFICIENTS

A VALUE OF 99.00000 IS PRINTED
IF A COEFFICIENT CANNOT BE COMPUTED.

	VARA	VARB	VARC	VARD
VARA	1.00000	0.51793	0.59005	0.47279
VARB	0.51793	1.00000	0.01092	0.05046
VARC	0.59005	0.01092	1.00000	0.06499
VARD	0.47279	0.05046	0.06499	1.00000

MULTIPLE REGRESSION RUN USING CARD INPUT

FILE PREDICTI (CREATION DATE = 11/30/82) OF QUENCHED TEMPERATURE

SUMMARY TABLE

VARIABLE	MULTIPLE R	R SQUARE	RSQ CHANGE	SIMPLE R	B
VARB	0.51793	0.26825	0.26825	0.51793	0.13473
VARC	0.78090	0.60981	0.34156	0.59005	3.50685
VARD	0.88217	0.77822	0.16841	0.47279	0.16046
(CONSTANT)					145.98135

MULTIPLE REGRESSION RUN USING CARD INPUT

FILE PREDICTI (CREATION DATE = 11/30/82) OF QUENCHED TEPPERATURE

DEPENDENT VARIABLE: VARA FROM VARIABLE LIST 1
REGRESSION LIST 1

SEQNUM	OBSERVED VARA	PREDICTED VARA	RESIDUAL
1	245.0000	286.9646	-41.96478
2	268.0000	294.9879	-26.98793
3	343.0000	311.0342	31.96574
4	367.0000	327.0803	39.91943
5	392.0000	343.1267	48.87311
6	225.0000	251.8963	-26.89630
7	245.0000	259.9194	-14.91946
8	285.0000	275.9656	9.034225
9	320.0000	292.0120	27.98790
10	340.0000	308.0583	31.94159
11	216.0000	216.8279	-0.8278297
12	230.0000	224.8510	5.149014
13	235.0000	240.8973	-5.897297
14	245.0000	256.9436	-11.94361
15	245.0000	272.9897	-27.98981
16	270.0000	305.5576	-35.55783
17	330.0000	329.6272	0.3726868
18	341.0000	345.6736	-4.673615
19	400.0000	361.7197	38.28006
20	250.0000	270.4893	-20.48935
21	285.0000	278.5125	6.487486
22	307.0000	294.5586	12.44117
23	343.0000	310.6050	32.39485
24	343.0000	326.6514	16.34854
25	220.0000	235.4209	-15.42088
26	236.0000	243.4440	-7.444035
27	248.0000	259.4902	-11.49035
28	245.0000	275.5366	-30.53665
29	260.0000	291.5828	-31.58286
30	330.0000	333.3125	-3.312677
31	341.0000	341.3357	-0.3358335
32	363.0000	373.4282	-10.42846
33	374.0000	389.4746	-15.47477
34	307.0000	298.2441	8.755800
35	285.0000	306.2673	-21.26735
36	331.0000	322.3135	8.688333
37	331.0000	338.3599	-7.359979
38	350.0000	354.4063	-4.406290
39	295.0000	263.1755	31.82426
40	319.0000	271.1987	47.80112
41	288.0000	287.2451	0.7548109
42	280.0000	319.3376	-39.33780
43	343.0000	359.7939	-16.79414
44	370.0000	375.8403	-5.840463
45	378.0000	391.8867	-13.88677
46	385.0000	407.9329	-22.93307
47	343.0000	324.7256	18.27432
48	354.0000	340.7720	13.22801
49	355.0000	356.8181	-1.818295
50	362.0000	372.8645	-10.86461
51	318.0000	281.6340	36.36595
52	330.0000	289.6570	40.34280
53	341.0000	321.7498	19.25017
54	300.0000	337.7959	-37.79813

DURBIN-WATSON TEST OF RESIDUAL DIFFERENCES COMPARED BY CASE ORDER (SEQNUM).

VARIABLE LIST 1, REGRESSICN LIST 1. DURBIN-WATSON TEST 1.28791

MULTIPLE REGRESSION RUN USING CARD INPUT

FILE PREDICTI (CREATION DATE = 11/30/82) OF QUENCHED TEPPERATURE

DEPENDENT VARIABLE: VARA VARIABLE LIST 1

REGRESSION LIST 1

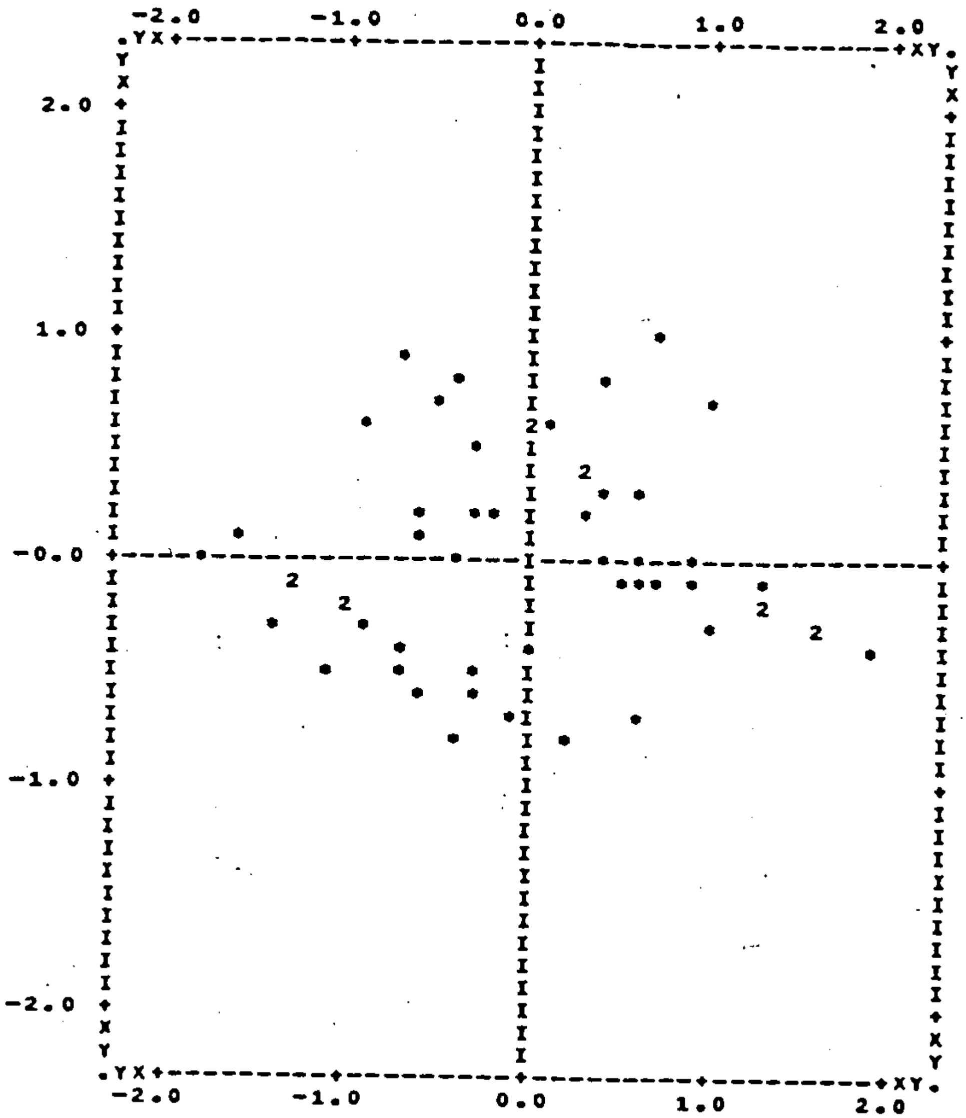

ROWS,COLUMNS Y: VALUES OUTSIDE (-3.0,3.0)

ROWS,COLUMNS X: VALUES IN (-3.0,-2.05) OR (2.05,3.0)

MULTIPLE REGRESSION RUN USING CARD INPUT

FILE PREDICTI (CREATION DATE = 11/30/82) OF QUENCHED TEMPERATURE

VARIABLE ERROR

MEAN	0.006
VARIANCE	0.000
RANGE	0.029

VALID OBSERVATIONS - 54

STD ERROR	0.001	STD DEV	0.007
KURTOSIS	0.816	SKEWNESS	1.195
MINIMUM	0.000	MAXIMUM	0.029

MISSING OBSERVATIONS - 0